Silica Sol-Gel Materials as a Catalyst Support for use in Microwave-Assisted Continuous-Flow Organic Synthesis

CHRISTOPHER SCHRUDER

A DISSERTATION SUBMITTED TO
THE FACULTY OF GRADUATE STUDIES
IN PARTIAL FULFILLMENT OF THE REQUIREMENTS
FOR THE DEGREE OF DOCTOR OF PHILOSOPHY

GRADUATE PROGRAM IN CHEMISTRY
YORK UNIVERSITY
TORONTO, ONTARIO

SEPTEMBER 2018

ABSTRACT

The Organ group used microwave irradiation as a means of heating flowed chemical reactions in the development of a microwave-assisted continuous-flow organic synthesis (MACOS) system, to combine the benefits of flow reactions and the effective heating of microwave radiation. MACOS was well suited to the use of heterogeneous catalysts contained within the reactor capillaries, and metal films proved to be effective to not only catalyze reactions, but also to act as a heating source. Unfortunately, the heating of bulk metal films under microwave irradiation was hard to control, leading to intense over-heating of reactions and destruction of the metal films.

Transition metal-loaded heterogeneous catalysts immobilized on microwave-transparent silica supports were prepared. The supported catalysts also act as a mixer within the flow channels to prevent laminar flow and allow for high catalyst surface area. The *in situ* palladium nanoparticle-loaded silica macrospheres were used to catalyze Heck cross-coupling reactions in MACOS, providing good product yield, and can be recycled several times without appreciable decrease in product formation.

Dithiocarbamate-functionalized ligands were prepared and used to form amphiphilic transition metal complexes to attempt to selectively load metals at the surface of silica macrospheres. Some selectivity for incorporation of the metal complexes towards the outer surface of the macrospheres was obtained, however, there was a penetration depth of metals into the interior of the macrospheres, and the complexes were not fully characterized.

Inorganic-organic hybrid macrospheres were prepared containing functional groups that could coordinate desired transition metals selectively on their surface. These inorganic-organic

hybrid catalyst supports were also used to perform Heck cross-coupling reactions in MACOS. Calcination of these metal-loaded macrospheres yielded silica macrospheres with palladium nanoparticles loaded selectively on their surface.

The inorganic-organic hybrid macrospheres were able to catalyze the Heck cross-coupling of aryl iodides in MACOS. They were re-usable without significant decrease in product conversion. The calcined macrospheres with palladium nanoparticles loaded selectively on their surface were able to catalyze the Heck cross-coupling of aryl iodides in MACOS, but significant leaching of the catalyst from the support was observed.

ACKNOWLEDGEMENTS

I would like to thank my supervisors, Professor Michael G. Organ and Professor William J. Pietro, for their guidance and support over the course of my graduate studies. I would also like to thank my research committee advisors: Professor Gino G. Lavoie, who has taught me many things both in class and during our yearly research evaluations; and Professor Jennifer I. L. Chen, who not only helped me during my Ph.D. studies, but also as a first year undergraduate student. In addition, I would like to thank both my internal examiner, Professor William van Wijngaarden, and my external examiner, Professor Cathleen Crudden, for agreeing to examine this thesis.

Thank you to all the past and current members of the Organ group for all of the guidance and fun times over the years. Also to the sole other member of the Pietro group, Xia Chen for being such a good friend. Also my friends Gabrielle, Henry and Viviana, Kristjan and Tiffany, Andres Consuelo, Julia, and Ha.

Finally, thank you to my parents for their love and support over the years. I owe you a lot for helping me get this far.

TABLE OF CONTENTS

LIST OF TABLES

LIST OF FIGURES

LIST OF SCHEMES

LIST OF ABBREVIATIONS

Ac	Acetyl
APTES	3-Aminopropyl triethoxysilane
Avg.	average
CFU	Continuous flow unit
DCM	Dichloromethane
DMA	Dimethylacetamide
DMF	N,N-dimethylformamide
DTC	dithiocarbamate
EDX	Energy-dispersive X-ray spectroscopy
h	Hour
ICP-AES	Inductively coupled plasma atomic emission spectrometry
IOMS	Inorganic-organic hybrid macrosphere
*is*CuSMSs	in situ copper-loaded silica macrospheres
*is*PdSMSs	in situ palladium-loaded silica macrospheres
MACOS	Microwave-assisted continuous-flow organic synthesis
MAOS	Microwave-assisted organic synthesis
Me	Methyl
MIOMS	3-Mercaptopropyl-functionalized inorganic-organic hybrid macrosphere
M_n	Number average molecular weight
MPTES	3-Mercaptopropyl triethoxysilane
MR	Microreactor

NHC	N-heterocyclic carbene
NMR	Nuclear magnetic resonance
PCD	Pressure creating device
Pd^{II}@MIOMSs	Palladium(II) acetate-loaded 3-Mercaptopropyl-functionalized inorganic-organic hybrid macrospheres
Pd^{0}@SMS	Silica macrospheres with palladium nanoparticles selectively on their surface
PEO	Polyethylene oxide
SEM	Scanning electron microscope
S_NAr	Nucleophilic aromatic substitution
tan δ	Loss tangent
TBOS	Tetrabutyl orthosilicate
TEM	Transmission electron microscope
TEOS	Tetraethyl orthosilicate
THF	Tetrahydrofuran
TMOS	Tetramethyl orthosilicate
ε’	Dielectric constant
ε”	Dielectric loss

Chapter 1: Introduction

1.1: Chemical Synthesis in Flow

Flow reactors are being investigated as an increasingly popular alternative for traditional batch reactors in many chemical syntheses.[1] Microfluidic techniques use capillaries with diameters of 10-500 μm that are ideal for efficient heat transfer and temperature control because of their high surface area to volume ratios.[1] However, larger diameter channels may be used for some flow processes.[1] In a batch reaction, all reagents are kept in a single vessel for the entire reaction timeframe, whereas flow reactors (Figure 1.1) use a stream of flowing reagents that are separated until the moment of reaction.

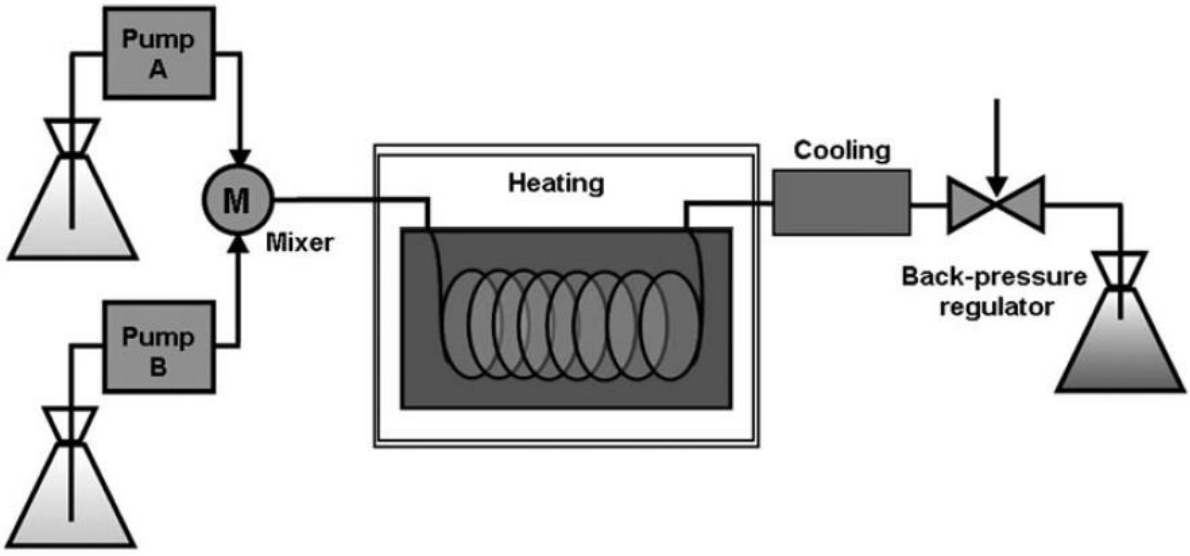

Figure 1.1: General Schematic of a flow reactor for chemical synthesis. Reprinted with permission from Reference [1]a [4]. Copyright 2010 John Wiley and Sons.

While batch syntheses in flasks are easily handled, allow for continuous visual observation of reactions, and do not generally require expensive specialized equipment, the advantages of performing reactions in a flow format usually outweigh these features. Some of the advantages of flow processes are cleaner reactions, efficient mixing of reagents, fast heat transfer, high

achievable temperatures and pressures, safer synthesis of hazardous compounds, easy scale-up, efficient use of recyclable immobilized catalysts, integrated analytics, and automated optimization/purification.[1] However, flow processes still have some significant drawbacks. For example, flow processes require significant investment in time and equipment to implement. As many industrial processes have already been optimized for the use of batch reactors, conversion to flow could be very costly.[1] In addition, reactions involving solid reagents or precipitating products generally cannot be effectively converted to flow processes due to clogging of the flow systems.

Reactions that generally benefit most from the use of flow techniques are those that are very fast and mostly rate-limited by mixing.[2],[3] These very fast reactions are classified as type A and B reactions, where type A reactions are extremely fast and controlled by mixing, whereas type B reactions are very fast and kinetically-controlled.[3] Type C reactions, however, are slower (>20 minutes) and may not gain rate benefits from flow techniques. However, such reactions could still take advantage of other benefits of flow.[3] These slower reactions may be performed in "mesofluidic" reactors, with diameters ≥500 μm, because mixing is a less critical factor for the reaction.

The continuous removal of products from starting materials in flow reactions allows for strict control of residence time, which can help to prevent the occurrence of possible side reactions. Flow processes allow for the products to be removed from the system and quenched immediately following reaction, thus reducing the propensity for side reactions to cause further reaction and loss of product. Very reactive intermediates can also be formed in flow and used immediately in a multi-step synthesis through the use of multiple inlets. The reduced occurrence of side

reactions in flow provides cleaner reaction mixtures that are easier to purify, reducing processing time and cost.

The fast heat transfer in flow syntheses stems from both the high surface-area to volume ratio of the flow system and the small amounts of reagents that will be reacting at a time in the flow system. The small volumes within the reactor capillaries heat and cool rapidly, allowing for high control and homogeneity of reaction temperatures. This has a safety advantage for extremely exothermic reactions, as well as possibly preventing undesired reactions caused by a large temperature range (Figure 1.2).[2],[4] Flow channels can also be formed into specific shapes to enhance mixing, heating, and cooling of reactions. Heating in flow can be achieved by simple submersion of the reactor capillary into a water[5] or oil bath.[6] However, more advanced setups can involve specialized equipment, such as embedded resistance heating wires,[7] Peltier elements, or microwave heating.[8],[9],[10]-[20]

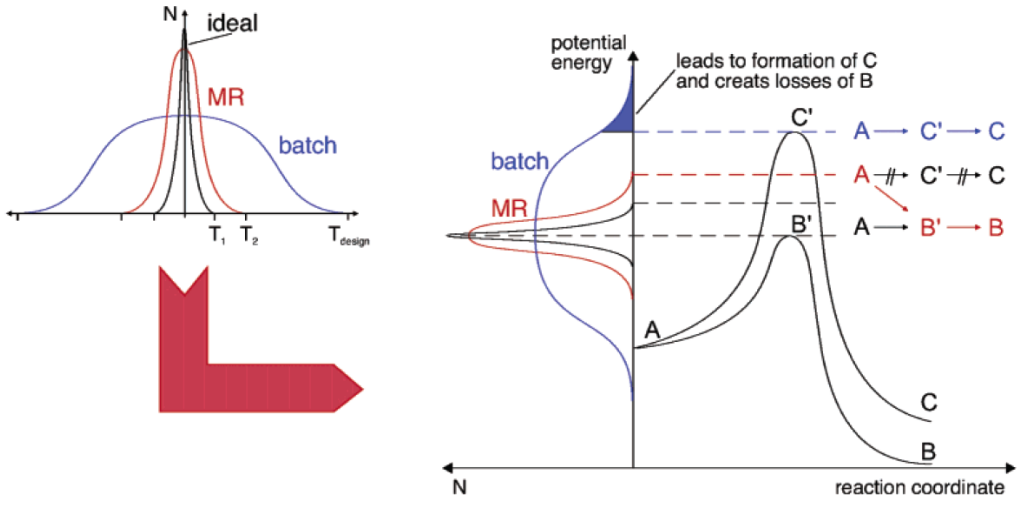

Figure 1.2: Normal distribution of temperatures for batch and flow microreactor (MR) systems (left). Reaction profile showing competing reactions with different activation energies, with normal distribution of temperatures imposed. Reprinted with permission from Reference [4]. Copyright 2004 American Chemical Society.

The small, enclosed nature of flow systems allows for high temperatures and pressures to be reached more readily and safely than in large-scale batch reactors. Stainless steel is commonly used as a reactor tube material owing to its ability to withstand high temperatures and pressures, as well as its corrosion resistance properties.[1] Reactions have been reported at pressures of up to 250 bar with a temperature of 340°C using stainless steel tubing in flow reactors.[21]

Having small volumes of reaction mixture also decreases the possible danger of explosion or leakage of highly exothermic or toxic reactions. The production of potentially dangerous or reactive intermediates can also be achieved safely due to the relatively short residence time of flow reactions compared to batch processes. Unstable or dangerous materials need not be stored or handled for long periods of time, or in large quantities at any given time.[1]

An additional advantage of flow reactors over the use of batch reactors involves large-scale or production reactions. Flow systems allow for scale-up by increasing the amount of time that the flow system is active (scale-out), or by increasing the number of systems running simultaneously (numbering up). This is actually an enormous advantage of flow reactions because optimization of the reaction only needs to be performed once, and is then usable for all conceivable scales of synthesis.[1] All material flowing through the system over time will theoretically experience the same conditions regardless of how long the system is run for and how much product has already been produced. As much or as little product can be prepared, as needed, using the same system. This can make on-demand production of some materials at any scale conceivable. Optimization can also be performed with great efficiency, allowing for fast screening of reaction conditions.

In-line analytics can also be incorporated into a flow system to allow for non-disruptive real-time analysis of chemical reactions.[18],[20] Using results from in-line analysis, automated processes for adjusting reaction conditions can be developed and implemented during a flow synthesis for automated reaction optimization.[18],[20] Since only a small amount of material will be needed for analysis, many different conditions can be quickly screened. This also has application for continual monitoring of flow reactions for quality control standards, identifying deviations from desired parameters and imposing corrections.[18],[20]

1.2: Heterogeneous Supported Catalysts in Flow Reactions

Continuous flow systems in chemical synthesis can be divided into four types (Figure 1.3), classified by the use of supported catalysts and reagents.[22] Type I and II systems are those that contain no catalysts. In Type I systems, all reactants and reagents flow through the reactor, but Type II systems will contain a reactant that is supported and confined in the reactor.[22]

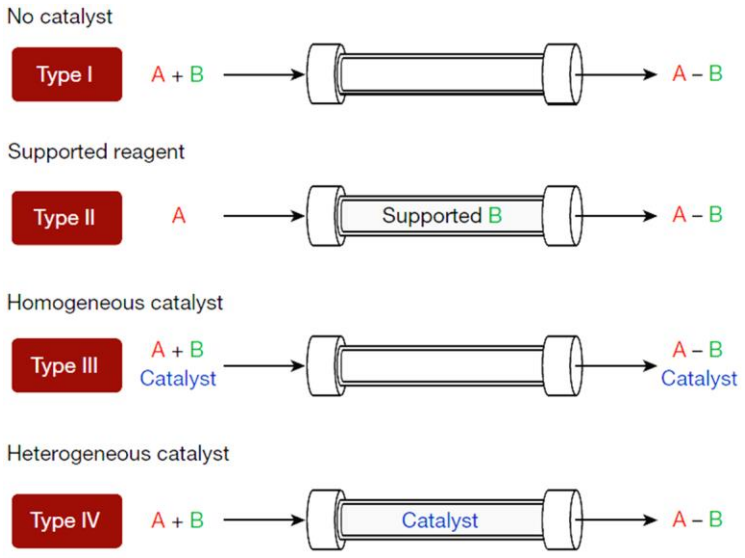

Figure 1.3: Types of continuous-flow systems used for organic synthesis. Reprinted with permission from Reference [22]. Copyright 2015 Springer Nature.

Purification in Type I systems will require unreacted A and B substrates, as well as side-products, to be separated from the desired product for purification. Type II systems will only require the separation of unreacted substrate A and side products for product purification, but the support will need to be replenished periodically. Type III and IV systems involve the use of a catalyst. Type III systems involve only a homogeneous catalyst, whereas Type IV systems use a supported catalyst that is confined within the reactor.[22] In Type, III systems, catalysts must be continuously added into the reaction, and will need to be separated from products at the end of the reaction for purification. Type IV systems still require removal of unreacted starting materials and side products for purification, but unlike Type III systems, do not require continuous addition of catalyst, or removal of a catalyst for product purification. Type IV systems are generally thought to be ideal due to the efficiency of reusable catalysts and reduced purification measures, potentially reducing processing times and costs.[22],[23] The catalyst being confined in the flow system in Type IV systems may also allow for significantly less catalyst to be necessary for a reaction, relative to a similar scale in Type III systems. Even with less overall catalyst, a higher effective catalyst loading may be achieved in Type IV systems due to the small reactor volumes.[24]

The use of heterogeneous transition metal catalysis in flow systems often involves the use of packed-bed reactors containing supported metal nanoparticles or tethered versions of homogeneous catalysts on chemically-inert materials.[1] Polymer, zeolite, and silica supports are commonly used for heterogeneous transition metal catalysts, where the catalyst can be attached to the support surface through covalent bonds (Figure 1.4),[25]-[27] adsorption,[19],[28] electrostatic interactions,[29] or encapsulation (Figure 1.5).[30],[31] The support material must be able to withstand the reaction conditions without degradation, and must be inert to reagents present.

Some supports may therefore be incompatible with certain types of reactions and conditions.[32] High surface-area and dispersion of catalyst are also desirable.

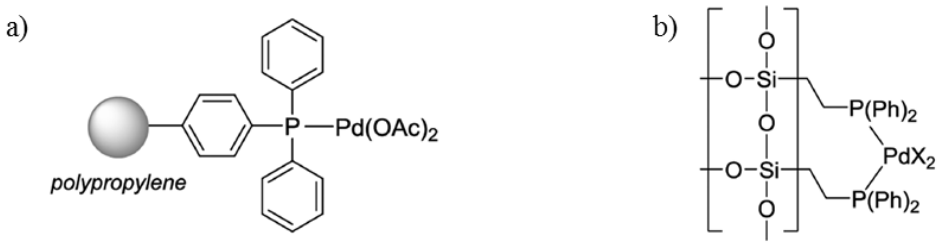

Figure 1.4: Supported catalysts covalently bound to polymer and silica supports. a) Polymer-bound FiberCat 1001.; b) Silica supported SiliaCat Catalyst. Adapted with permission from Reference [32]. Copyright 2015 American Chemical Society.

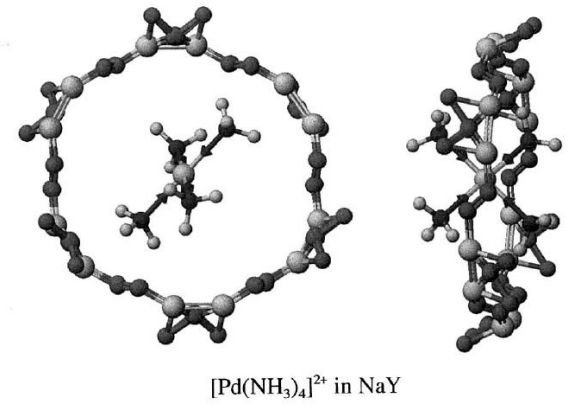

Figure 1.5: Palladium catalyst encapsulated in NaY zeolite cage support. Adapted with permission from Reference [30]b. Copyright 1999 Elsevier.

The use of supported palladium catalysts has become very common due to the large number of important coupling reactions for which palladium can be used.[1],[32] Supported palladium catalysts have been used to perform Suzuki-Miyaura,[14],[33] Mizoroki-Heck,[14],[19],[34] Sonogashira,[35] and Negishi[25] coupling reactions in flow using packed-bed catalyst systems or functionalized reactor capillaries.

Unfortunately, there are several problems associated with the use of packed-bed supported catalysts in flow processes. One problem is caused by the randomness of the packing of the catalyst beds. This can result in high resistance to flow, leading to high backpressures, stagnation zones, and broad residence time distributions for flow reactions.[23],[36] Monolithic catalyst supports can overcome these issues, and have a very high porosity, but suffer from more difficult synthesis, higher fragility, and lower catalyst loadings than catalyst beads.[36] Monolithic catalyst supports also may experience laminar flow of solutions through the channels, limiting the exposure of reagents to the catalyst as well as mixing.[36]

A second issue, which is not unique to packed-bed reactors, is the leaching of catalysts from the support. While, in a batch reaction, leached catalyst may remain active in solution or re-adsorb onto a catalyst support, flow reactions are more likely to have the catalyst washed out of the reactor, where it cannot re-adsorb.[32],[37],[38] This leads to loss of catalyst and reduction of

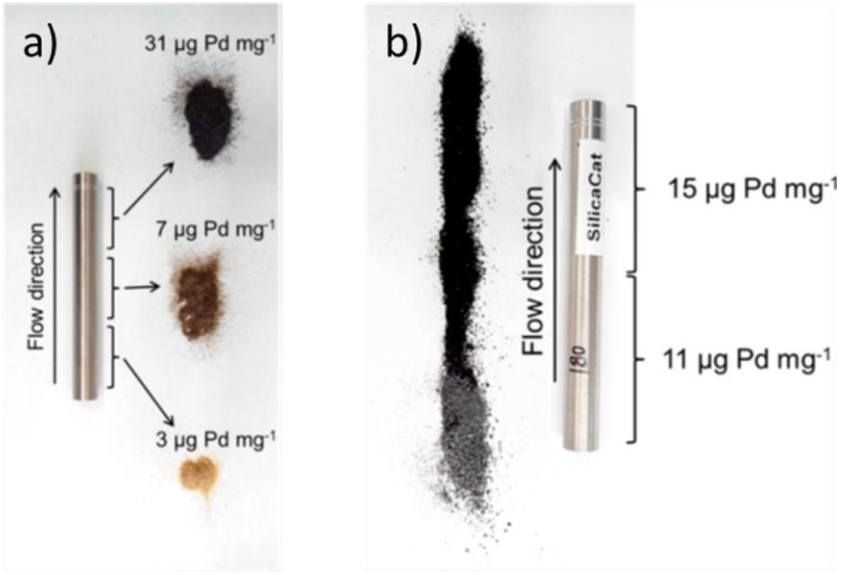

Figure 1.6: Visual representation of the contents of used supported catalyst cartridges after a continuous-flow Suzuki-Miyaura cross-coupling reaction showing the movement of catalyst along the cartridge. a) Polymer-bound FiberCat 1001.; b) SiliaCat DPP-Pd. Reprinted with permission from Reference [32]. Copyright 2015 American Chemical Society.

catalytic activity over time. Contamination of the products with catalyst may also be an issue, requiring separation during purification. As reactants are flowed for longer periods of time, the catalyst can dissolve and re-adsorb to the support, moving down the reactor bed and creating a gradient in catalyst concentration within the reactor (Figure 1.6).[32] This movement of the catalyst along the reactor bed leads to inhomogeneity in the catalyst loading, which can cause shorter contact-time of the substrates with the catalyst.

The leaching of metal from catalyst supports is concentration-dependent, with low concentrations of reactants usually leading to negligible amounts of catalyst in the product solution.[32] In some of these cases, the support may merely act as a reservoir for a homogeneous active catalyst, but re-adsorption is essential for high catalyst lifetimes. The use of coordinating functionality to help bind metals to the support, rather than simple adsorption, was found to decrease the amount of leaching and degradation of the catalyst (Figure 1.6b), but the degree is highly-dependent on the solvent system used.[32]

1.3: Silica Catalyst Supports Prepared Through Sol-Gel Processes

Silicate materials are good candidates for supported catalysts because they generally have greater chemical, mechanical, and thermal stability than polymer materials.[39],[40] They are also able to be prepared from versatile sol-gel techniques, giving great control over the composition and morphology of the resulting materials through even minor changes in synthesis conditions.

The sol-gel formation of silica materials proceeds through the hydrolysis and condensation of silicon alkoxides, which may be catalyzed by either acidic or basic conditions (Scheme 1.1).[41] The structure of the resulting silica materials can be greatly influenced by whether the sol-gel

formation is acid or base catalyzed, as both have different mechanisms that affect the growth and morphology of the resulting gels (Figure 1.7).[42]

a)

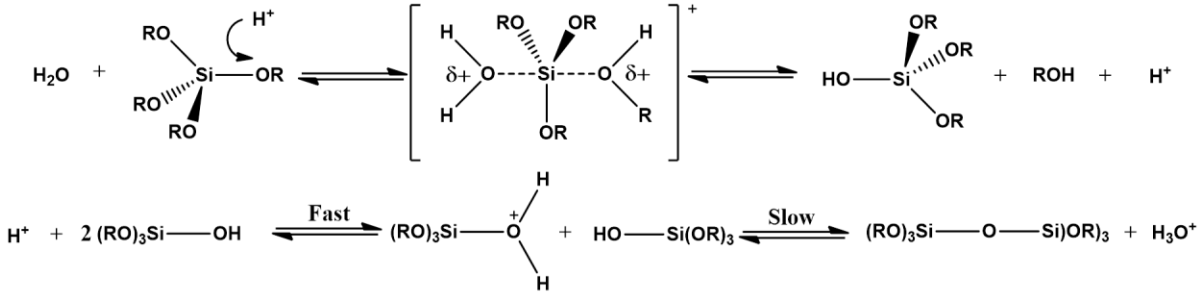

b)

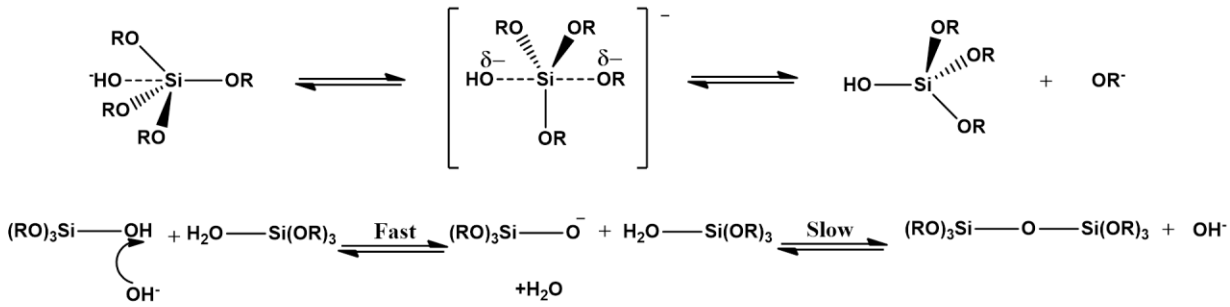

Scheme 1.1: Hydrolysis and condensation reactions in the formation of silica sol-gel materials. a) acid-catalyzed; b) base-catalyzed.

In acid-catalyzed conditions (Scheme 1.1a), each subsequent hydrolysis reaction to replace an alkoxy group on the silicon atom with hydroxyl becomes slower. As a result, in acid-catalyzed conditions, condensation reactions to form crosslinkages between silicon atoms is more likely to begin before hydrolysis is complete. This leads to the formation of chain and network-like morphologies as the networks grow, because it is the terminal alkoxides that are most likely to undergo hydrolysis and then condensation.[42]

However, under base-catalyzed conditions (Scheme 1.1b), each subsequent hydrolysis of the alkoxysilane proceeds faster. In these conditions, it is the fully-hydrolyzed species that is likely to begin crosslinking through condensation reactions.[42] As there are many sites that are able to undergo hydrolysis at the same time, these conditions lead to the formation of small, highly-branched agglomerates that eventually crosslink together to form the larger gel structure.[42]

The rates of hydrolysis for alkoxysilanes can also be influenced by the relative amounts of water present in the system, the sterics of the alkoxy groups, and by the addition of solvents to influence mixing of the silicon alkoxides and water.[42] Other additives can also be used to reduce hydrolysis and condensation rates to influence the morphology of the resulting materials.

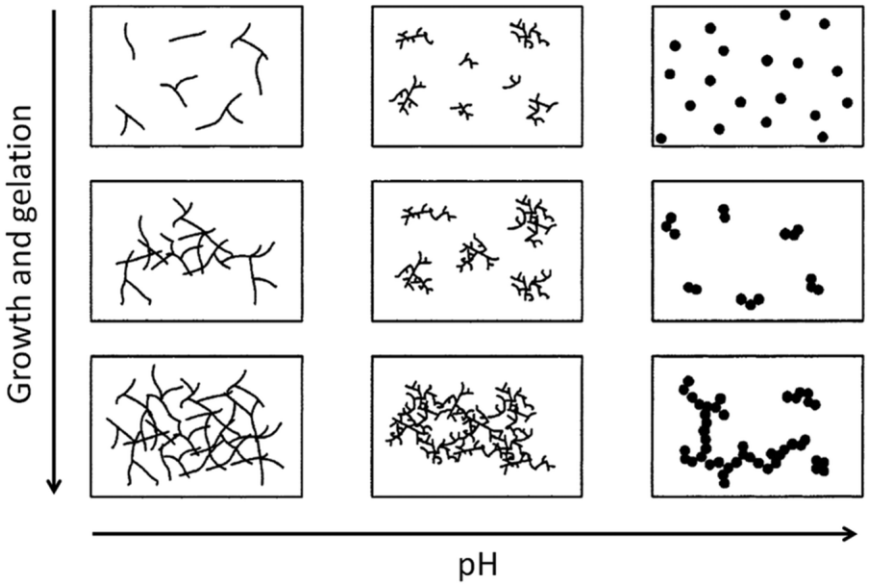

Figure 1.7: The effect of pH on the growth and morphology of silica sol-gels. Reprinted with permission from Reference [42]. Copyright 2004 American Chemical Society.

As the amount of crosslinking increases, small colloidal particles are eventually formed, creating a sol. The colloidal particles will eventually link together as the amount of crosslinking further increases over time, forming a three-dimensional network. This point is when gelation

occurs, and the sol becomes a much more viscous gel that can be shaped. The gel is then aged over time, allowing condensation and hydrolysis reactions to continue, strengthening the structure. The gels can eventually be dried to remove liquid trapped within pores in the structure, and may undergo additional sintering steps to further strengthen the resulting solid network by increasing crosslinking. Drying and sintering steps greatly affect the final structure of the material formed because cracking can occur due to capillary stresses caused by the removal of liquid from pores within the structure. The pore structure can also collapse as additional cross-linkages are formed. Sintering can also be used to remove any remaining organic surfactants or additives still present within the sol-gel after formation.

A major advantage of sol-gel processes for the formation of solid supports is the ability to control both the macroscopic and mesoscopic properties of the resulting material. The shape and porosity of the final structures can be customized through variation of synthesis conditions. Silica materials can be formed from a sol-gel process with a wide variety of morphologies (Figure 1.8), such as films, mesoporous powders,[39],[43] porous monoliths,[44] fibres,[45]-[49] wires,[50] tubes,[47],[51], gyroids,[48] nanospheres,[43],[48] hollow spheres,[51] macrospheres,[52],[53] and with functionality incorporated after[25]b,[26],[54],[55] or during[26],[27] ,[55],[56] synthesis.

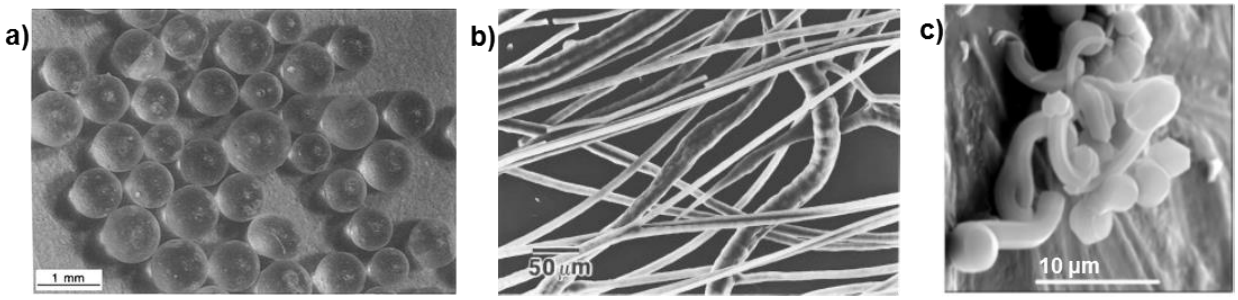

Figure 1.8: SEM images of silica a) macrospheres. Reprinted with permission from Reference [52]. Copyright 1997 American Chemical Society.; b) fibres. Reprinted with permission from Reference [49]. Copyright 1997 American Chemical Society.; and c) spiral wires prepared via a sol-gel method. Reprinted with permission from Reference [50]. Copyright 2005 IEEE.

Metal catalysts have been loaded onto silica supports by various means. Common methods include adding a metal catalyst to the sol during preparation to directly encapsulate the catalyst into the support structure,[19],[57]-[60] or through functionalization of the support with covalently-bound ligands to bind the metal to the support.[25]b,[26],[56],[60]-[63] A metal catalyst encapsulated directly into the silica support can be added as pre-formed nanoparticles,[57] or the nanoparticles may be formed within the matrix after incorporation of a precursor metal salt.[19],[58]-[62],[64]

Nanoparticles embedded in a silica matrix tend not to aggregate as long as their concentration is kept low, allowing for high monodispersity in size and high dispersion throughout the network. The support can also stabilize metal nanoparticles to hinder oxidation.[58],[59] Fonseca et al. prepared a silica support matrix containing a dispersion of nickel nanoparticles with an average diameter of ~6 nm through the addition of nickel(II) nitrate to a sol-gel preparation (Figure 1.9).[59]

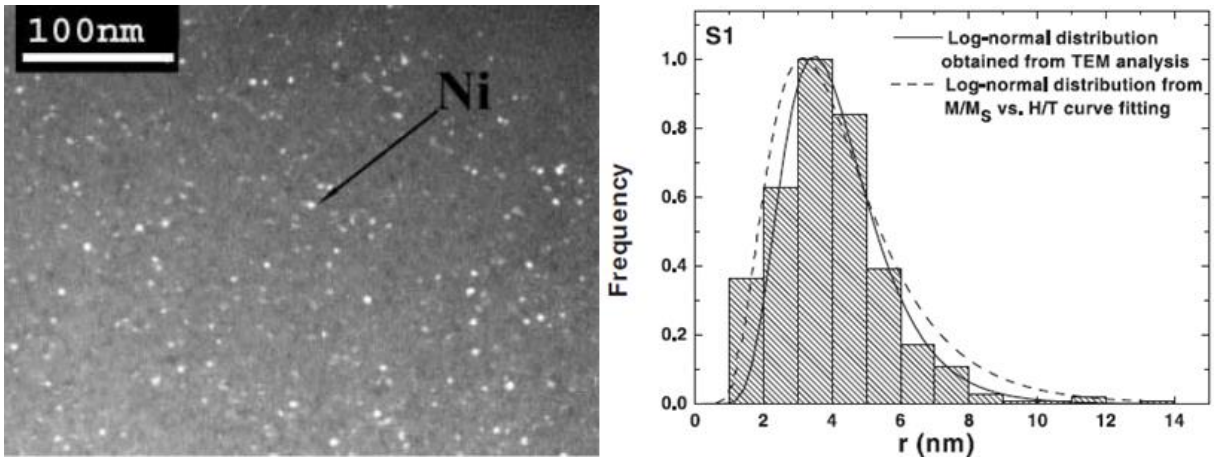

Figure 1.9: TEM image of a suspension of nickel nanoparticles in a silica matrix prepared by addition of nickel(II) nitrate to a sol-gel procedure (left), and histogram of particle size distribution (right). Adapted with permission from Reference [59]. Copyright 2003 Springer Nature.

Metal nanoparticles with high monodispersity can also be prepared in a silica sol-gel support through coordination of a metal salt within the support, followed by chemical or thermal reduction of the metal ions, leaving monodisperse metal nanoparticles, which can be used for catalysis or other applications (Figure 1.10).[60]-[63] The metal may also be used as a catalyst, without reduction, using the binding group as a ligand to prevent leaching of the catalyst from the support.[25]b,[26],[27]

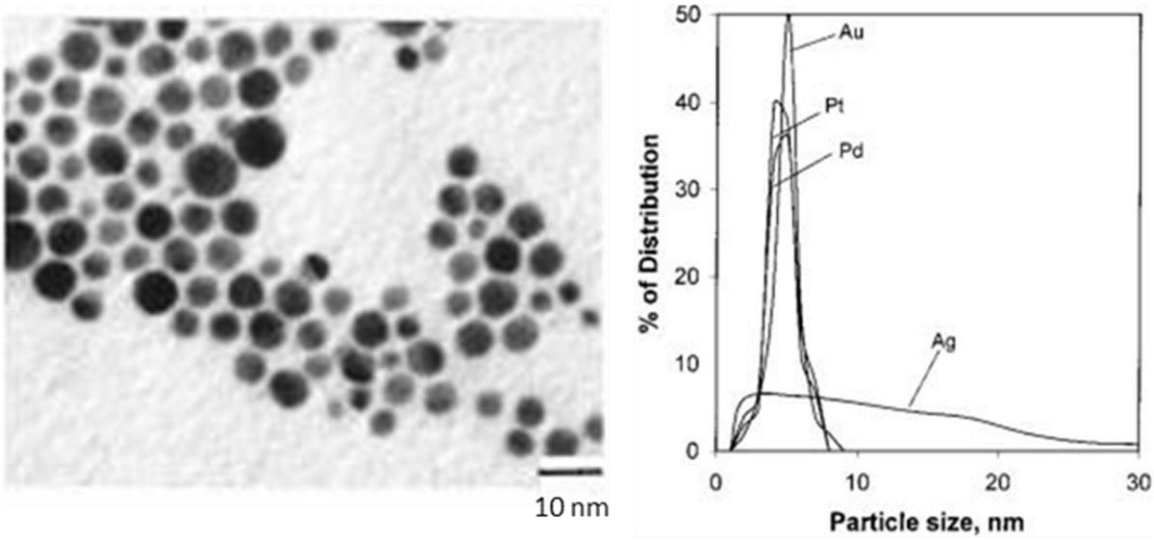

Figure 1.10: TEM image of gold nanoparticles suspended in a silica matrix prepared from a sol-gel mixture of N-[3-(trimethoxysilyl)propyl]ethylenediamine and chloroauric acid (100:1) following reduction with sodium borohydride (left). Particle size distribution shown for gold, palladium, platinum, and silver nanoparticles suspended in a silica matrix prepared using the same procedure (right). Adapted with permission from Reference [60]. Copyright 1999 American Chemical Society.

Different functional groups containing nitrogen-,[65]-[71] sulfur-,[26],[27] and phosphorus-[27]b,[72],[73] donor atoms, as well as carbenes,[25]b,[74] have been used as ligands to bind palladium catalysts to supports as a means to increase catalytic stability and reusability. Thiol-functionalized, high-surface area, silica supports were prepared by Shimizu et al.[26] and Crudden et al.[27]a to be used heterogeneous catalysts, as well as scavengers for leached palladium ions in

Suzuki-Miyaura and Heck cross coupling reactions. The thiol-functionalized silica was able to scavenge palladium metal from solution to then use as a recyclable heterogeneous catalyst with little catalyst leaching.[27]a Tests were also performed to confirm that catalysis was actually occurring from the supported palladium species, rather than the support merely acting as a reservoir and trap for homogeneous catalysts. The thiol coordination was also found to reduce aggregation and deactivation of the catalytic species on the support, improving the recyclability of the catalysts when ligating groups were present.[26]

1.4: Microwave Heating of Chemical Reactions

Typically, heating of chemical reactions in research laboratories is accomplished through the use of hotplates with oil or water baths, heating mantles, etc., that rely on external heat applied to the walls of the reaction vessel. Convection and mixing of the contents of the reaction are then needed to distribute the heat throughout the reaction mixture. Achieving uniformity of heating, however, becomes increasingly difficult as the size of the reaction vessel increases, leading to

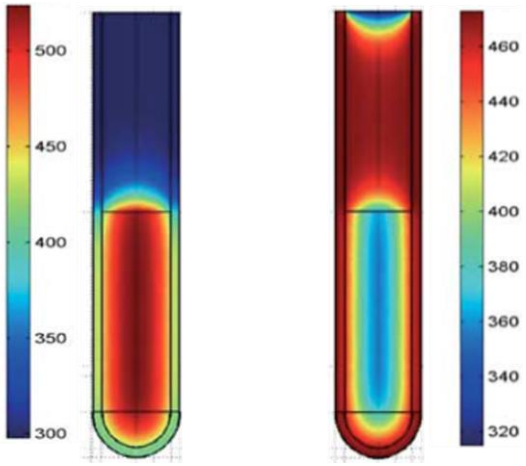

Figure 1.11: Temperature profiles of a reaction heated by microwave irradiation (left) and by immersion in an oil bath (right). Adapted with permission from Reference [75]. Copyright 2003 Springer Nature.

significant temperature differences between the outer walls of a reaction vessel and the centre.[4],[75]-[77] In the worst cases, these variations in temperature could result in the promotion of undesired alternative side reactions, or decomposition of the desired products after formation.[4] Both of these processes serve to decrease both yield and purity of the desired products, greatly reducing the efficiency of a chemical synthesis.

Microwave irradiation (Figure 1.12) was investigated as a substitute for the use of oil baths or heating mantles because it is able to penetrate the glass reaction vessels typically used in laboratory synthesis. Rather than relying on several degrees of external heat transfer, it allows for direct heating of reaction mixtures to give more uniform heating of solutions (Figure 1.11).[75],[76] This led to the development of microwave-assisted organic synthesis (MAOS). In the early days of MAOS, it was thought that there may be a unique microwave-effect, beyond purely a heating mechanism, because reactions were found to occur faster,[76] and with a decreased occurrence of side reactions,[78]-[80] than the same reactions conducted using a hot plate and oil bath. However, the energy of a standard microwave photon (2.45 GHz) is too low (0.0016 eV) to be able to break most chemical bonds, so microwave irradiation itself should be incapable of inducing

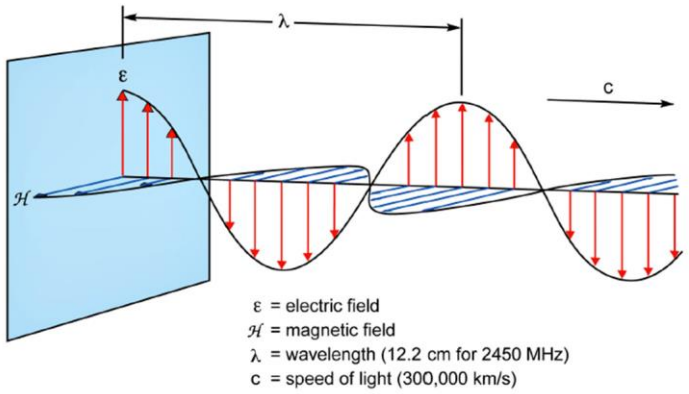

Figure 1.12: Microwave radiation from a standard microwave oven.[77]

chemical reactions.[81]-[83] It is now believed that most of these observed unique microwave effects can be explained by the uniform and rapid heating of reactions through microwave irradiation, which is difficult to achieve in traditional convection-reliant heating methods.[84] Non-thermal effects of microwave irradiation such as an induced orientation of dipolar molecules, which could affect the rates of some reactions, have been suggested but so far have not been proven.[78]-[80]

A drawback of microwave-irradiative heating for organic synthesis is that there is a possible limit for solvents that can be used. The reaction solution must be microwave-absorbing to a sufficient degree or the desired reaction temperatures may not be achieved. Microwave irradiative heating in MAOS works mainly through the processes of dipolar polarization and ionic conduction, which result from the electric component of the microwave radiation. The electric component of microwave radiation induces alignment of molecules' dipoles with its field, but realignment is necessary as the field continuously oscillates. This realignment causes energy loss through molecular friction and dielectric loss in the form of heat. However, heating does not occur for solutions for which the dipole re-alignment is too slow to keep up with the oscillating electric field, or if it is too fast that it follows the orientation of the field exactly.[82],[83] The limit to the microwave heating ability of the solvent can be compensated for by the reagents present in solution, or by use of additional microwave-absorbing additives. Heating due to ionic conduction allows ionic reagents or additives to reaction mixtures to assist in heating if the solvent itself is incapable of heating sufficiently under microwave irradiation.

The degree to which a material is microwave-absorbing is described by the loss tangent (tan δ). tan δ is related to the dielectric loss (ε"), which is the efficiency with which electromagnetic

radiation is converted to heat, and the dielectric constant (ε'), which is the ability of the molecules to be polarized by the electric field, by the equation $\tan\delta = \varepsilon''/\varepsilon'$. Based on their tanδ values, substances are considered to have high (tan δ >0.5), medium (0.5> tan δ>0.1), or low (tan δ<0.1) microwave-absorption abilities.

The tan δ values at 2.45 GHz and 20°C of several common organic solvents are shown in Table 1.1. Many common polar solvents used in organic synthesis have a high enough tan δ value to be used in MAOS without much difficulty in achieving high temperatures, but the presence of polar solutes can also increase the tan δ of the solution. These values are all dependent on the frequency of the irradiation and temperature. The ε" value generally decreases at high temperatures, causing a decrease in tan δ, and making solutions more difficult to heat further the higher the temperature becomes (Figure 1.13)**.**

Table 1.1: tan δ of various solvents at 2.45 GHz and 20°C.[77]

Solvent	**tan δ**	**Solvent**	**tan δ**
ethylene glycol	1.350	chloroform	0.091
ethanol	0.941	acetonitrile	0.062
DMSO	0.825	ethyl acetate	0.059
2-propanol	0.799	acetone	0.054
methanol	0.659	THF	0.047
1-butanol	0.571	dichloromethane	0.042
DMF	0.161	toluene	0.040
water	0.123	hexane	0.020

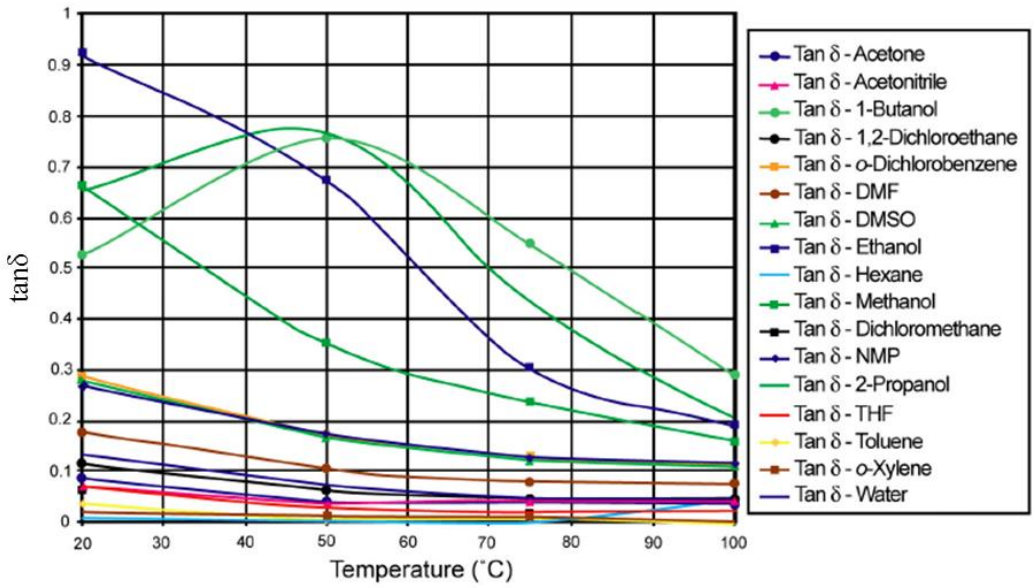

Figure 1.13: tan δ of various solvents at 2.45 GHz and various temperatures.[77]

Microwave irradiation can also be used to heat semiconducting and conducting solid materials in reactions, allowing them to be used as a heating mechanism. In these materials, the magnetic component of the microwave radiation is also responsible for causing the material to heat.[87],[88] Heating occurs by the induced formation of electrical currents within the solid by the mechanisms of conduction loss (Figure 1.14) and eddy current loss (Figure 1.15). In these heating methods, the heat is generated by movement of electrons within the material in opposition to the changing electromagnetic field of the microwaves. Conduction loss occurs due to movement of the electrons induced by the electric component of the microwaves, while eddy current loss is due to circular electron currents created within the material to create a magnetic field to oppose the magnetic field component of the microwave radiation.[88]

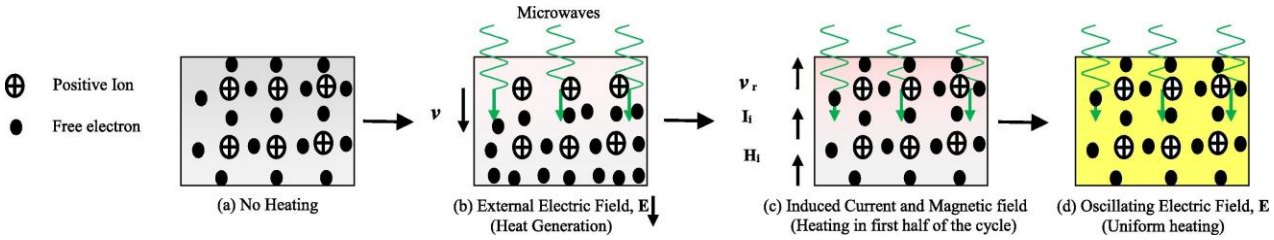

Figure 1.14: Conduction loss heating mechanism of microwave radiation. Reprinted with permission from Reference [88]. Copyright 2016 Elsevier.

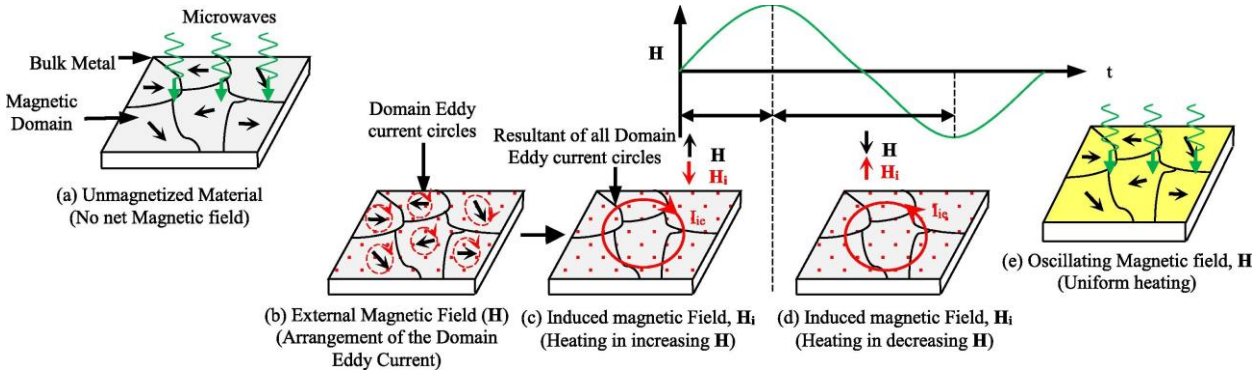

Figure 1.15: Eddy current loss heating mechanism of microwave radiation. Reprinted with permission from Reference [88]. Copyright 2016 Elsevier.

Microwave irradiative heating is becoming commonplace in research laboratories and is beginning to make its way into industry. There are, however, challenges for large reaction vessels, as the microwave irradiation can only penetrate a small distance before convection currents become the dominant method of heating within the reaction.[85]

1.5: Microwave-Assisted Continuous-Flow Organic Synthesis

Microwave-assisted continuous-flow organic synthesis (MACOS) was developed to combine the benefits of both MAOS and microfluidic techniques to allow for efficient heating and scale-up of reactions in organic synthesis.[10]-[20] The small diameters of flow reactors are ideal for use with microwave irradiation to provide uniform heating of reactions.

The original reactor for MACOS used by the Organ group (Figure 1.16) consisted of a glass capillary suspended within the microwave cavity of a Biotage Smith Creator Synthesizer, through which reagents are flowed using syringe pumps.[10] Capillaries of diameters ranging from 200-1150 μm could be inserted into the microwave reactor, and multiple reagent streams for multi-component reactions can be implemented through the use of multiple syringe pumps and a mixing chamber.[10] Residence time is therefore determined by the combination of the capillary size and flow rate used. The use of multiple capillaries within a single microwave cavity simultaneously (Figure 16B) allows for scale-up by numbering up with a single microwave.[10]b Heating is achieved through dielectric heating of the reaction mixture, and adjusted through variation of the microwave power applied. In this reactor, the maximum temperature achievable is the boiling point of the solvent used, as the formation of bubbles can push solution out of the reactor, but will also depend on the tan δ of the reaction solution.

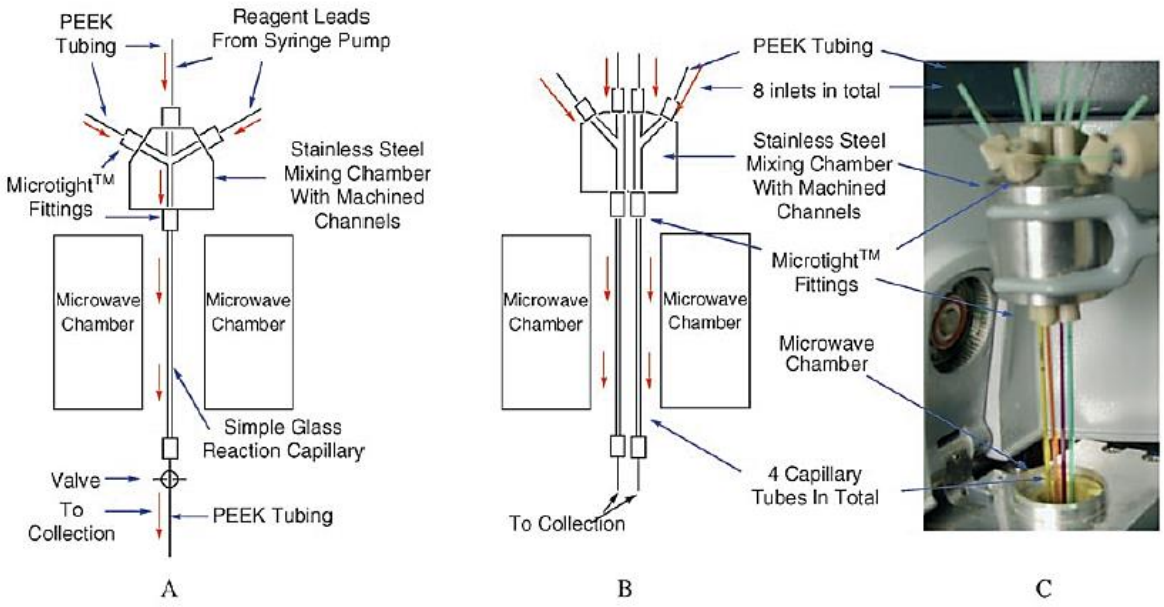

Figure 1.16: Schematic of the original reactor design used for MACOS. A) single-capillary system.; B) parallel multi-reactor system.; C) photograph of the parallel multi-reactor system. Reprinted with permission from Reference [10]b. Copyright 2005 John Wiley and Sons.

Performing reactions in MACOS allows for efficient and fast library development using a variety of reactions, which is useful for the discovery and development of drug candidates.[10],[12] Libraries have been created by use of a sequential-flow approach, in which a constant stream of the general reagents was used, accompanied by sequential plugs of varying additional substrates to prepare a variety of compounds.[10]b

The early MACOS reactor effective for a variety of reactions, such as Suzuki-Miyaura[10],[14] and Heck[10]b,[14] cross-couplings, nucleophilic aromatic substitution,[10]b ring-closing metathesis,[10]a Wittig reactions,[10]a Claisen rearrangements,[17] Diels-Alder cycloadditions,[14]c hydrosilylation reactions,[15]c and gold-catalyzed benzannulation.[15]a

In many cases where homogeneous metal catalysts were used, a film of metal was found coated on the walls of the capillary at the end of the reaction, accompanied by higher than usual conversions (Table 1.2).[10]a The metallic films were tested as a heterogeneous catalyst and found not only to be catalytically-active, but also made it easier to heat reactions to higher temperatures. With this discovery, reactor capillaries coated with metallic films were investigated as both a heterogeneous catalyst, and as a method of heating in MACOS.[10],[14]-[16] Metal films were coated on the inside walls of capillaries to act as both a catalyst and heating mechanism, or on the outside of capillaries to act purely as a heating mechanism.

Table 1.2: Suzuki-Miyaura cross-coupling reactions performed in MACOS with various palladium catalysts.[10]a

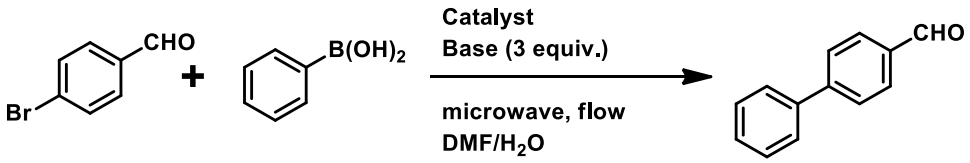

Conditions	Power (W)	Flow rate (Residence Time)	Conversion (%)[a]
$Pd(OAc)_2$ (5 mol%) K_2CO_3	170	30 μL/min (4m 13s)	38%
$Pd(OAc)_2$ (5 mol%) KOH (Pd coating present on capillary after reaction)	170	30 μL/min (4m 13s)	100 (reduced starting material present)
Pd-Coated Capillary from pre KOH	150	20 μL/min (5m 30s)	89 (reduced starting material present)
$Pd(PPh_3)_4$ (5 mol%) KOH	170	30 μL/min (4m 13s)	100

[a]Determined by ^{1}H-NMR spectroscopy relative to residual aryl halide

Glass capillaries with porous metallic palladium films coated on their inside walls were prepared as reactor capillaries for palladium-catalyzed reactions in MACOS (Figure 1.17).[14] These palladium-coated capillaries were found to be effective as a recyclable heterogeneous catalyst for Suzuki-Miyaura (Table 1.3) and Heck (Table 1.4) cross-coupling reactions, as well as Diels-Alder cycloadditions in MACOS.[14] The increased heating provided by the metal films under microwave irradiation was also essential for some reactions to be completed using MACOS within a reasonable timeframe.[14]b

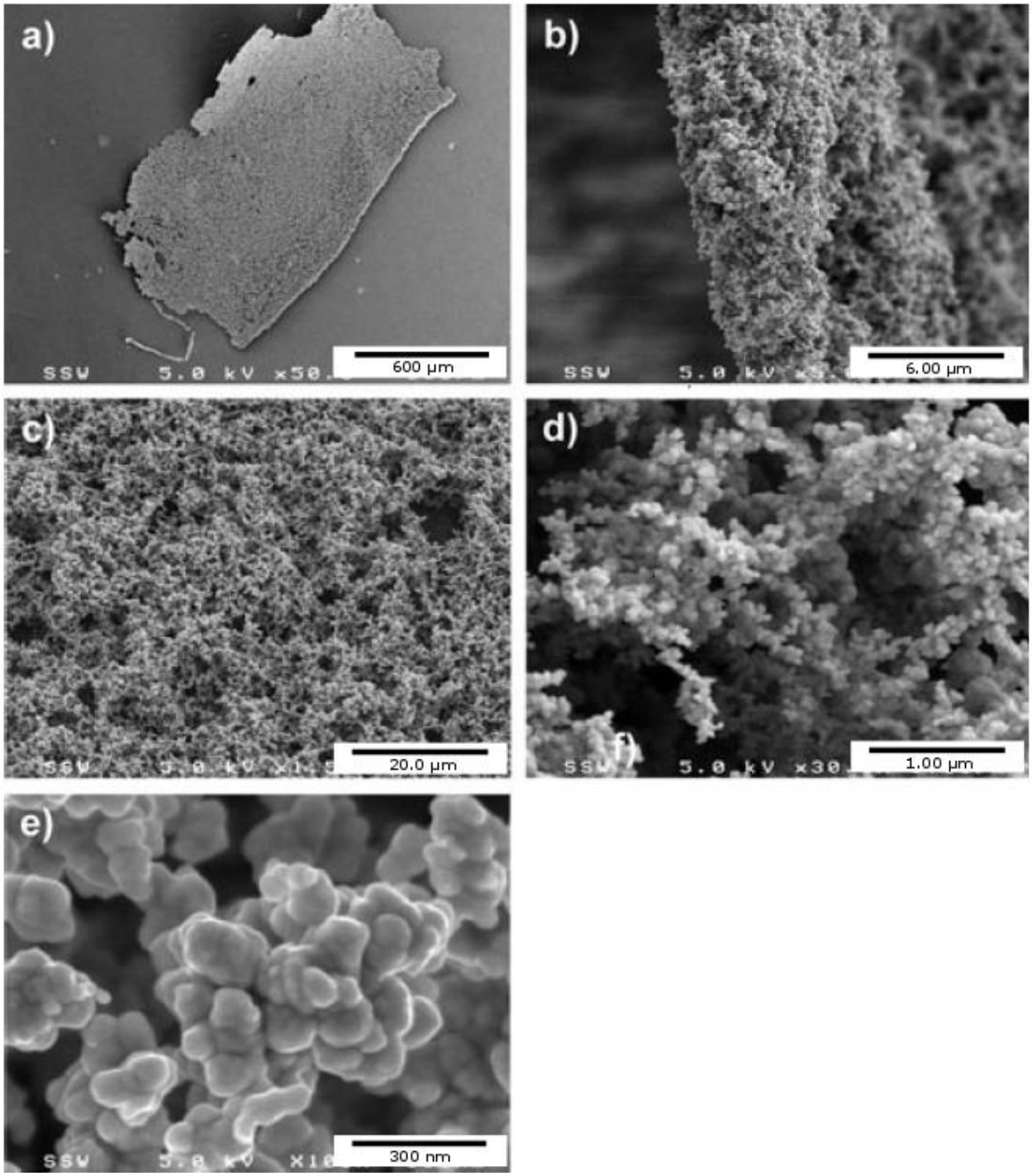

Figure 1.17: SEM image of the porous metallic palladium films prepared inside a glass capillary and removed at a) ×50.0 magnification. b) × 5000, c) ×1500, d) ×30000, and e) ×100000. Adapted with permission from Reference [14]a. Copyright 2006 John Wiley and Sons.

Table 1.3: Suzuki-Miyaura cross coupling reactions in MACOS using metallic palladium film-coated reactor capillaries.[14]a

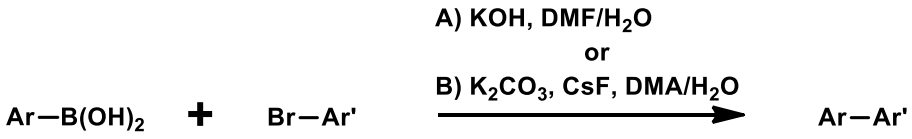

Ar-B(OH)$_2$	Br-Ar'	Conditions	Temperature (°C)	Conversion (%)[a]
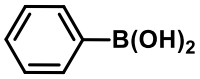	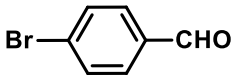	A	205	88
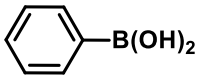	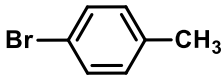	A	205	95
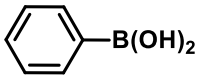	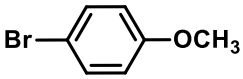	A	205	97
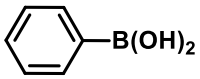	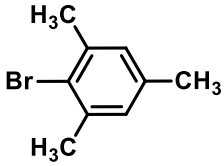	A	200	92
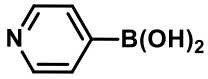	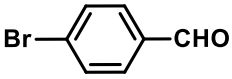	B	215	93
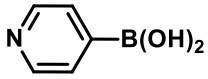	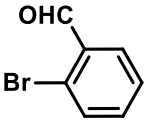	B	220	59
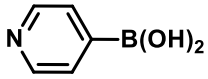	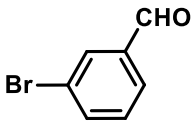	B	210	73
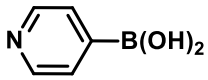	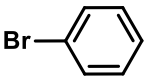	B	215	81
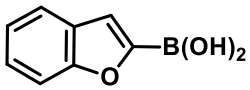	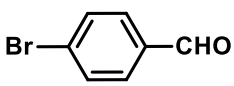	B	225	84

[a] Determined by ^{1}H-NMR spectroscopy relative to residual aryl halide

Table 1.4: Heck cross coupling reactions in MACOS using metallic palladium film-coated reactor capillaries.[14]a

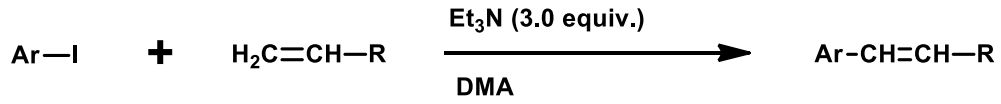

Ar-I	R	Temperature (°C)	Conversion (%)[a]
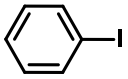	CO_2CH_3	205	80
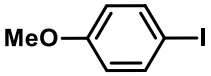	CO_2CH_3	200	58
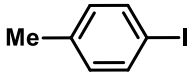	CO_2CH_3	205	89
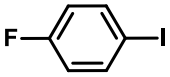	CO_2CH_3	200	89
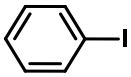	$CO_2C(CH_3)$	215	99
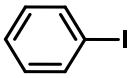	CN	220	99

[a] Determined by ^{1}H-NMR spectroscopy relative to residual aryl halide.

Unfortunately, the use of metallic films as a heating mechanism under microwave irradiation was problematic due to incredibly high and inhomogeneous temperatures being achieved, even at low microwave power settings.[16] Temperatures reached over 900°C, with uneven heating over the film (Figure 1.18).[16] The high temperatures obtained when using metal film-coated capillaries were difficult to control, even under low microwave power, and were high enough to cause damage to both the metal film itself and even the glass capillaries (Figure 1.19).[16]

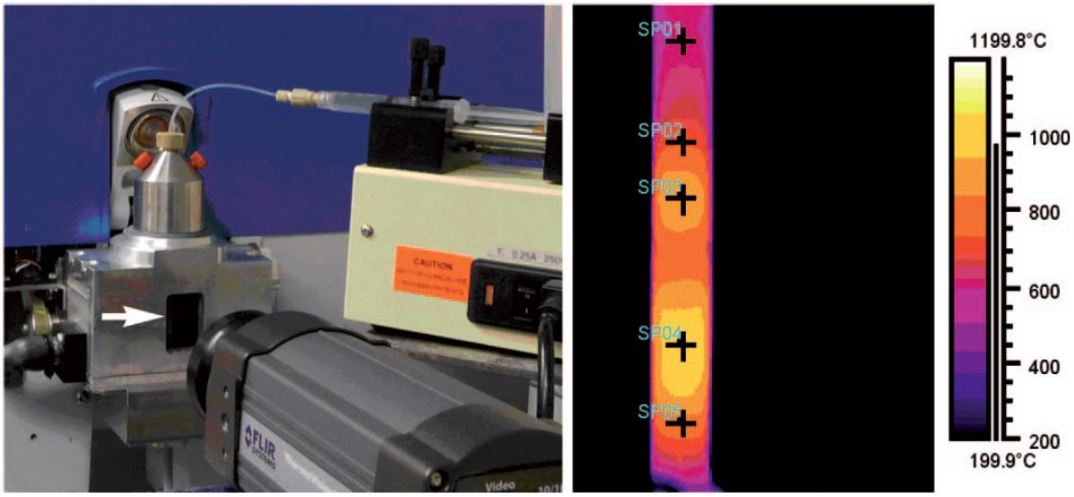

Figure 1.18: MACOS setup using a modified Biotage Initiator Synthesizer with a hole machined into the end of the waveguide to allow for temperature measurements to be made using a FLIR Systems Thermovision™ A320 camera and the temperature profile of a Cu-coated flow capillary under microwave irradiation. Reprinted with permission from Reference [16]. Copyright 2009 John Wiley and Sons.

Figure 1.19: Metal-coated glass capillaries damaged due to extreme heating under microwave irradiation.[89]

Due to the problems associated with the use of a metal film for microwave-irradiative heating, flow capillaries made from the semiconducting material silicon carbide were also utilized as a method of heating reactions in MACOS. In this method, the silicon carbide capillary itself would heat up upon absorption of microwave irradiation and transfer it to the solution. When using a silicon carbide reactor capillary, the heating under microwave irradiation is

independent of both the solution flowing through the capillary, and the flow rate used (Figure 1.20).[17] Therefore, the heating is purely due to absorption of microwave irradiation by the silicon carbide capillary.

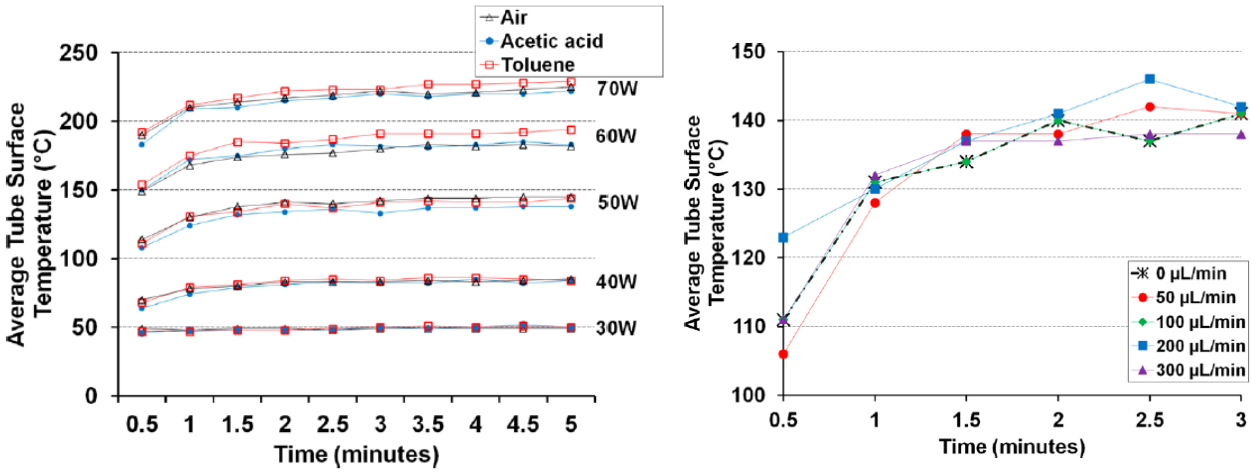

Figure 1.20: Temperature of silicon carbide reactor capillaries when heated with microwave irradiation. Adapted with permission from Reference [17]. Copyright 2014 American Chemical Society.

The use of backpressure in MACOS allows for reaction temperatures above the boiling point of the solvents at atmospheric pressure while still maintaining a liquid-phase reaction.[14]c Without backpressure, it was observed that gas pockets would occasionally form within the flow system during reactions, which reduces residence time by pushing material out of the reactor.[16]

Due to the importance of backpressure for achieving high temperatures and reaction rates in MACOS, a second-generation MACOS system was developed.[17] The addition of a pressure ballast system, referred to as the pressure creating device (PCD), into the MACOS reactor system allowed for backpressures up to 1100 psi to be used in flow reactions (Figure 1.21). The PCD in MACOS uses pressure exerted by gas, rather than a physical device, so it does not have

carryover and cross-contamination problems that can occur with conventional backpressure-creating devices.[17] Since the PCD uses gas to apply backpressure onto the system, it also allows for reactions to be carried out under an inert atmosphere in flow.

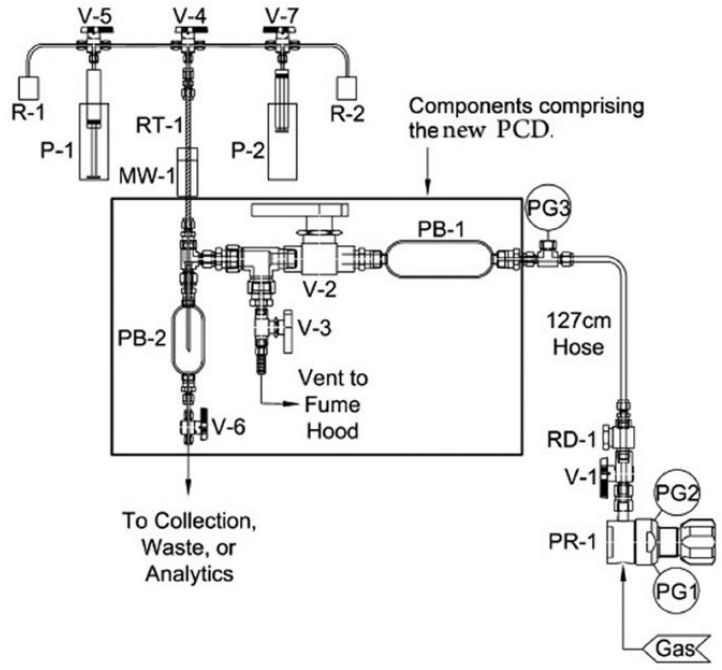

Figure 1.21: Schematic of the MACOS system with addition of a PCD to introduce backpressure into the reactor. P-1 and P-2: syringe pumps, R-1 and R-2: reagent reservoirs, V-1 to V-6: valves, RT-1: reactor tube, MW-1: Microwave, PG1 to PG3: pressure gauges, PB-1 and PB-2: pressure ballasts. Reprinted with permission from Reference [17]. Copyright 2014 American Chemical Society.

Somerville et al.[18] more recently described further improvements upon the MACOS reactor design. Functionality for automation and in-line analytics were added, as well as improvements upon the microwave reactor and infusion system. This second-generation MACOS system (Figure 1.22) uses pairs of syringe pumps (P1 and P2) accompanied by a 4-port, 2-position valve (V1), referred to collectively as a continuous flow unit (CFU) to continuously flow reagent

solutions into the MACOS system. As one syringe pump is infusing reagents into the reactor, the other is refilling from the reagent reservoir. Multiple CFUs can be used for a single reaction, allowing for multiple reagents solutions to be infused simultaneously, or in a sequence.

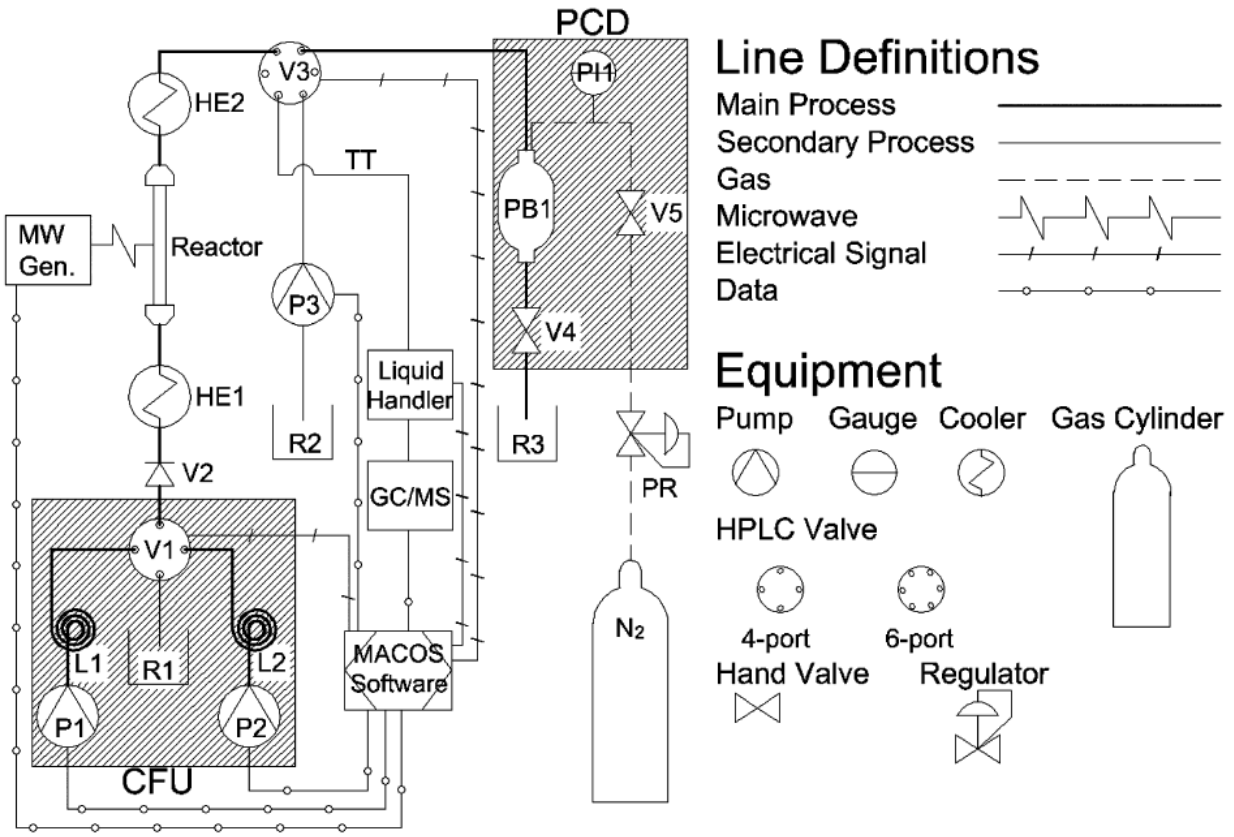

Figure 1.22: Schematic of the second-generation MACOS system with automation and in-line analytical capabilities. P1 and P2: syringe pumps, P3: carrier solvent pump, L: holding loop, R1: reactant reservoir, R2: carrier solvent reservoir, R3: product collection reservoir, V: valve, V3: sampling valve, HE: heat exchanger, PB: pressure ballast, PI: pressure indicator, PR: pressure regulator, TT: transfer tube. Reprinted with permission from Reference [18]. Copyright 2014 American Chemical Society.

A new microwave generator, the Arrhenius One, was also employed to give a longer microwave-irradiation zone than when using the modified Biotage Initiator in the original

MACOS reactor. This allows for longer residence times without the need to slow flow rates, while still using a single straight tube reactor.

The addition of a sampling method for analysis of reactions while they are in progress allows for reaction conditions to be quickly evaluated and adjusted to aid in optimization of reactions, as well as perform quality control analysis periodically throughout a reaction.[18] The eventual goal is to allow for automated analysis and optimization of reactions using the MACOS reactor.

1.6: Plan of Study

There were several problems associated with the use of bulk metal films as catalysts in MACOS. The bulk metal films could break and flake off of the reactor capillaries during reaction due to their intense and inhomogeneous heating under microwave irradiation. This would lead to a reduction in the amount of catalyst present within the reactor and contamination of product mixtures with significant amounts of metal. Intense local heating also limited control over the reaction temperatures. Thus, a new method of introducing heterogeneous catalysts into the reactor capillaries was needed. Ideally, this catalyst would have a high surface area to allow for contact with the reagents, not heat significantly under microwave irradiation, and be sufficiently thermally, mechanically, and chemically-stable to be used in a flow reactor for extended periods of time without decomposition.

With these requirements, silica sol-gel materials were considered as an ideal candidate for a catalyst support in MACOS. A packed-bed reactor should allow for a high catalytic surface area and limit laminar flow of reagents, which may limit the contact of reagents with catalytic surfaces. The versatility of preparing silica sol-gel materials with a wide variety of properties, such as functionality, sizes, and levels of porosity, allows for customization of the catalyst

support. In addition, the low microwave heating ability of silica should prevent them from heating significantly under microwave irradiation. The high chemical and thermal resistance of silica should also prevent degradation of the support, allowing them to be used for continuous flow reactions over long periods of time.

Figure 1.23: Schematic of a reactor capillary for MACOS filled with a bed of metal-loaded silica macrospheres.

Macrospheres were considered as a good candidate for the structure of the silica supports, as they could be prepared with a controlled monodisperse size. The macrospheres should be small enough to fit within the reactor capillaries and allow for high catalyst surface area, but be large enough to not simply fill the capillary and cause clogging issues (Figure 1.23). Several types of transition metal-containing silica sol-gel supported catalysts with different functionalities were prepared, and the palladium-loaded catalysts were tested for their catalytic ability in Suzuki-Miyaura and Heck cross-coupling reactions in MACOS.

Chapter 2: Silica Sol-Gel Supports Impregnated *in situ* with Metal Nanoparticles

2.1: Introduction

Silica sol-gel materials were chosen as potential candidates for catalyst supports in MACOS due to their transparency to microwave radiation and control over the morphology of the resulting material. A packed bed of silica-supported catalysts was also desirable for use in flow to act as a mixer to prevent the occurrence of laminar flow. Porous materials with high surface areas are also beneficial, as they allow for higher catalytic surface contact areas.

Porous silica structures formed from a sol-gel procedure were first examined as potential candidates for heterogeneous catalyst supports in MACOS. A packed bed of porous supports may provide high catalyst surface area, while also reducing the occurrence of laminar flow.

The monodisperse, controlled-size silica macrospheres prepared through a sol-gel method by Huo et al.[52] are a good candidate for a catalyst support in flow. The size of the macrospheres prepared could be chosen to fit within the capillaries without need of further modification. In the case of large, non-porous, spherical beads, the reaction solution would flow around the beads in the reactor capillary. The size of the macrospheres relative to the reactor capillary diameter is therefore very important for several factors. Smaller beads would have a higher overall surface-area, but could be resistant to mass-transfer through the reactor capillary and cause blockages. Small beads may also take up a large proportion (up to 74%) of the reactor capillary volume, greatly reducing reaction residence time or throughput. The diameters of the quartz and silicon carbide reactor capillaries used in the MACOS system are 2000 and 1750 μm respectively, so macrospheres with diameters of 500-1000 μm were considered for forming the packed-bed catalyst support.

2.2: Experimental

2.2.1: Materials and Methods

Tetraethyl orthosilicate (TEOS), tetrabutyl orthosilicate (TBOS), polyethylene oxide (PEO) (avg. M_n 100000), bromobenzene, 4-bromotoluene, 3-bromoanisole, 4-bromoanisole, 4-bromoacetophenone, 4-bromobenzonitrile, iodobenzene, 4-iodotoluene, 4-iodoanisole phenylboronic acid, *tert*-butyl acrylate, methyl acrylate, triethylamine, ethanol (95%), N,N-dimethylformamide (DMF), tetrahydrofuran (THF) and dichloromethane (DCM) were purchased from Sigma Aldrich. Palladium(II) acetate trimer (Pd 45.9-48.4%) was obtained from Alfa Aesar. Cetyltrimethylammonium bromide (CTAB) was purchased from British Drug Houses.

Samples were prepared for SEM imaging by mounting on an aluminum stub using carbon tape. SEM images and EDX spectra were recorded on a FEI XL30 ESEM equipped with an EDAX energy dispersive spectrometer. TEM samples were prepared by grinding macrospheres, suspending the resulting powder in ethanol, then placing onto a copper grid. TEM imaging was performed on a Philips EM201 electron microscope. NMR spectroscopy was performed using a Bruker ARX 400 MHz spectrometer. PXRD spectra were recorded on a Siemens D5000 Diffractometer System operating at 50 kV/35 mA. Thermal imaging was performed using an FLIR Systems ThermoVision A320 infrared camera fitted with a 24° fixed FOV lens and an AP1 1200°C filter. Elemental analysis was performed at Galbraith Laboratories, Inc. in Knoxville TN.

2.2.2: Preparation of Porous Silica Sol-Gel Supports

In a 20-mL scintillation vial, the desired proportion of PEO (average molecular weight 100000) was added to 17.5 mL 1.0M nitric acid with stirring. Silver nitrate or palladium(II)

acetate may also be added at this point to impregnate the resulting sol-gel with metal. With continued stirring, 14.0 mL TEOS was added. Two phases formed and were stirred until the solution became homogeneous. The solution was capped and placed in an oven and heated at 50°C for 6 days. The cap was then removed and the solution dried over a week at 50°C. The dried white monolith was then placed into a muffle furnace and heated to 600°C over 3 hours, then kept at 600°C for 2 hours. A white monolith was then obtained after cooling.

2.2.3: Preparation of Silica Macrospheres

To a 250-mL round-bottom flask, 0.60 g CTAB, and 35 mL distilled water are added. Metal-impregnated macrospheres are prepared by the addition of 0.28 mmol palladium(II) acetate, copper(II) acetate, or nickel(II) acetate. The contents were stirred at 500 rpm with a 3/4" "+"-shaped stir bar for 10 minutes, until a cloudy solution the colour of the metal salt added formed. Once the solution became homogeneous, 3.5 mL of a 2M aqueous solution of sodium hydroxide was added, causing the solution to become clear. This solution was kept stirring at 500 rpm for 10 minutes, then 5.0 mL of TBOS was added slowly. The solution was stirred at 500 rpm overnight. Silica spheres with a diameter of approximately 2 mm were then filtered from clear solution and dried in air for 24 hours, during which time they shrank to a diameter of approximately 1 mm. After drying, the spheres were calcined in a muffle furnace overnight at 500°C.

For reduction of the metal species, the metal-impregnated macrospheres were placed in a tube furnace with flowing hydrogen gas and heated to 350°C. The macrospheres were then kept under a static pressure of flowing hydrogen gas at 350°C for 3 hours, after which they were cooled to room temperature.

2.2.4: Batch Suzuki-Miyaura Cross-Coupling Reactions Using *is*PdSMSs

Aryl halide (0.60 mmol) and phenylboronic acid (7.2 mmol) were dissolved in 5.0 mL of ethanol/water solution in a 5-mL microwave vial. Potassium carbonate (1.80 mmol) were then added to the solution. 0.030 g *is*PdSMSs (containing 0.012 mmol palladium) was then added to the vial. The vial was sealed and heated under microwave irradiation at 150°C.

The crude reaction mixture was concentrated to remove ethanol, and the products were extracted from the aqueous solution using DCM, dried over anhydrous magnesium sulfate, and concentrated using a rotary evaporator. Purification of the product was performed using column chromatography.

2.2.5: Batch Heck Cross-Coupling Reactions Using *is*PdSMSs

Aryl iodide (0.40 mmol), methyl or *tert*-butyl acrylate (0.60 mmol), triethylamine (0.084 mL, 0.60 mmol) and 2.0 mL DMF were added to a 5-mL microwave vial. *is*PdSMSs (0.020 g) and a stir bar were added to the vial, and the vial then sealed. The vial was heated at 130ºC in the batch microwave for the desired amount of time. The resulting pale amber solution with black solid pieces of the macrospheres was extracted with DCM, adding water to cause separation from the DMF phase. The solution was extracted several times with water to remove DMF from the DCM phase, and the DCM phase was concentrated. The resulting material was then re-dissolved in diethyl ether, extracted again several times with distilled water to remove DMF, and then concentrated to obtain the desired product. Filtering through a plug of silica was sometimes necessary to remove residual DMF.

2.2.6: Batch Huisgen Dipolar Cycloaddition Using *is*CuSMSs

Benzyl azide (0.50 mmol), phenylacetylene (0.75 mmol) and THF were added to a 5-mL microwave vial. *is*CuSMSs (0.0098 g) and a stir bar were added to the vial and the vial sealed. The vial was heated at 100ºC in the batch microwave for 1 hour. The solution was filtered through Celite and concentrated *en vacuo*.

2.3: Results and Discussion

2.3.1: *in situ* Metal-Impregnated Porous Silica Sol-Gel Supports

Porosity could be incorporated into a silica sol-gel by the addition of a polymer into the sol-gel precursor mixture, followed by pyrolysis to remove the polymer after formation. Certain metal salts could also be added *in situ* to the sol-gel precursor solution to incorporate desired metals into the sol-gel structure in a one-pot synthesis. Silica sol-gels containing palladium(II) acetate, palladium(II) chloride, silver nitrate, copper(II) acetate, and nickel(II) acetate were prepared in this manner.

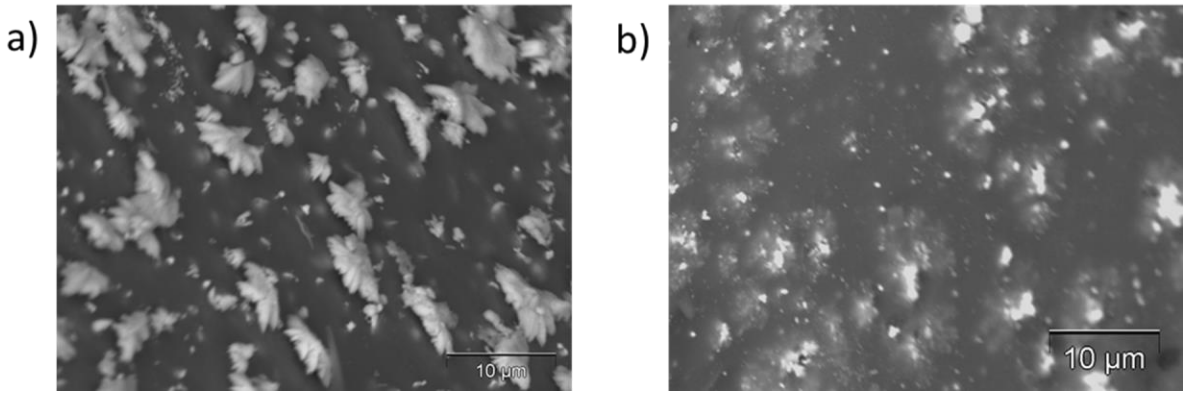

Figure 2.1: SEM images using a backscatter detector of silica sol-gel with a) silver nitrate added to sol-gel precursor mixture. b) palladium(II) acetate added to sol-gel precursor. Lighter areas represent higher atomic number elements.

Scanning electron microscope (SEM) images using a backscatter detector of the metal salt-loaded silica sol-gels show metal particles present on the surface of the silica as bright areas (Figure 2.1). Energy-dispersive X-ray spectroscopy (EDX) also confirmed the presence of metals on the surface of the silica after preparation, showing that the metal salts were indeed incorporated into the sol-gel structure from this one-pot synthesis.

Porous metal-loaded silica sol-gels were prepared by adding a combination of PEO and the desired metal salt to the sol-gel precursor solution containing TEOS. Increasing the relative mass of PEO formed smaller, more uniform pores. This is due to gelation of the sol-gel occurring before phase separation proceeds, leading to smaller PEO/silica and solvent phase domains.[90] The addition of a metal salt also decreased the pore sizes. Low metal loadings (~1%) decreased the pore diameters relative to only adding PEO, but higher metal loadings (5%) completely prevented any large scale porosity from forming.

Table 2.1: Silica sol-gels prepared with PEO and in situ addition of metal salts.

Entry	PEO/SiO_2 (w/w)[a]	$Ag(NO_3)/SiO_2$ (%)[a]	$Pd(OAc)_2/SiO_2$ (%)[a]	Pore Diameter (μm)[b]
1	-	8.3	-	0
2	-	-	5.0	0
3	0.26	-	-	>50
4	0.37	-	-	5±1
5	0.47	-	-	0.9±0.3
6	0.26	5.0	-	0
7	0.26	1.0	-	11±2
8	0.37	1.0	-	3.8±0.8
9	0.26	-	1.0	1.0±0.2

[a] Relative to theoretical amount that could be formed based on added TEOS. [b] Measured from SEM images.

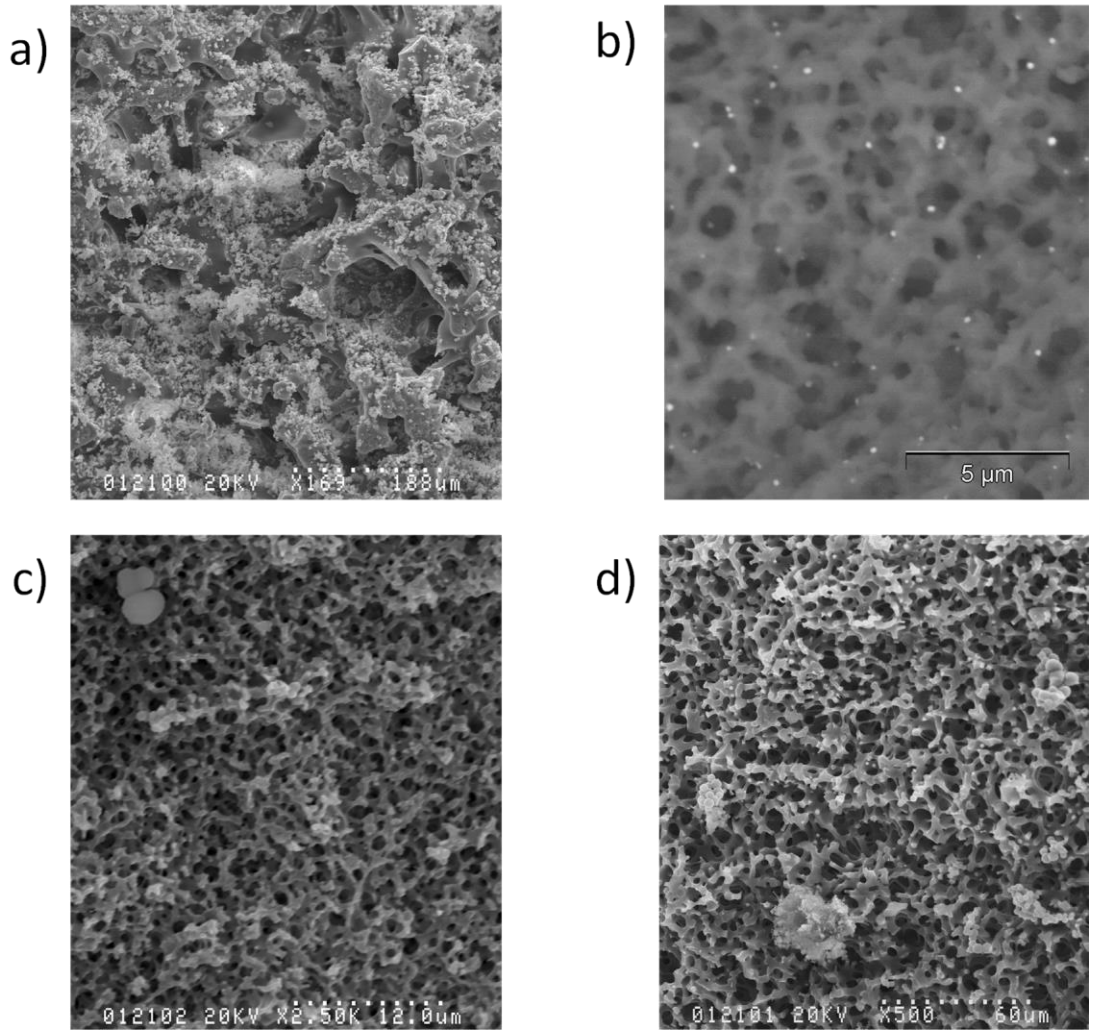

Figure 2.2: SEM images of porous silica sol-gels prepared with a) 0.26 PEO/SiO_2 (Table 2.1, Entry 3); b) 0.26 PEO/SiO_2 and 1% $Pd(OAc)_2/SiO_2$ (Table 2.1, Entry 9) taken using backscattermode. Lighter areas represent highter atomic number elements; c) 0.37 PEO/SiO_2 (Table 2.1, Entry 4); and d) 0.47 PEO/SiO_2 (Table 2.1, Entry 5).

While the metal-loaded porous silica supports may give high catalytic surface-area and loading, they cannot be used as formed. The bulk sol-gel must be broken into smaller pieces to fit into the reactor capillaries for use in flow. This also leads to a non-uniformity in the size of the broken pieces, with some unusable in flow. Larger pieces would not fit within the reactor

capillaries, and smaller pieces have the possibility of clogging the flow system. It was a time-consuming and irreproducible process to break up the supports and sort them into pieces appropriate for use in MACOS. Due to these issues, a method of forming supports with controlled size, which could be tailored to use in the reactor capillaries of the MACOS system, was desired.

2.3.2: *in situ* Metal Nanoparticle-Impregnated Silica Macrospheres

The use of tetrabutyl orthosilicate (TBOS) as the silica source, rather than TEOS or tetramethyl orthosilicate (TMOS), was necessary to ensure the phase separation of water and the alkoxysilane required for the formation of macrospheres. The longer, more hydrophobic, alkyl chains are necessary to allow for the formation of large macrospheres rather than fine powders or irregular pieces.[52],[53] Serrano et al.[53] studied the mechanism of formation of the silica macrospheres (Figure 2.3), and found that the macrospheres are formed by the aggregation and fusion of smaller spherical droplets in the emulsion. The macrospheres are very soft after initial formation, and lose their spherical morphology if the stirring is stopped, leading to irregularly shaped pieces. Since TBOS undergoes hydrolysis and condensation more slowly than alkoxysilanes with shorter alkyl chains, a longer timeframe is probably necessary for sufficient crosslinkages to form from the hydrolysis and condensation of the TBOS to stabilize the structure. The macrospheres stabilized after a synthesis time of about 10 hours, at which point stirring could be stopped with the macrosphere structure being retained.

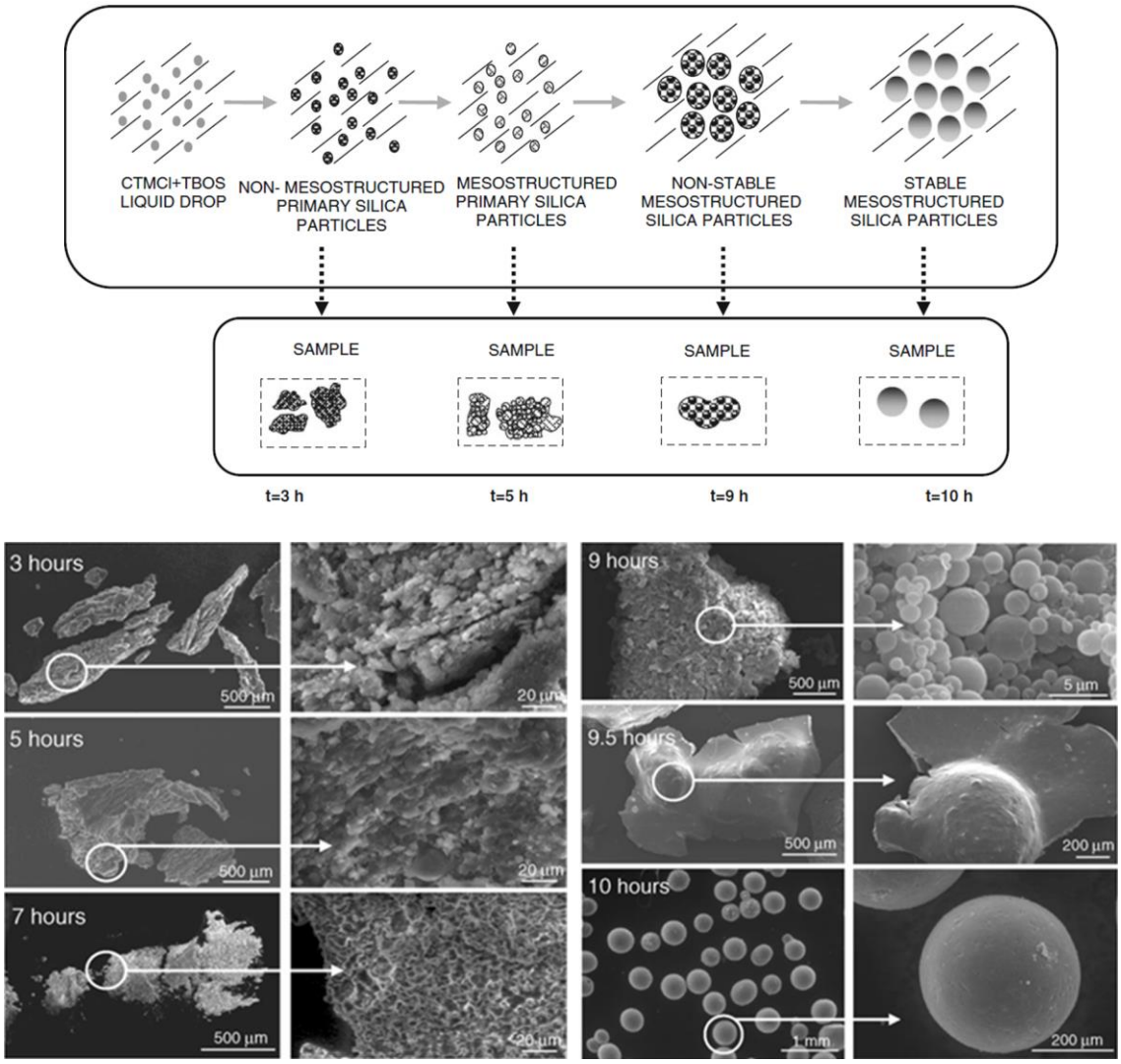

Figure 2.3: Process of formation of silica macrospheres from an emulsion of TBOS in water (top). SEM images of the contents of the emulsion at different synthesis times (bottom). Adapted with permission from Reference [53]. Copyright 2009 Springer Nature.

Palladium films, similar to those coated on the walls of the MACOS reactor capillaries, were also coated on silica macrospheres to load them with metal (Figure 2.4). Unfortunately, the coatings were non-uniform, broke off of the sphere surface, and heated to the point of glowing under microwave irradiation. Since these palladium film-coated macrospheres exhibited many of the same problems the metal-coated reactor capillaries had, a more dispersed metal nanoparticle

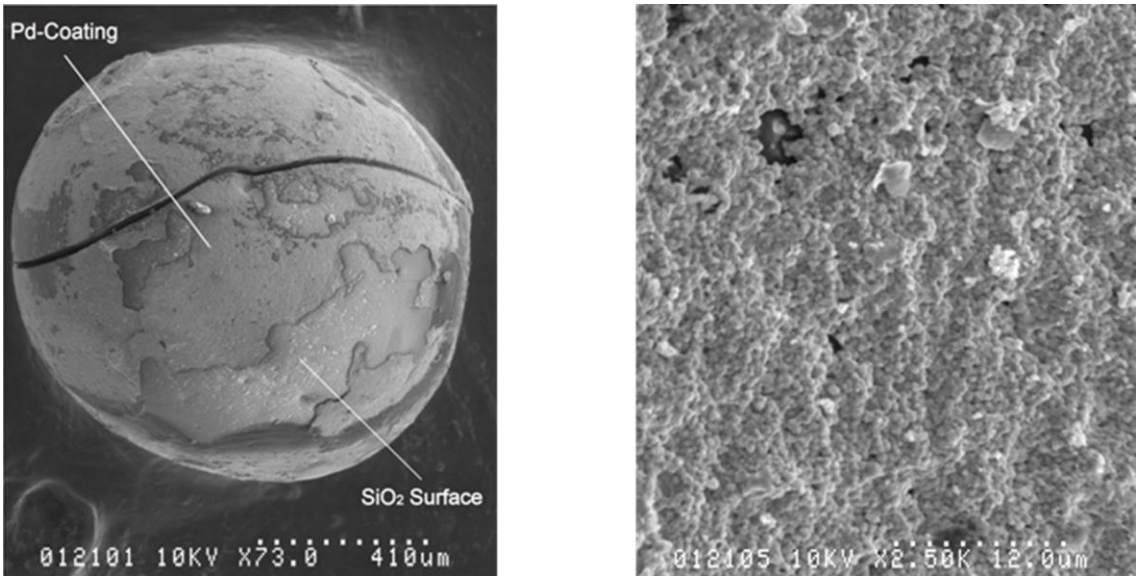

Figure 2.4: SEM images of silica macrosphere coated with a palladium film (left) and morphology of the film (right).

catalyst was desired. Therefore, metal salts added *in situ* to the sol-gel precursor emulsion seemed to be a better option for catalyst loading.

The silica macrospheres could also be loaded with metals by the addition of a metal salt to the sol-gel precursor emulsion, similarly to the *in situ* loading of the porous silica. Ideally, a metal salt with higher solubility in the sol-gel precursor phase than the aqueous phase would be selected to efficiently load the desired metal into the macrospheres. However, when used in the formation of *in situ* metal-impregnated silica macrospheres, high metal loadings prevented macrosphere formation. Loadings of up to 2.0 mol% palladium(II) acetate relative to TBOS in the sol-gel precursor emulsion still allowed for formation of large spherical structures. Addition of the metal salt after macrosphere formation, but before hardening, caused the spherical structures to destabilize, giving amorphous pieces without the metal being incorporated into the sol-gel. Since the mixing is very important for obtaining large spherical structures, and the

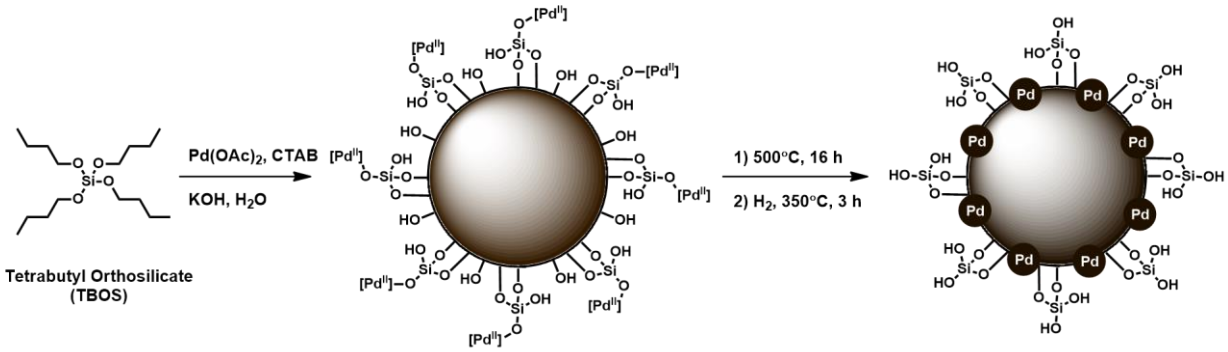

Scheme 2.1: Formation of *is*PdSMSs prepared from TBOS using a sol-gel emulsion.

macrospheres are not fully stable after initial formation, disruptions to the mixing before hardening can cause loss of spherical morphology. The preparation of the in situ palladium-loaded silica macrospheres (*is*PdSMSs) is shown in Scheme 2.1. Calcination of the *is*PdSMSs was performed at 500°C for 16 hours to remove remaining organic surfactants from the macrospheres, further harden the structures, and promote the formation of palladium nanoparticles from the palladium(II) acetate dispersed through the macrosphere structure.

The *is*PdSMSs were able to be prepared as monodisperse macrospheres with controllable diameters from 760-1310 μm by changing the stirring rate of the emulsion (Table 2.2). SEM images using a backscatter detector show bright spots dispersed over the surface of the

Table 2.2: Diameters of *is*PdSMSs prepared from TBOS using a sol-gel emulsion.

Stirring Rate (rpm)	Macrosphere Diameter (μm)[a]
450	No sphere formation
500	1310±80
550	1070±100
600	1010±100
650	940±120
700	840±100
750	760±90

[a] Measured from SEM images.

*is*PdSMSs (Figure 2.5d), suggesting that metal particles may be present on the surface of the macrospheres. EDX also confirmed the presence of palladium on the surface and in the interior of the macrospheres, with approximately equal ratios of palladium to silicon (Figure 2.6). Residual amounts of carbon, sodium, and bromide were also present from the synthesis.

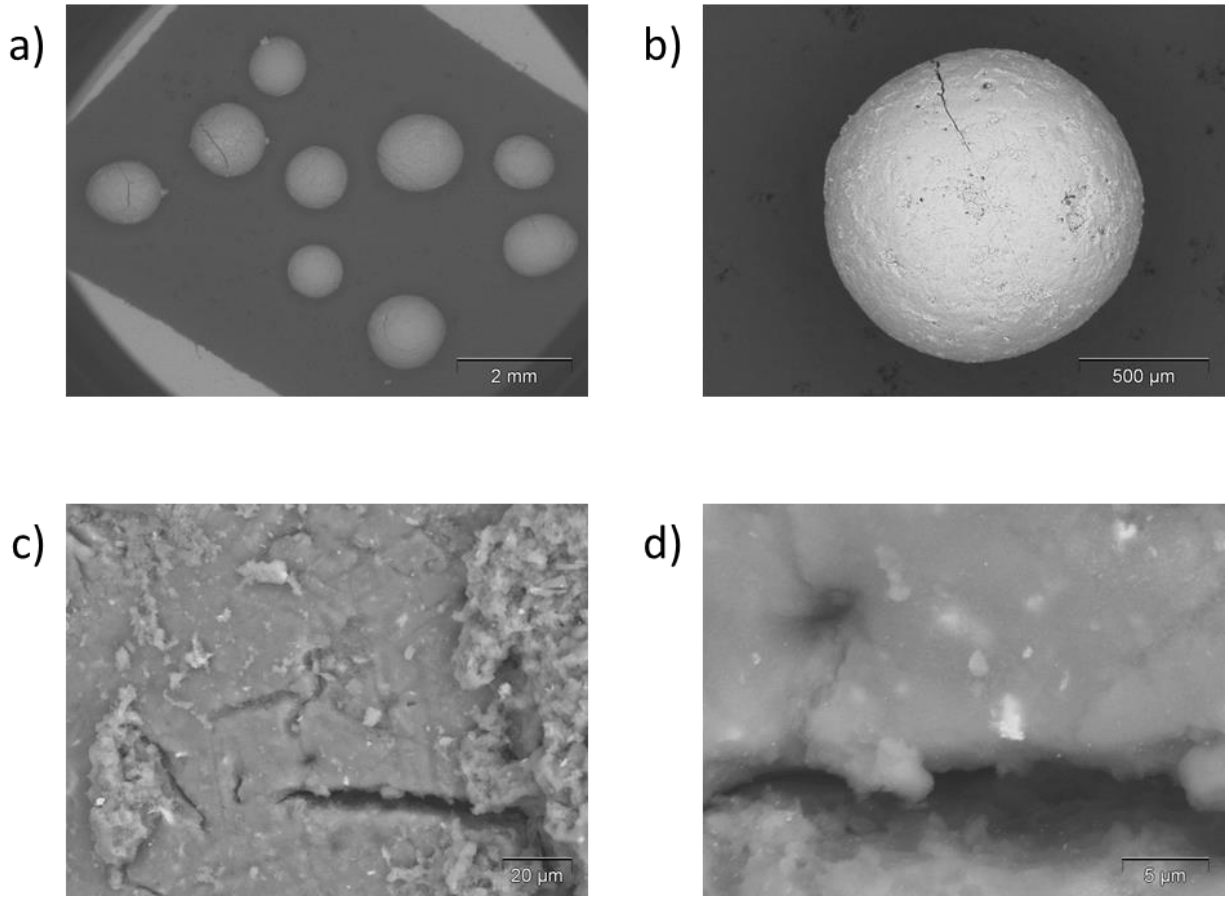

Figure 2.5: SEM images of the surface of *is*PdSMSs using a backscatter detector.

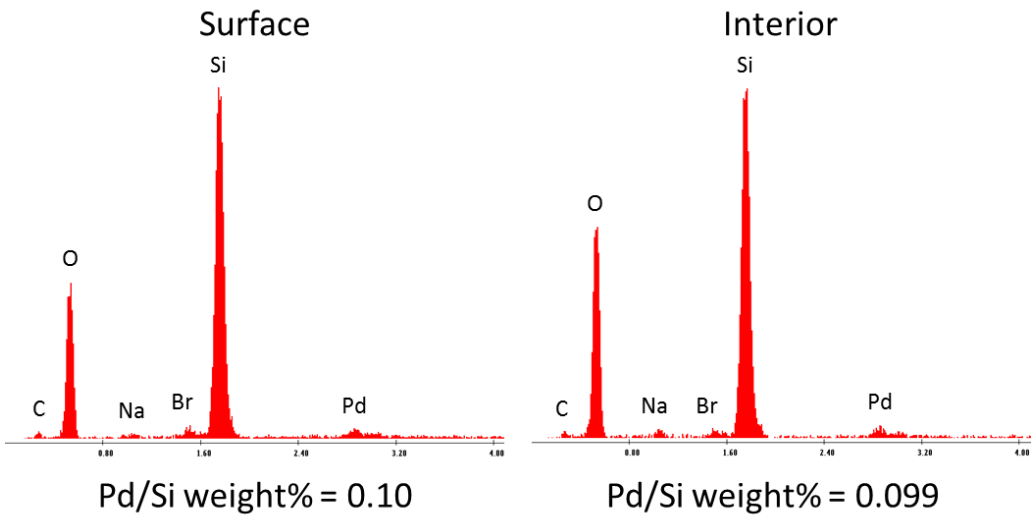

Figure 2.6: EDX spectra of the surface and interior of *is*PdSMSs. Pd/Si weight% determined by EDX.

Table 2.3: Composition of the *is*PdSMSs.

Element	Composition (Weight%)
C	< 0.5[a]
H	1.3[a]
N	< 0.5[a]
Si	40[b]
Pd	4.3[b]

[a] Determined by combustion analysis. [b] Determined by ICP-AES.

The palladium composition of the *is*PdSMSs was also measured using inductively coupled plasma atomic emission spectrometry (ICP-AES) (Table 2.3). The *is*PdSMSs had a palladium composition of 4.3 weight%, which, when compared to the silicon weight%, shows a 0.11 palladium/silicon weight ratio. This is in agreement with the values of 0.10 and 0.099 calculated from EDX spectra. The palladium loading of the *is*PdSMSs determined by ICP-AES is

approximately 2.9 mol% palladium relative to silicon, which is nearly 50% higher than the 2.0 mol% palladium(II) acetate to TBOS added during preparation. This suggests that the majority of the palladium(II) acetate is being incorporated into the macrospheres, but there is a significant quantity of the TBOS that is not reacting or being incorporated into the macrospheres.

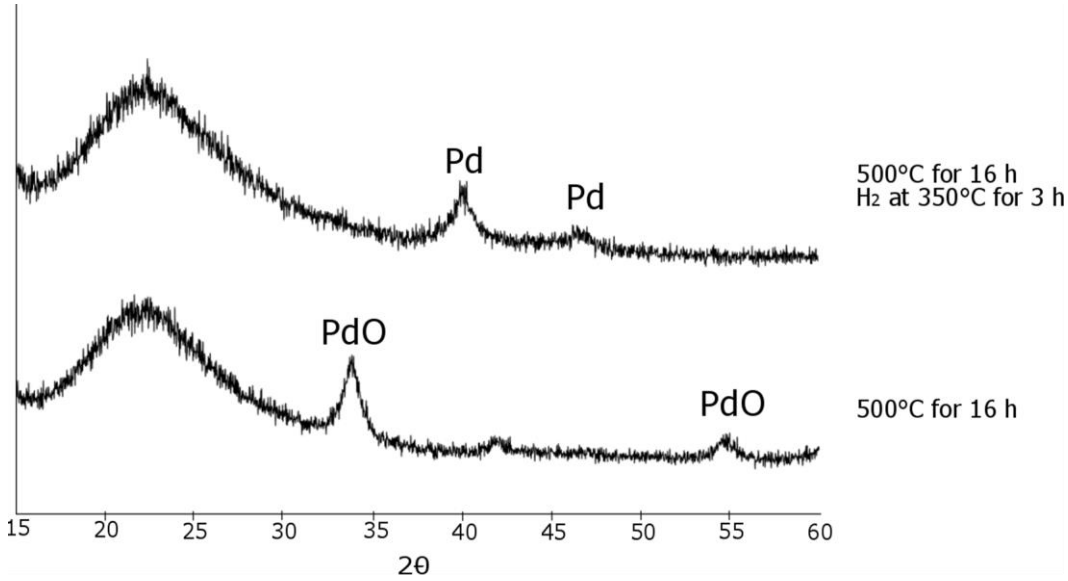

Figure 2.7: PXRD spectra of *is*PdSMSs before and after reduction under H_2 at 350°C.

The powder X-ray diffraction (PXRD) spectrum of the *is*PdSMSs after calcination (Figure 2.7) shows only peaks for palladium oxide, with no discernible peaks for metallic palladium. However, after treatment of the *is*PdSMSs under hydrogen gas at 350°C for 3 hours, peaks for metallic palladium appeared in the PXRD spectrum, while the palladium oxide peaks completely disappeared. This suggests there is complete reduction of the palladium particles encapsulated in the *is*PdSMSs, even those buried in the centres of the macrospheres. There was no obvious large scale porosity observed in the *is*PdSMSs structure from the SEM images, but they must be

permeable to hydrogen gas for this complete reduction to have occurred. Therefore the macrospheres must contain some degree of porosity. Since mesoporosity was observed by Huo et al.[52] and Serrano et al.[53] in their preparations of silica macrospheres using this preparation, it is possible that it is present in the *is*PdSMSs as well to some degree. The broadening of the palladium peaks in the PXRD spectra is characteristic of very small crystalline domains, suggesting that the palladium particles present within the *is*PdSMSs are either very small or made up of aggregates of smaller particles, which is desirable to give high catalytic performance and not heat under microwave irradiation.

The *is*PdSMSs were too large to image directly with transmission electron microscopy (TEM), so they were ground to a powder before imaging to examine the palladium particle size and distribution within the macrospheres. A dispersion of palladium nanoparticles was observed, confirming that the palladium was present as encapsulated nanoparticles in the silica matrix, and dispersed throughout the structure of the *is*PdSMSs. A TEM image of a piece of the ground *is*PdSMSs showing the dispersion of palladium nanoparticles and a histogram of particle size, measured from analysis of TEM images, are shown in Figure 2.8. The majority of palladium particles were in the range of 2-3 nm in diameter, but some larger particles were observed. Porosity was not observed in the macrosphere pieces imaged, but it was noted by Serrano et al.[53] that samples prepared using TBOS rather than TEOS were less ordered, containing worm hole-like channels. The pieces analyzed have been ground from the bulk structure, so are not uniform, and may not fully represent the morphology of the silica in the macrospheres. The complete reduction of palladium particles within the *is*PdSMSs suggests that pores must be present, although they were not observed, with the palladium particles possibly within them.

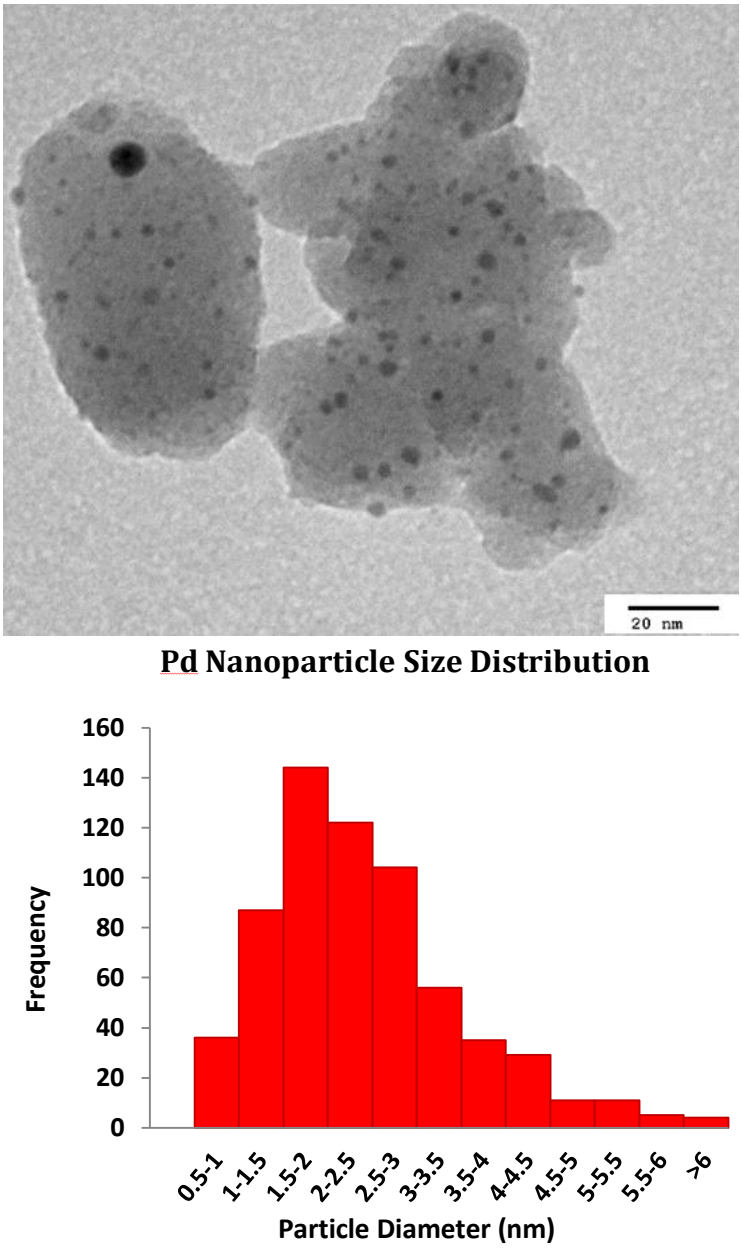

Figure 2.8: TEM image of broken pieces of *is*PdSMSs and histogram of particle size distribution measured using TEM analysis.

The dispersion of palladium nanoparticles throughout the silica matrix not only provides a high catalyst surface area, but may also prevent the particles from heating under microwave irradiation due to a size-induced metal to insulator transition.[91] To test the microwave heating

ability of the *is*PdSMSs, a sealable microwave vessel was filled with the macrospheres. Pentane was used to fill the spaces between the macrospheres and conduct heat to the walls of the microwave vessel. The *is*PdSMSs were then heated under microwave irradiation while measuring the temperature of the vessel with an external IR camera, and compared to the heating of water and DMF (Figure 2.9). At a microwave power of 30 W, there was negligible heating of both pentane and the *is*PdSMSs, while water (tan δ = 0.123 at 20°C, 2.45 GHz) and DMF (tan δ = 0.161 at 20°C, 2.45 GHz) both heated significantly. In contrast, the metal films coated on the capillary walls had been found to heat to incredibly high temperatures at the same microwave power.[16] Higher microwave power settings began to show some heating of the *is*PdSMSs and pure silica macrospheres, but to a significantly lesser degree than the water or DMF.

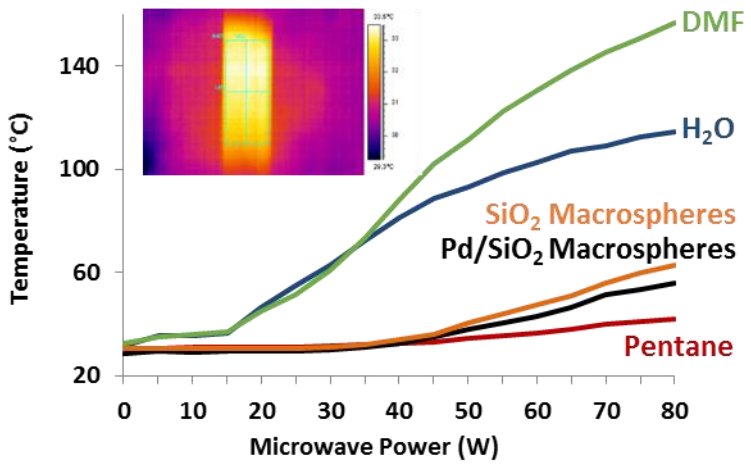

Figure 2.9: IR camera image of *is*PdSMSs in pentane being heated by microwave irradiation (embedded) and temperatures of DMF, water, pentane, silica macrospheres, and *is*PdSMSs in pentane at various microwave power settings.

The *is*PdSMSs did not heat to a significantly different degree than silica macrospheres that did not contain metal nanoparticles. Due to this, it was thought that the heating of the *is*PdSMSs

under microwave irradiation is not due to the palladium nanoparticles, but may instead be due to water present within the macrospheres. In order to investigate this, the silica macrospheres were left open to air for several days and heated under microwave irradiation again (Figure 2.10). The temperature achieved for the silica macrospheres left exposed to air was significantly higher than before exposure, suggesting that adsorbed water within the macrospheres does contribute to heating under microwave irradiation. Upon further heating *in vacuo* at 130°C for 10 hours, the silica macrospheres exhibited a 4% mass loss, presumably from loss of absorbed water.

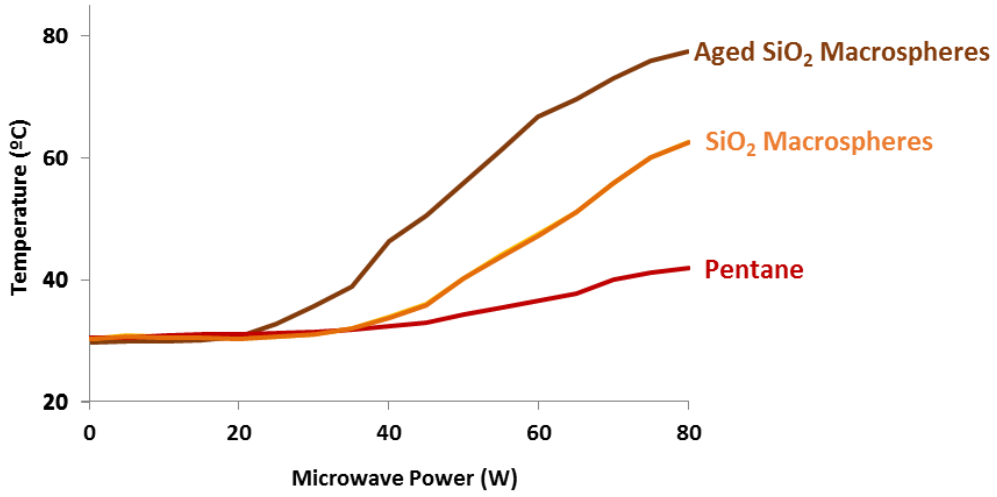

Figure 2.10: Temperature of silica macrospheres in pentane under microwave irradiation.

These results suggest that there was insignificant heating due to the palladium particles loaded into the macrospheres. The sizes of the particles are too small to individually heat under microwave irradiation, and the dispersion seems to be high enough that percolative conduction does not occur, preventing heating.[91] Since the degree of heating from the palladium-loaded macrospheres is less than from solvents with medium microwave absorption capabilities, heating in reactions containing the *is*PdSMSs should be due only to microwave absorbance of the solvent

and reagents. This should prevent the formation of hot spots due to inhomogeneous heating of the metal catalyst, as was observed when using metal films.[16]

Copper-loaded macrospheres (*is*CuSMSs) were also prepared in a similar manner to the *is*PdSMSs by the addition of copper(II) acetate to the sol-gel emulsion used to form the macrospheres.

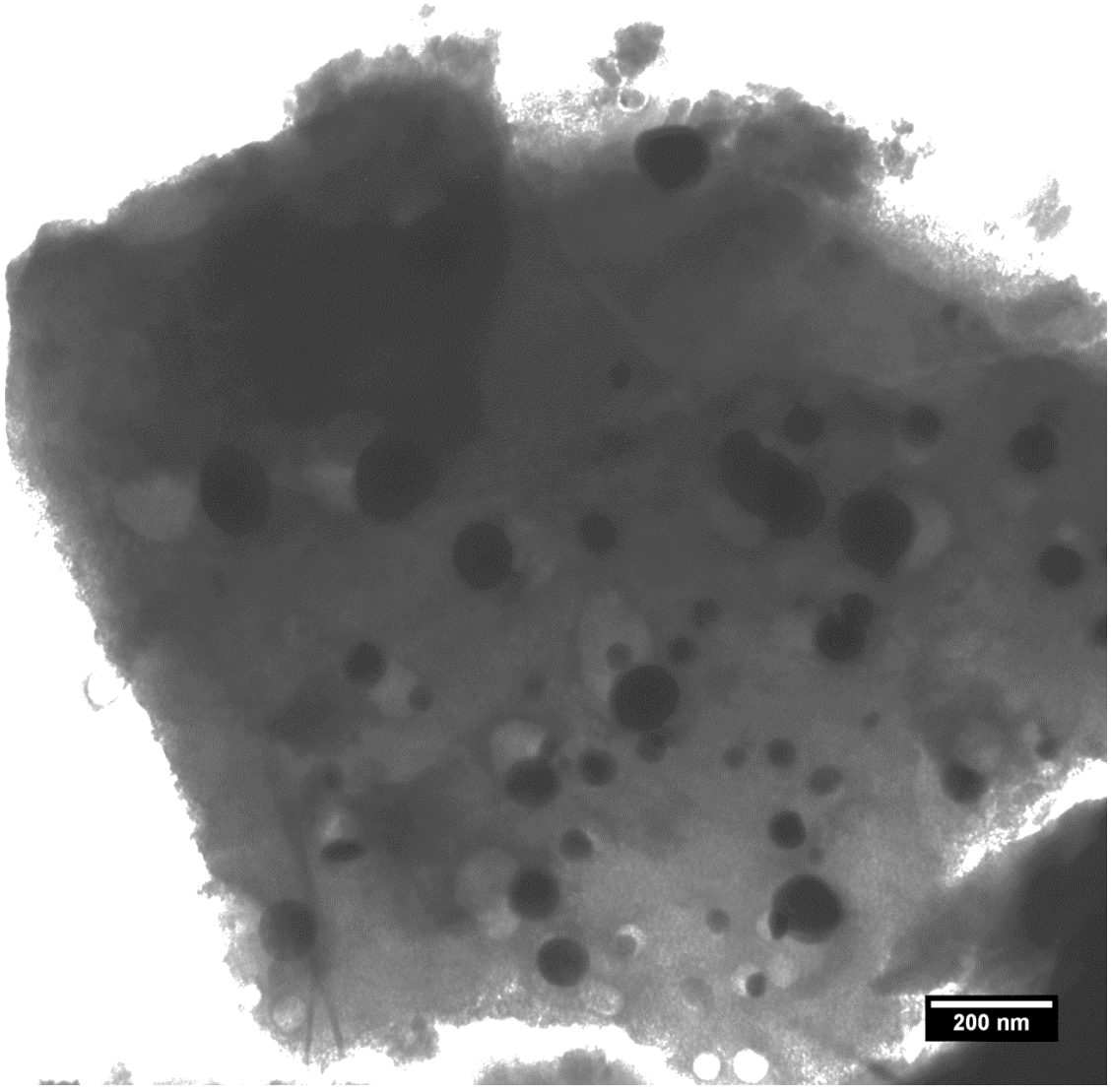

Figure 2.11: TEM image of ground pieces of *is*CuSMSs showing a dispersion of metal particles in a silica matrix.

However, the *is*CuSMSs began to turn green after several days, indicating that the copper within the macrospheres was becoming oxidized. TEM images also showed a dispersion of polydisperse copper particles with diameters ranging from about 20-120 nm (Figure 2.11), significantly larger than the 2-3 nm palladium nanoparticles in the *is*PdSMSs.

To attempt to load the macrospheres with palladium selectively on their surface, the addition of palladium(II) acetate was delayed until after formation of macrospheres. Addition soon after formation of the macrospheres caused loss of structure, but waiting several hours until after hardening did not cause destruction of the macrosphere structure. SEM images of the surface and interior of the macrospheres using a backscatter detector (Figure 2.12) show several large palladium clusters on the surface of the macrosphere (Figure 2.12b), but the distribution is uneven and sparse. EDX spectra also confirm that, although the palladium appears to have been selectively incorporated onto the surface of the macrospheres, it was in very small quantities (Figure 2.13). Examination of the flask after synthesis showed much of the palladium(II) acetate remaining in the flask, unincorporated into the macrospheres. Pure silica macrospheres also adsorbed negligible amounts of palladium when soaked in a palladium salt-containing solution.

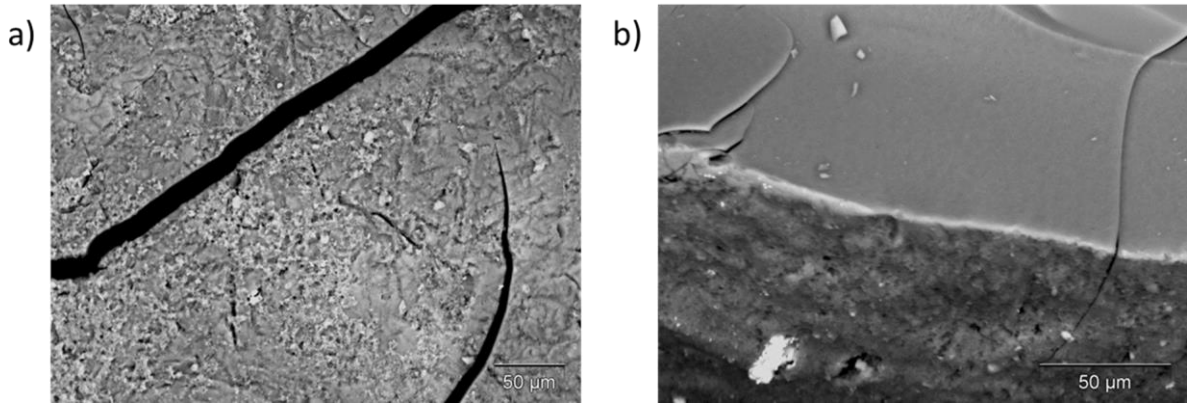

Figure 2.12: SEM images using a backscatter detector of a) the surface and b) the interior of silica macrospheres prepared with addition of palladium(II) acetate to the emulsion after hardening of the macrospheres. Lighter areas represent higher atomic number elements.

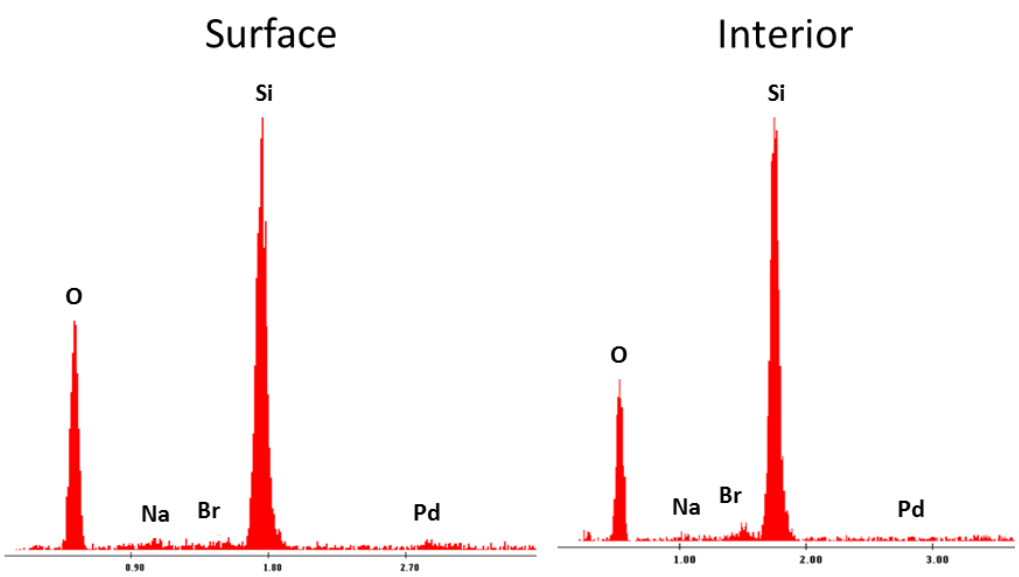

Figure 2.13: EDX spectra of surface and interior of silica macrospheres prepared with addition of palladium(II) acetate delayed until after formation and hardening of the macrospheres.

2.3.3: Catalytic Activity of Metal-Loaded Macrospheres in Batch Microwave Conditions

The catalytic ability of the *is*PdSMSs was evaluated in MAOS under batch conditions to ensure that the palladium nanoparticles were catalytically active. The *is*PdSMSs were able to catalyze the Suzuki-Miyaura cross-coupling of several aryl halides with phenylboronic acid in MAOS, even with a short reaction time and 1.0 mol% theoretical catalyst loading (Table 2.4). Although 1.0 mol% of palladium nanoparticles, based on the palladium content of the *is*PdSMSs determined by ICP-AES, relative to the aryl halide was added for each reaction, not all catalyst may be available for reaction. A significant proportion of the palladium nanoparticles present within the macrospheres are encapsulated in areas within the interior of the macrosphere structure. Despite the macrospheres being broken due to stirring during reaction, some catalyst may still have remained inaccessible.

Table 2.4: Suzuki-Miyaura cross coupling reactions in batch MAOS catalyzed by *is*PdSMSs.

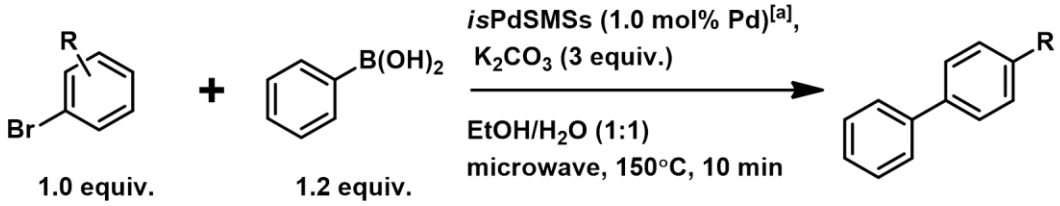

Entry	ArX	Yield (%)
1	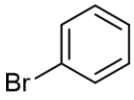	86
2	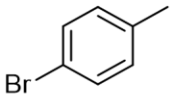	93
3	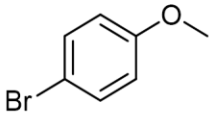	90
4	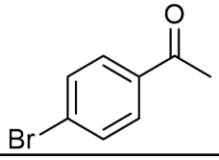	85
5	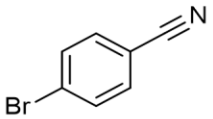	90
6	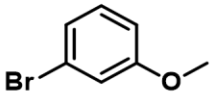	93

[a] Based on the total palladium content of the *is*PdSMSs determined by ICP-AES.

These results were promising for the use of the *is*PdSMSs as a supported catalyst in MACOS for palladium-catalyzed cross-coupling reactions. However, a possible problem for the potential application of supported catalysts for Suzuki-Miyaura cross-coupling reactions in MACOS was

the precipitation of product from solution as the temperature decreased, as these precipitates could potentially cause blockages in the flow system.

Heck cross-coupling reactions were also performed using the *is*PdSMSs in batch MAOS conditions (Tables 2.5 and 2.6). Unlike for the Suzuki-Miyaura cross-coupling catalyzed by the *is*PdSMSs, aryl bromides were unreactive, even with a 2.0 mol% palladium loading and 20 minute reaction time. Although, the effective catalyst loading will actually be much lower than this due to encapsulation of the palladium nanoparticles in the interior of the macrospheres or broken remains. Aryl iodides were coupled in near quantitative yield under similar conditions as was attempted for the cross-coupling of aryl bromides (Table 2.6). For substrates with lower

Table 2.5: Heck cross-coupling of aryl bromides in batch MAOS catalyzed by *is*PdSMSs.

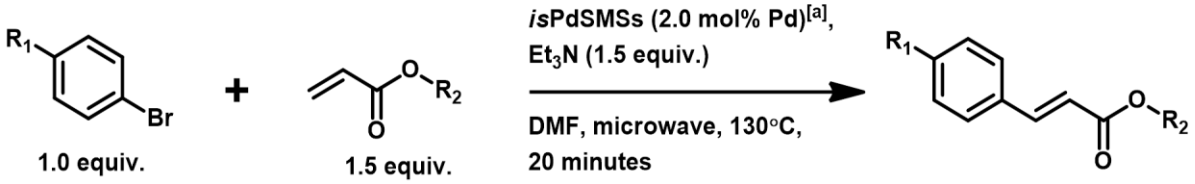

Entry	R_1	R_2	Conversion (%)[b]
1	H	Me	0
2	H	t-Bu	0
3	Me	Me	0
4	Me	t-Bu	0
5	OMe	Me	0
6	OMe	t-Bu	0

[a] Based on the total palladium content of the *is*PdSMSs determined by ICP-AES. [b] determined by ^{1}H-NMR spectroscopy of the crude reaction mixture.

yields, such as iodobenzene, longer reaction times or increased catalyst loadings were able to increase yields. In the case of the Heck reaction products, there were no solids observed, apart from the remains of the *is*PdSMSs.

Table 2.6: Heck cross-coupling of aryl iodides in batch MAOS catalyzed by *is*PdSMSs.

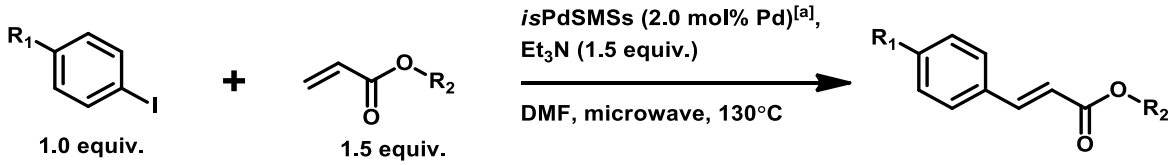

Entry	R_1	R_2	Palladium Loading (mol%)[a]	Time (minutes)	Yield (%)
1	H	Me	2.0	30	99
2	H	Me	2.0	20	89
3	H	Me	2.0	10	85
4	H	t-Bu	2.0	20	81
5	H	t-Bu	3.0	20	94
6	Me	Me	2.0	30	99
7	Me	Me	2.0	20	97
8	Me	t-Bu	2.0	30	99
9	Me	t-Bu	2.0	20	99
10	OMe	Me	2.0	30	98
11	OMe	t-Bu	2.0	30	95

[a] Based on the total palladium content of the *is*PdSMSs determined by ICP-AES.

The *is*CuSMSs were used in batch microwave conditions as a catalyst for Huisgen dipolar cycloadditions (Scheme 2.2), but only traces of product were observed in ^{1}H-NMR spectra after 1 hour of reaction time. This suggests that this reaction cannot be effectively used in flow with this catalyst, as the activity is too low.

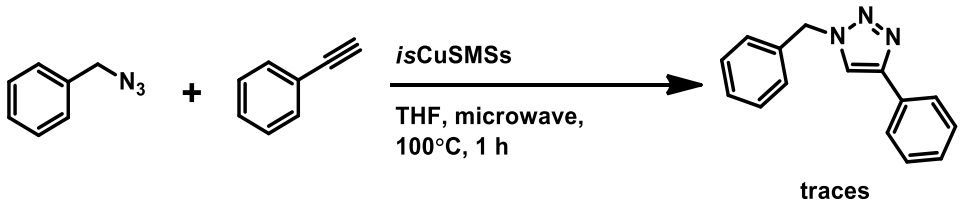

Scheme 2.2: Huisgen dipolar cycloaddition catalyzed by *is*CuSMSs in batch MAOS.

2.4: Conclusions

Monodisperse, metal nanoparticle-loaded silica macrospheres with a diameter around 1 mm were prepared from a sol-gel emulsion technique. Microporosity was not observed in the macrosphere structure, but mesoporosity may be present due to the permeability of the macrospheres to hydrogen gas.

Palladium could be loaded into the macrospheres up to 4.3 weight%, while still maintaining formation of macrospheres, in the form of highly dispersed metallic nanoparticles. The palladium nanoparticles were mostly 2-3 nm in diameter and dispersed throughout the entire structure of the macrospheres. These palladium-loaded silica macrospheres did not heat significantly under microwave irradiation, with the heating that did occur seemingly due to water trapped by the macrospheres. Copper-loaded silica macrospheres were also prepared, but the copper nanoparticles were prone to oxidation.

The palladium-loaded macrospheres were catalytically active for both Suzuki-Miyaura and Heck cross-coupling reactions in batch MAOS reactions. Heck cross-couplings of aryl bromides were unsuccessful, but near quantitative conversion to product was achieved for aryl iodides.

Chapter 3: Suzuki-Miyaura and Heck Cross-Coupling Reactions in MACOS Using *is*PdSMSs

3.1: Introduction

The use of bulk metal films in MACOS had proved problematic due to the intense and uncontrollable heating of the metal films under microwave irradiation, as well as the low catalytic surface area and laminar flow reducing reagent contact with catalytic surfaces.[16],[89] While the metal films had proven to be effective catalysts, the technical problems associated with their use limited their application and reusability.

The *is*PdSMSs had proven to be catalytically active for Suzuki-Miyaura cross-coupling reactions under batch reaction conditions, as well as not heat under microwave irradiation. The macrosphere diameter was also tailored for incorporation into the reactor capillaries used in MACOS without causing significant backpressure issues. With a microwave-transparent supported palladium nanoparticle catalyst in hand, cross-coupling reactions using MACOS were performed using reactor capillaries containing packed beds of *is*PdSMSs.

3.2: Experimental

3.2.1: Materials and Methods

Phenylboronic acid, *tert*-butyl acrylate, methyl acrylate, 4-bromoanisole, 4-bromoacetophenone, iodobenzene, 4-iodotoluene, triethylamine, ethanol (95%), DMF, and DCM were purchased from Sigma Aldrich.

NMR spectroscopy was performed using a Bruker ARX 400 MHz spectrometer. Thermal imaging was performed using an FLIR Systems ThermoVision A320 infrared camera fitted with a 24° fixed FOV lens and an AP1 1200°C filter. Elemental analysis was performed at Galbraith Laboratories, Inc. in Knoxville TN.

3.2.2: Preparation of a Macrosphere-Filled Reactor Capillary

A quartz (2000 µm inner diameter) or silicon carbide (1750 µm inner diameter) capillary was fitted with Vespel™/graphite ferrules and stainless steel Swagelok® tube fittings. Glass wool was used to fill the bottom of the tube fittings to prevent the macrospheres, or pieces of them, from exiting the tube and being transported to other parts of the MACOS system where they may cause blockages. One end of the tube was blocked off with the tube fittings, leaving one end open, and the tube was then filled with the macrospheres. The second tube fitting was then attached, blocking off both ends of the capillary.

The volume of the reactor was then measured by attaching a syringe filled with DMF to one end of the reactor and filling the capillary with DMF until it reached the other tube fitting. For the quartz tubes, the solution was withdrawn and infused again until no air bubbles were observed in the capillary. Since the silicon carbide capillaries are opaque, the solution was drawn out and pushed through again until no more air bubbles were observed coming out of the tube fittings and consistent volume measurements were obtained for subsequent measurements.

3.2.3: Continuous-Flow Suzuki-Miyaura Cross-Coupling Reactions Using the First-Generation MACOS System

The reaction solution was prepared by the combination of aryl halide (0.60 mmol) and phenylboronic acid (7.2 mmol), and K_2CO_3 (1.80 mmol) dissolved in 5.0 mL of ethanol/water solution.

A 15-cm quartz capillary loaded with *is*PdSMSs was placed through the microwave irradiation zone of a Biotage® initiator that has been modified for flow reactions to allow the

microwave to be active while the chamber lid is open. A needle at the end of the reactor capillary was used to puncture a sealed vial, and the system was pressurized using compressed air.

The solvent of the reaction to be performed was infused at a flow rate of 20 μL/min. Once the solvent began to collect in the vial, the microwave is turned on and the power is gradually increased until a temperature of 150°C, measured using the external ThermoVision A320 infrared camera, was reached. Continual adjustment of the microwave power was necessary to maintain this temperature. The valve was then closed, and the syringe switched to one containing the reaction mixture. The valve was opened, and the reaction mixture was infused at a flow rate of 20 μL/min.

3.2.4: Continuous-Flow Heck Cross-Coupling Reactions Using the MACOS System

A 23 cm long silicon carbide reactor capillary containing *is*PdSMSs was placed within the microwave chamber of the second-generation MACOS system and attached to the rest of the system. The MACOS system was flushed with 10 mL of the reaction solution (aryl iodide (5.00 mmol), methyl or *tert*-butyl acrylate (7.5 mmol), and triethylamine (7.5 mmol) diluted to 25.00 mL with DMF) at a flow rate of 100 μL/min. The MACOS system was then pressurized to 200 psi and the reactor was heated to 130ºC with the microwave. The reaction solution was then infused at a flow rate of 30 μL/min. Once 4 mL of the reaction solution was infused, the valve connected to the sampling loops switched, isolating 510 μL of the reaction solution from the MACOS system. That collected solution was pushed out of the sampling loops to a vial with 3 mL DMF, using a third syringe pump. The reaction solution continued being infused into the MACOS system at 30 μL/minute, and the sampling valve switched once again after an additional 1 mL of reaction solution was infused. The collected solution was then pushed through the

sampling loops using 6 mL DMF and the sampling flow system was drained by pushing air through it to collect all solution.

The pale amber solution obtained from the sampling loops was extracted with DCM, adding water to cause separation from the DMF phase. The solution was extracted several times with water to remove DMF from the DCM phase, and the DCM phase was concentrated. The resulting material was then re-dissolved in diethyl ether, extracted again several times with distilled water, and then concentrated to obtain the desired product. Filtering through a plug of silica was sometimes necessary to remove residual DMF.

For subsequent reactions using the same reactor capillary, only 2 mL of reaction solution was used for the initial priming of the MACOS system. The system was flushed after use by infusing 10 mL of air at a flow rate of 500 µL/minute.

3.3: Results and Discussion

3.3.1: Suzuki-Miyaura Cross-Coupling Reactions Using *is*PdSMSs in MACOS

Since the *is*PdSMSs had shown to be active in batch microwave conditions, Suzuki-Miyaura cross-coupling reactions were also performed using the first-generation MACOS system (Figure 3.1). A quartz reactor capillary was used, meaning that the heating of the reaction would only be due to the absorption of microwave radiation by the reaction mixture, since the *is*PdSMSs have shown to not heat under microwave irradiation. Backpressure was applied using compressed air and sealing the system.

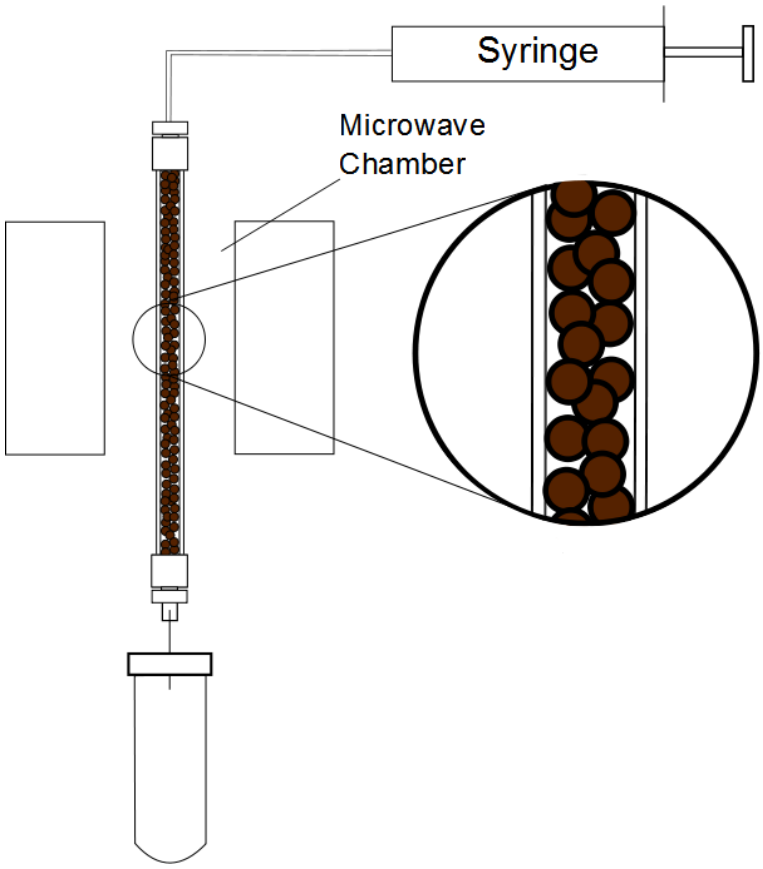

Figure 3.1: Schematic of the first-generation MACOS system used for Suzuki-Miyaura cross-coupling reactions catalyzed by *is*PdSMSs. The system was pressurized with compressed air and then sealed.

The macrospheres were packed in the reactor capillary and placed in the microwave chamber of a Biotage® Initiator, modified to allow for operation with the cavity open. The quartz capillaries had an inner diameter of 2000 μm, and were cut to a length of 15 cm, but a large proportion of the volume was filled with the *is*PdSMSs. Due to this, the actual reactor volume would be very small, however the effective catalyst loading would be much higher than the reactants would experience in batch conditions. The microwave irradiation chamber in the Biotage® Initiator is only about 4 cm long, so the residence time within the heated area would only be about 17 minutes at the flow rate used without the macrospheres present. The

temperature in the microwave-irradiated zone was monitored using an IR camera, and adjusted as necessary during reaction.

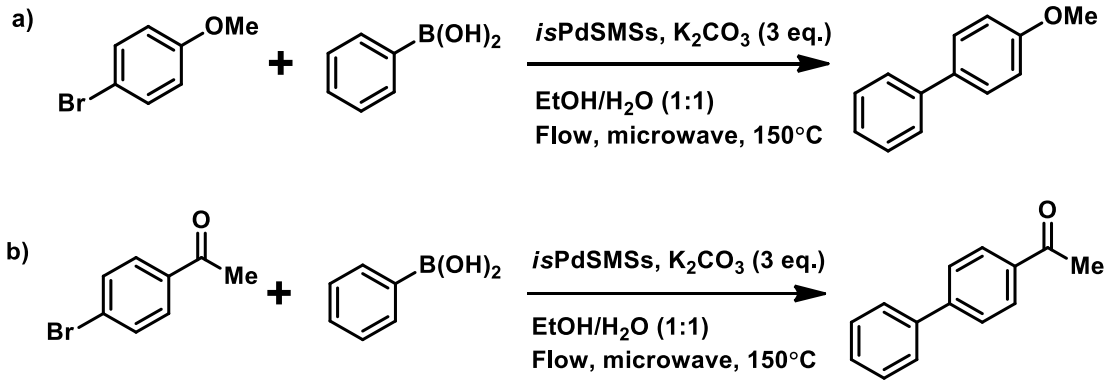

Scheme 3.1: Flow Suzuki-Miyaura cross-coupling reactions attempted in the first-generation MACOS system using the *is*PdSMSs. The formation of precipitates blocked the reactor capillary and prevented further infusion of reagents.

The reactions shown in Scheme 3.1 were attempted in the first-generation MACOS system using the isPdSMSs as a catalyst. Unfortunately, the formation of precipitates caused clogging of the capillary. Precipitates formed around the *is*PdSMSs in the reactor capillary could be observed through the quartz reactor capillaries (Figure 3.2). Due to this, Suzuki-Miyaura cross-coupling reactions often failed when using the *is*PdSMSs in MACOS.

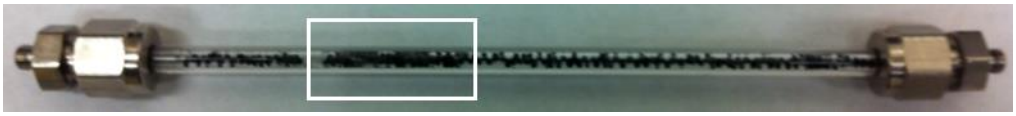

Figure 3.2: Quartz reactor capillary for MACOS filled with *is*PdSMSs after being used for a Suzuki-Miyaura cross-coupling reaction. White box highlights the area in which the white solid was present.

The blockages always occurred just below the microwave-irradiated area of the reactor capillary, meaning precipitation may have been induced upon cooling of the reaction mixture.

Conversions were determined by ^{1}H-NMR spectroscopy by comparing product to starting material peaks from the collected solutions were very low. However, precipitation of products from the solution could reduce apparent yields if they remain trapped in the reactor capillary.

3.2: Heck Cross-Coupling Reactions Using *is*PdSMSs in MACOS

The development of the second-generation MACOS system and use of silicon carbide reactor capillaries allowed for many advantages over the first-generation system. The second-generation MACOS system uses a microwave applicator with a much longer microwave-irradiation zone than the Biotage® Initiator, allowing for increased residence time without the need to decrease the reaction throughput. Silicon carbide reactor capillaries, rather than quartz ones, were also used because silicon carbide itself heats controllably under microwave irradiation, providing heating in place of the reaction mixture. This further ensures a large and uniform heating zone because the capillary remains stationary within the microwave cavity, unlike the reaction mixture, transferring heat along its length independent of the flow rate used (Figure 1.21).[17]

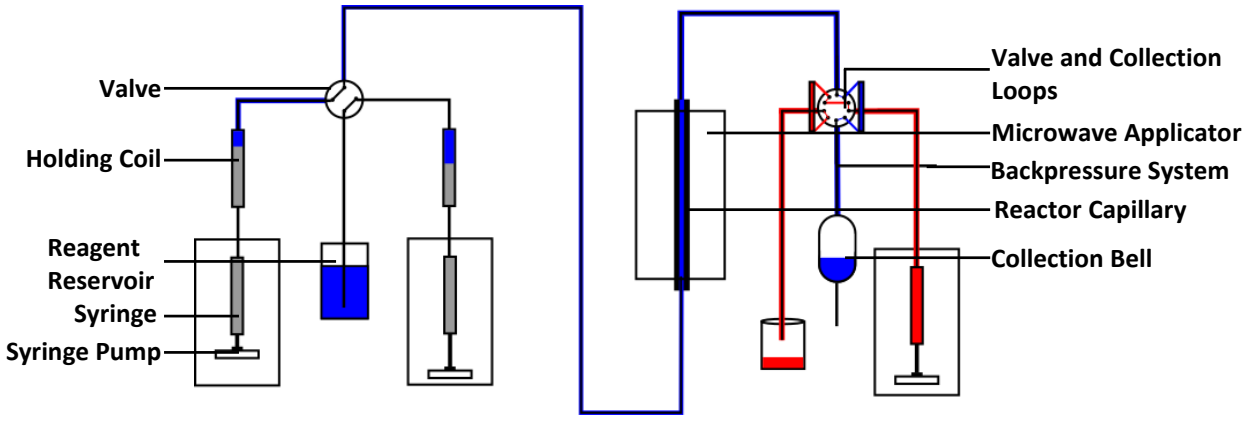

Figure 3.3: Schematic of the second-generation MACOS system used to test the *is*PdSMSs for Heck cross-coupling reactions.

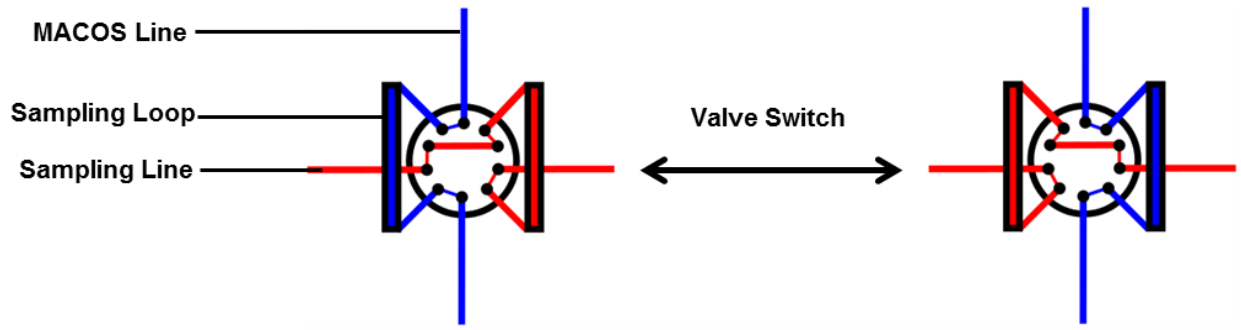

Figure 3.4: Valve with sampling loops used for sampling during flow. Switching of the valve can switch the lines connected to the sampling loops to bring a known volume of solution in and out of the pressurized MACOS system (shown in blue).

A schematic of the second-generation MACOS system used is shown in Figure 3.3. A single CFU was used to infuse the pre-mixed reaction solution. The reactor capillary consisted of a silicon carbide capillary with 1750 μm inner diameter loaded with *is*PdSMSs. A backpressure of 200 psi of argon was applied using the PCD to prevent boiling of the reaction solution. This system also uses an additional valve with two sampling loops that can be switched between the MACOS system and a secondary sampling flow system at atmospheric pressure (Figure 3.4). By switching this valve, a known volume of the reaction mixture stream can be taken out of the MACOS system without interruption of flow or causing depressurization. This aliquot of the reaction mixture can then be collected separately by pushing it through the sampling flow system using solvent. Since the concentrations of starting materials the reaction solution and volume of the sampling loops are known, the amount of product expected in the collected aliquot can be determined and used to assess the reaction. The extraction of the aliquot can be repeated at set times in continuous flow to continually monitor reactions over extended periods of time.

Table 3.1: Heck cross-coupling reaction of aryl iodides performed in MACOS using *is*PdSMSs.

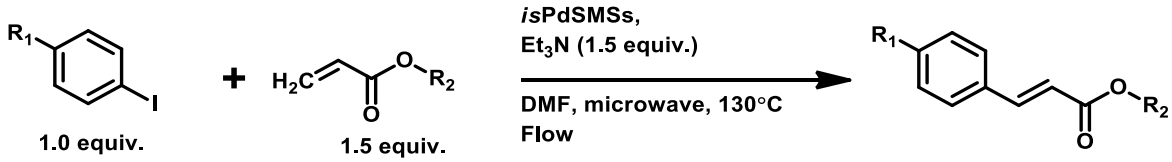

R_1	R_2	*is*PdSMSs (g)	Residence Time (min)[a]	Isolated Yield (%)[b]				
				1st Use	2nd Use	3rd Use	4th Use	5th Use
H	Me	0.257	8.6	78	80	81	82	79
H	*t*-Bu	0.267	9.0	94	88	85	88	89
Me	Me	0.278	10	89	87	89	86	84
Me	*t*-Bu	0.281	10	88	91	84	87	90

[a] Reaction solution was infused at a flow rate of 30 µL/minute, giving a throughput of 0.36 mmol/hour based on aryl iodide concentration, until 5.00 mL of reaction solution was infused. Residence time was calculated based on the measured total measured volume of the reactor capillary, subtracting the measured volume of the fittings, and the flow rate used. [b] Yield was determined from the combination of two aliquots of solution removed after 8000 s (4 mL reaction solution infused) and 10000 s (5 mL reaction solution infused) of reaction time.

Heck cross-coupling reactions of aryl iodides performed in MACOS using *is*PdSMSs gave near quantitative conversions, and good isolated yields over repeated use of the catalyst (Table 3.1). The same reactor capillary filled with the *is*PdSMSs was used repeatedly, without removing the macrospheres from the capillary. These conversions are in line with, or better than, those obtained when using the palladium film-coated reactor capillaries (Table 1.4). The use of silicon carbide reactor capillaries and a dispersed metal nanoparticle catalyst allowed for more controllable and uniform heating of reactions, as well as reusability of the reactor capillaries. There did not appear to be significant reduction in product yield over multiple uses of the supported catalyst. Elemental analysis of the resulting reaction mixtures determined 6-15 ppm of palladium in solution, showing that there is some leaching of catalyst from the *is*PdSMSs over

time. Even with this small amount of leaching, 5 uses of the supported catalyst was not enough to significantly affect its performance.

The residence time within the reactor capillary varied somewhat, due to variation of the packing of the macrospheres within the capillary, but was generally around 8-10 minutes. The total volume of the silicon carbide reactor capillary used is approximately 550 μL, meaning the macrospheres filled about 45-53% of the total reactor volume.

3.4: Conclusions

Suzuki-Miyaura cross-coupling reactions were unsuccessful in MACOS using the *is*PdSMSs due to the formation of precipitates. The precipitates clogged the reactor capillary, preventing further infusion of the reaction mixture.

The Heck cross-coupling of aryl iodides was performed using the *is*PdSMSs in the second-generation MACOS system. Good yields were obtained for the cross-coupled products in each reaction, and precipitates were not an issue. The same *is*PdSMSs-loaded reactor capillary was used multiple times with no significant change of yield upon subsequent uses, up to 5 times.

Chapter 4: Selective Surface Metal Loading of Silica Macrospheres Through the Use of Amphiphilic Transition Metal Complexes

4.1: Introduction

An unfortunate aspect of the *is*PdSMSs is that the palladium nanoparticles are dispersed throughout the entire macrosphere structure, not exclusively on the surface where they will be able to come into contact with the reaction solution. Since the nanoparticles are dispersed uniformly through the macrosphere structure, a large majority of the catalyst will be inaccessible to reagents flowing around the macrospheres in the reactor capillary. Attempts at coating silica macrospheres with metals after formation were unsuccessful, as bulk metal films were unstable and heated significantly under microwave irradiation. Methods of selectively incorporating metals on the surface of the macrospheres, such as delaying the addition of metal salts towards the beginning of macrosphere formation during synthesis disrupted the macrosphere stability, causing collapse of the spherical structure or low uptake of metals by the macrospheres.

Another possible method of selectively incorporating metals at the surface of the macrospheres during formation would be to employ transition metal-containing surfactant molecules. Surfactants that contain transition metals as an integral part of their structure are referred to as metallosurfactants. Metallosurfactants behave in similar ways to typical purely organic surfactants, and are able to form micelles as well as films at air-water interfaces.[92]

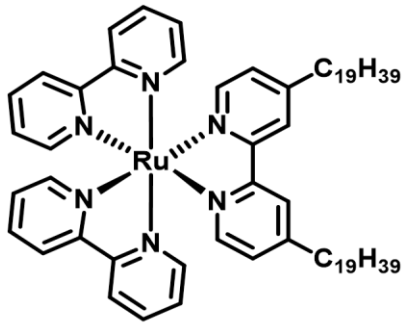

Figure 4.1: Ruthenium-containing metallosurfactant used to template the formation of porous silica sol-gels with metal nanoparticles deposited on the pore surfaces.[93]

Metallosurfactants containing ruthenium (Figure 4.1) have been shown to be capable of templating the sol-gel formation of mesoporous silica while incorporating ruthenium nanoparticles onto the pore walls.[93]

It was thought that the use of amphiphilic transition metal complexes could exploit the oil-in-water nature of the macrosphere synthesis to promote the incorporation of metal salts on the outer surface of the macrospheres at the oil and water interface. If the concentration of the metallosurfactant is kept below the critical micelle concentration, the metallosurfactants may assemble at the interface between the macrospheres and the aqueous solution during macrosphere formation

Dithiocarbamate (DTC)-functionalized ligands were considered because they can be easily prepared from a wide variety of commercially available amines, with the desired hydrophilic functionality already incorporated, and chelate to desired catalytic metals to be incorporated into the macrospheres (Scheme 4.1).[94]

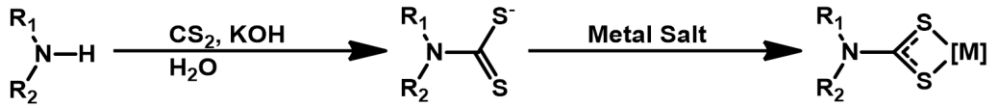

Scheme 4.1: Preparation of DTC transition metal complexes from amines.

4.2: Experimental

4.2.1: Materials and Methods

TBOS, carbon disulfide, diethylamine, diethanolamine, N-ethylethanolamine, dibutylamine, bis(2-ethylhexyl)amine, 6-aminohexanoic acid, 12-aminododecanoic acid, N-methyl-D-glucamine, sodium bisulfite, and DMF were purchased from Sigma Aldrich. Palladium(II)

acetate trimer (Pd 45.9-48.4%) was obtained from Alfa Aesar. CTAB was purchased from British Drug Houses.

Samples were prepared for SEM imaging by mounting on an aluminum stub using carbon tape. SEM images and EDX spectra were recorded on a FEI XL30 ESEM equipped with an EDAX energy dispersive spectrometer. IR spectroscopy was performed using a Perkin-Elmer PE-1750 FTIR spectrometer with samples prepared as KBr pellets. Elemental analysis was performed at Galbraith Laboratories, Inc. in Knoxville TN.

4.2.2: Synthesis of Dithiocarbamate Complexes (1-17)

In a 20-mL scintillation vial, 0.40 mmol of amine was dissolved in 9.5 mL distilled water. The solution was allowed to stir for 10 minutes, and 0.5 mL of a 2M aqueous solution on KOH was added to the solution. The solution was allowed to stir for an additional 10 minutes, followed by the addition of 0.41 mmol carbon disulfide. The carbon disulfide was immiscible with the aqueous solution and stirred vigorously for 2 hours until a clear yellow solution was obtained. A solution of the metal salt (0.20 mmol) was then added dropwise to the solution (nickel(II) acetate tetrahydrate or zinc(II) acetate dihydrate in 2.0 mL distilled water, or palladium(II) acetate in 2.0 mL DMF) and allowed to stir overnight.

The metal complex was precipitated by adding a 1M solution of $NaHSO_4$ dropwise until no further precipitation was observed. The solution was then centrifuged to collect the solid precipitate and the solution was decanted. The precipitate was washed with distilled water and centrifuged again, disposing of the aqueous solution The precipitate was then re-dissolved in slightly basic (KOH) solution and centrifuged again. Any remaining solid that was insoluble in basic solution was collected separately. The solution was then acidified through dropwise

addition of 1M $NaHSO_4$ to cause precipitation, and centrifuged again. Again, the precipitate was washed with distilled water and centrifuged. The solution was decanted and the precipitate dissolved yet again in basic solution. The solution was extracted three times with diethyl ether and centrifuged to remove any remaining traces of precipitate that was insoluble in basic solution. The solution was then acidified to induce precipitation and centrifuged to collect the solid. The precipitate was then washed once again with distilled water and dried under vacuum to yield a brown (palladium), green (nickel), or white (zinc) powder.

4.2.3: Preparation of Metal-Loaded Silica Spheres Using Dithiocarbamate Complexes

These macrospheres were prepared in a similar manner to the preparation of *in situ* metal-loaded silica macrospheres described in Chapter 2.2.3. However, instead of the addition of a metal acetate salt, a 0.1-0.6 g portion of the dithiocarbamate metal complex was added

Silica spheres the colour of the dithiocarbamate complex added, with a diameter of approximately 2 mm, were then filtered from solution and dried in air for 24 hours, during which time they shrank to a diameter of approximately 1 mm. After drying, the spheres were calcined in a muffle furnace overnight at 500°C.

4.3: Results and Discussion

4.3.1: Amphiphilic Transition Metal Complexes

A variety of amines with varying chain lengths and functionality were used for the formation of DTC complexes of nickel, zinc, and palladium (Figure 4.2). The complexes were characterized by IR spectroscopy to ensure DTC formation and coordination (Table 4.1).

Complexes with hydrophilic and hydrophobic chain-ends were prepared, as it was not known whether the metal would comprise a hydrophobic or hydrophilic group.

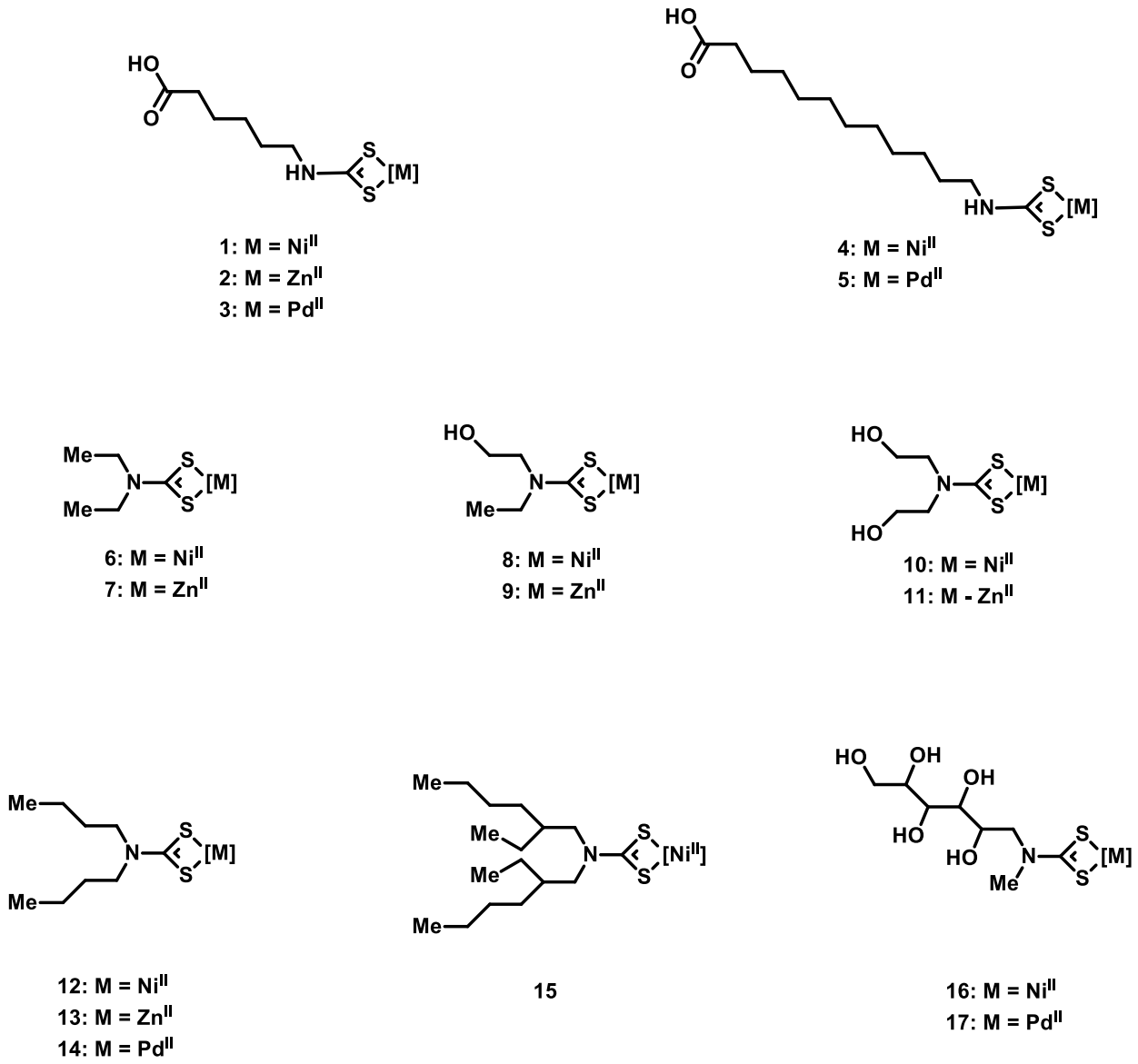

Figure 4.2: DTC ligands synthesized and coordinated to transition metals.

Table 4.1: Selected IR stretching frequencies of DTC transition metal complexes.

Complex	ν(N-CS_2) (cm^{-1})	ν(C-S) (cm^{-1})
1	1521	943
2	1506	946
3	1522	935
6	1520	993
7	1502	993
8	1514	991
9	1502	986
10	1513	976
11	1491	989
12	1506	966
13	1497	957
14	1512	972
15	1506	979
16	1535	966
17	1533	966

Both primary and secondary amines with and without polar functionality were used for the formation of the DTC ligands. Carboxylic acid and alcohol functionalities were used to promote hydrophilicity at the chain end for those complexes. Secondary amines were chosen in addition to primary amines, as they will not undergo the base-mediated decomposition pathway possible for the primary amine DTCs (Scheme 4.2). However, the acid-mediated decomposition pathway is still possible, which can lead to re-formation of the amine and carbon disulfide (Scheme 4.3).

Table 4.2: Elemental analysis results of DTC complex **3**.

Element	mass% Composition	Actual Empirical Composition	Expected Empirical Composition[c]
C	26.4[a]	8.9	7
H	4.01[a]	16.2	12
N	3.6[a]	1.0	1
S	25.7[b]	3.3	2
Pd	26.1[b]	1	1

[a] Determined by combustion analysis. [b] Determined by ICP-AES. [c] Based on expected coordination of 1 DTC ligand.

The DTC complexes were not completely characterized, so the complex structures are not known. Elemental analysis of DTC complex **3** (Table 4.2) suggests a single DTC ligand coordinated to the palladium center. The additional sulfur atom per palladium may be due to coordination of hydrogen sulfide formed during the preparation of the DTC complex by possible acid-mediated decomposition of DTCs. There is likely a mixture of complexes present, which have not been fully identified.

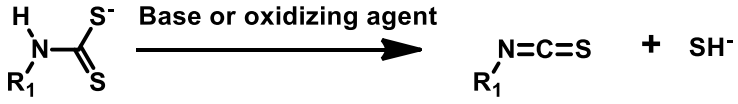

Scheme 4.2: Base-mediated decomposition of DTCs to alkyl isothiocyanates.

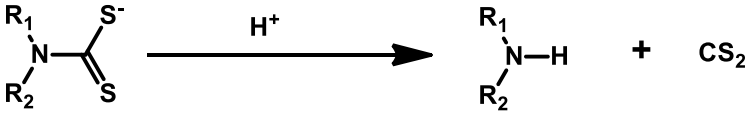

Scheme 4.3: Acid-mediated decomposition of DTCs.

4.3.2: Preparation of Silica Macrospheres Using Amphiphilic Transition Metal Complexes

Even though they were not fully characterized, a selection of the DTC complexes were used in the formation of silica macrospheres. EDX was used to determine if they provided any selectivity in metal incorporation.

For most of the DTC complexes, no selectivity for metal incorporation was observed using SEM and EDX. Silica macrospheres formed using complexes with DTC ligands containing no hydrophilic functionality contained metals both on the surface and in the interior of the macrospheres (Figures 4.3-4.5). The macrospheres prepared using DTC complexes that contained alcohol functionality appeared to contain very small amounts of metal (Figures 4.6 and 4.7). It is possible that the complex remained in the aqueous solution rather than being incorporated into the macrospheres.

The most promising results were obtained from complexes **3** and **5**, which contained carboxylic acid functionality. Macrospheres prepared with the addition of complex **3** contained a marked selectivity for the incorporation of metals towards the surface, confirmed by EDX (Figure 4.8). SEM images using a backscatter detector show a distinct preference of metal incorporation towards the outer surface of the macrospheres when looking at a cross-section of a broken macrosphere. Complex **5** showed less selectivity than complex **3**, as the interior of the macrospheres was also found to contain palladium by EDX (Figure 4.9). The longer alkyl chains of complex **5** may increase hydrophobicity, causing the complex to be present in the interior of the macrospheres to a greater extent. However, even with the increased selectivity of metal incorporation towards the surface of the macrospheres, a significant portion was still present in the interior of the macrospheres.

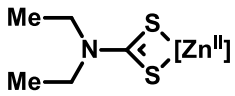

7

Interior

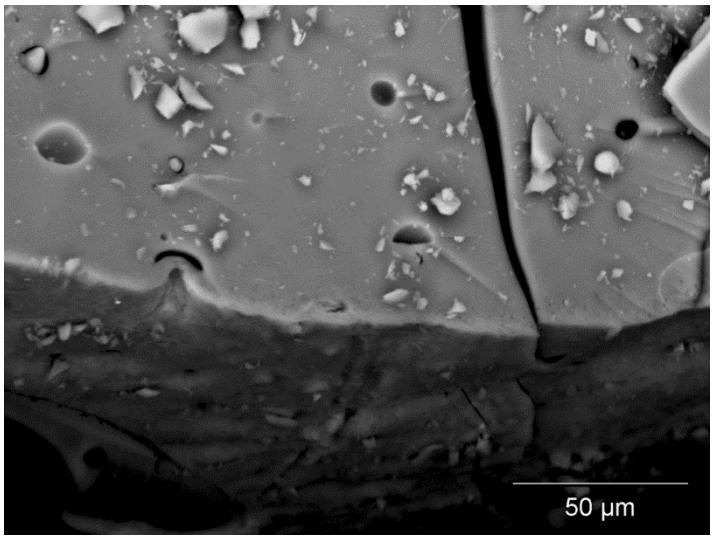

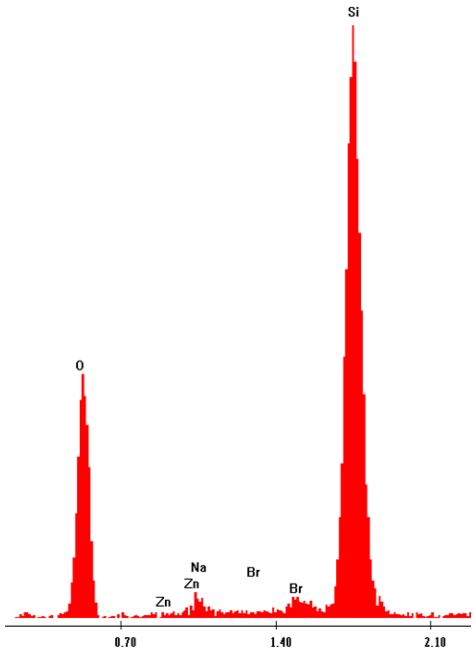

Surface

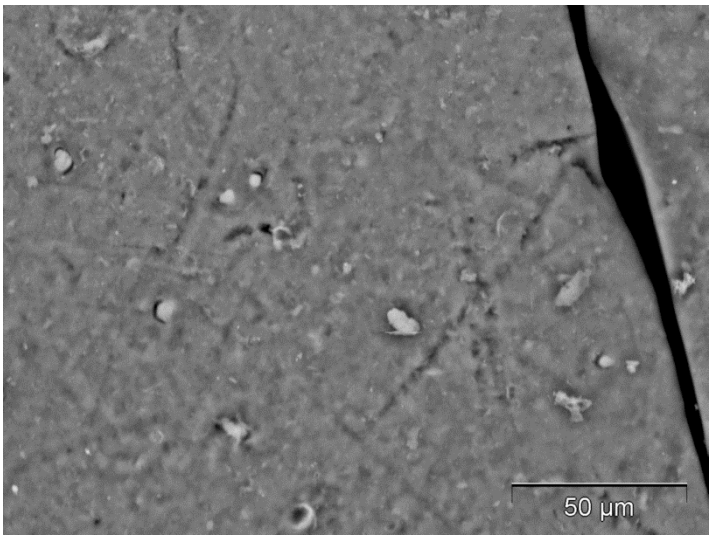

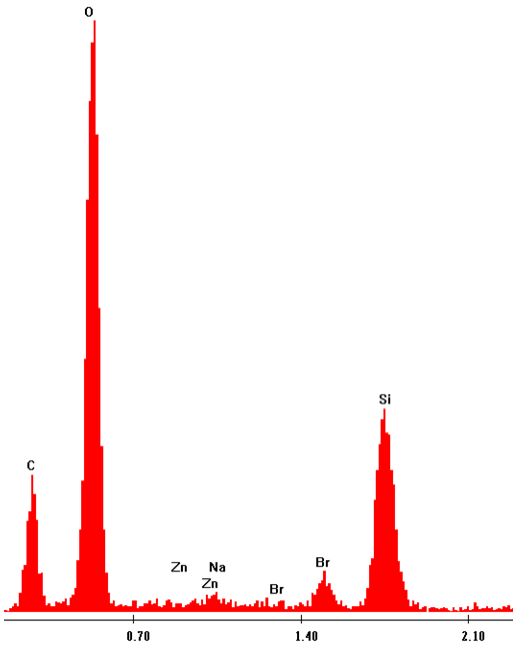

Figure 4.3: SEM images using a backscatter detector and EDX spectra of silica macrospheres prepared using DTC complex **7**.

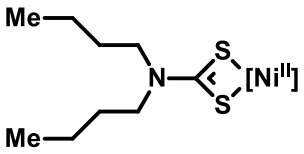

12

Interior

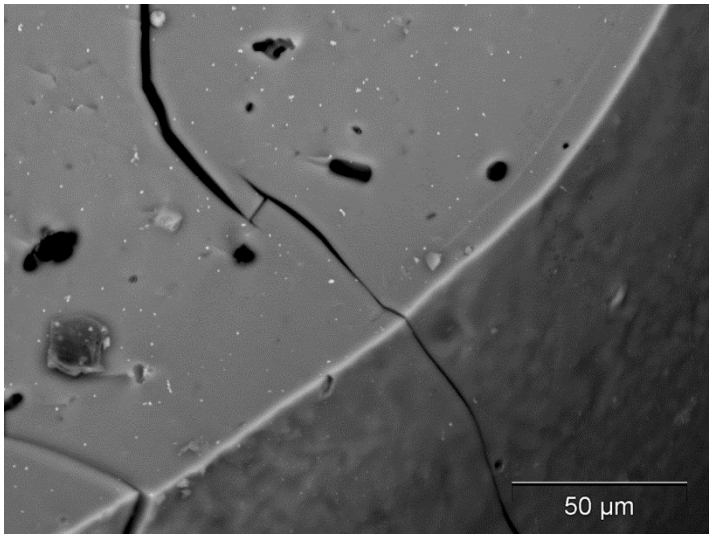

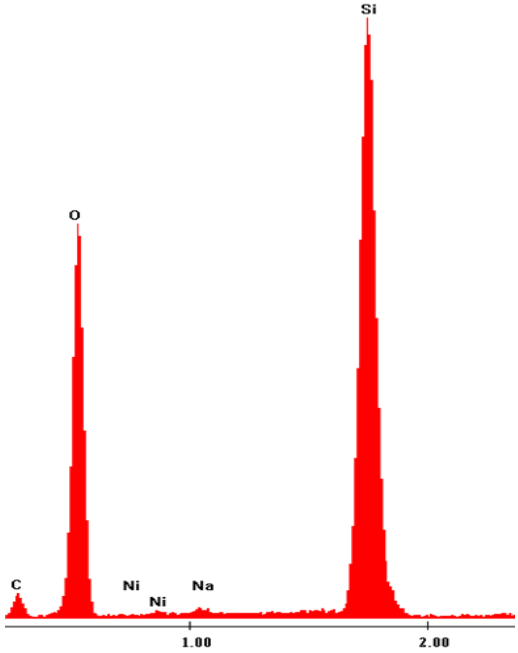

Surface

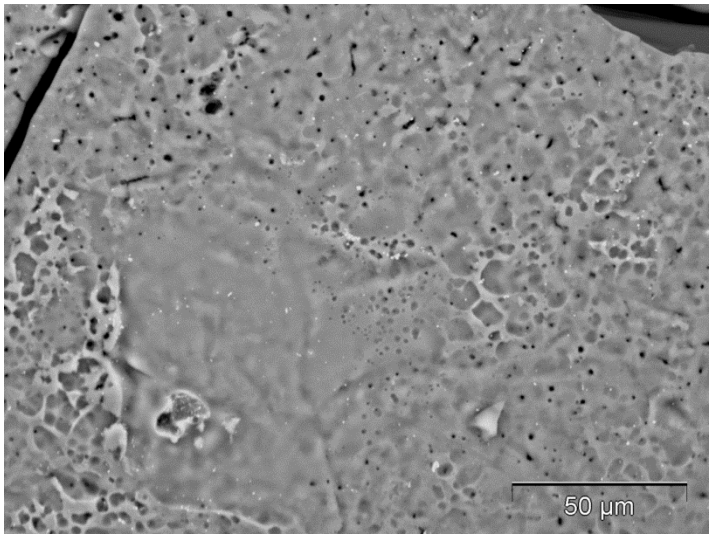

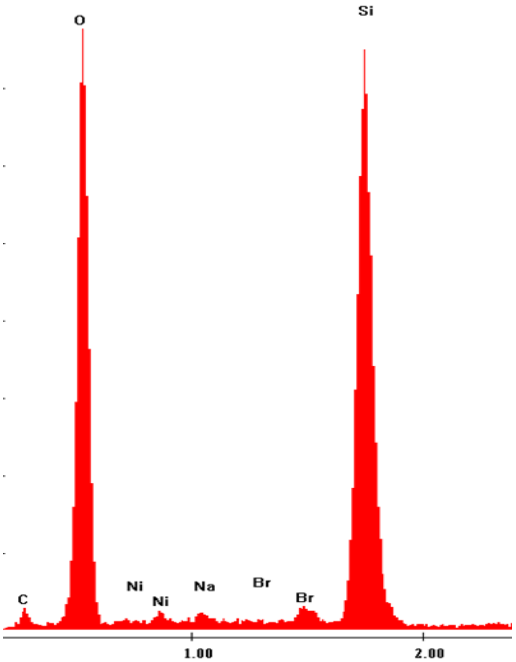

Figure 4.4: SEM images using a backscatter detector and EDX spectra of silica macrospheres prepared using DTC complex **12**.

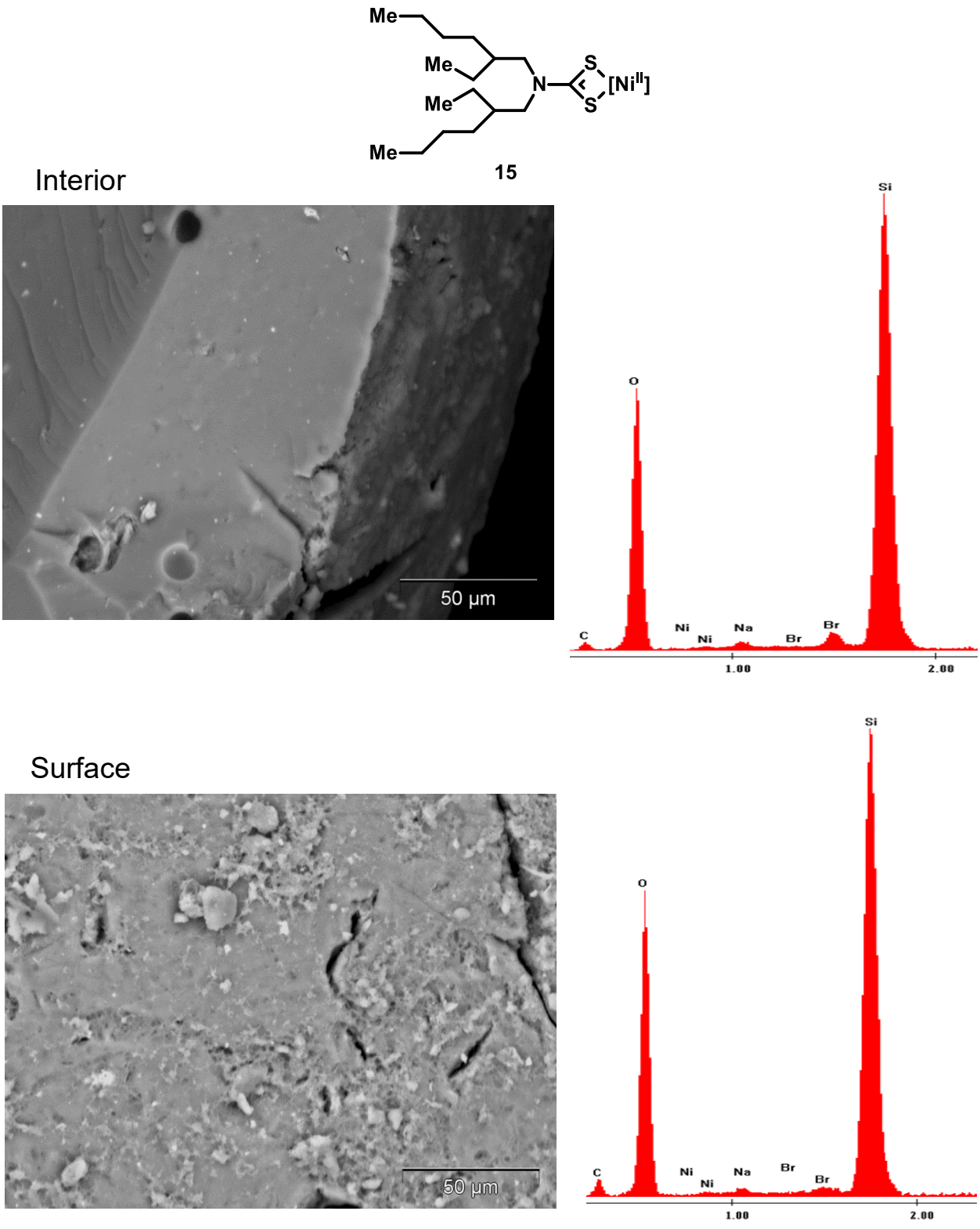

Figure 4.5: SEM images using a backscatter detector and EDX spectra of silica macrospheres prepared using DTC complex **15**.

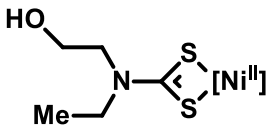

8

Interior

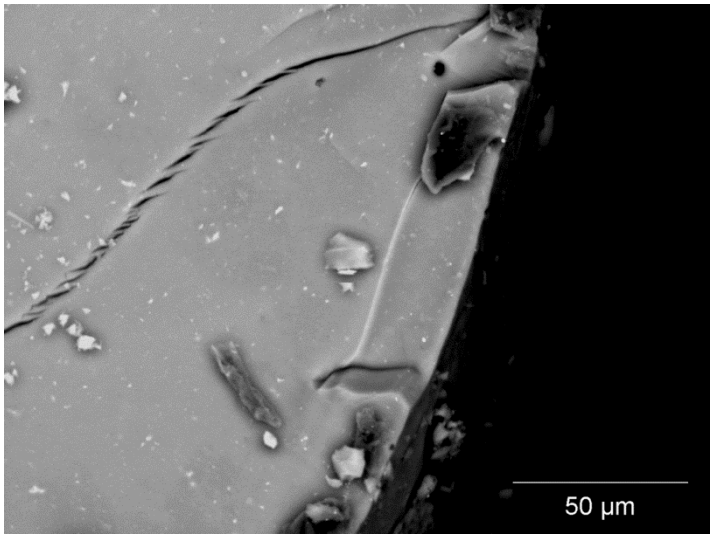

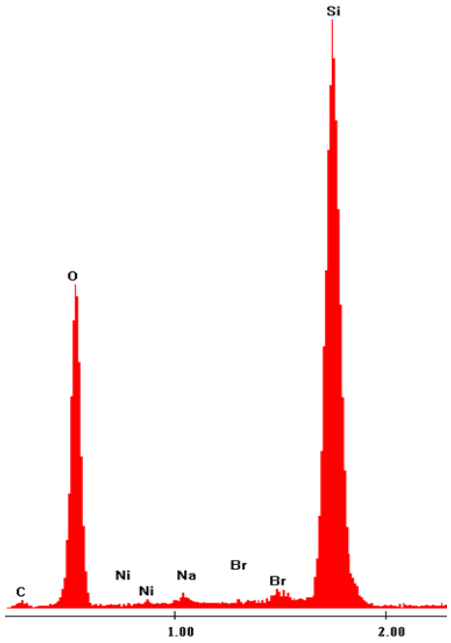

Surface

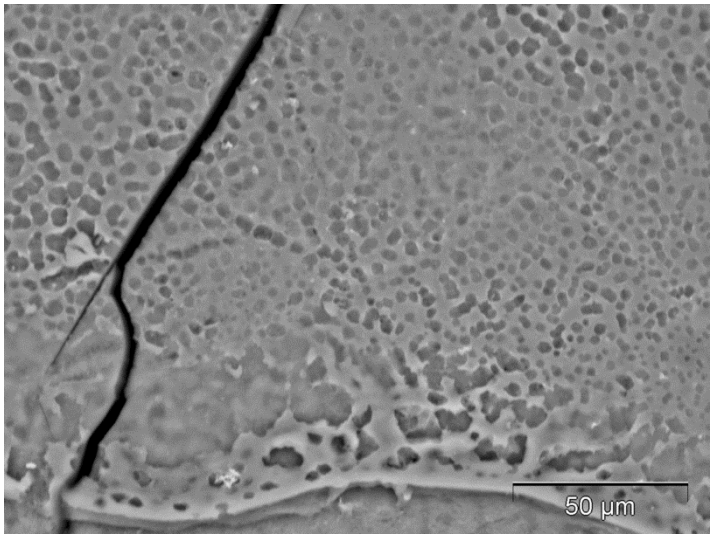

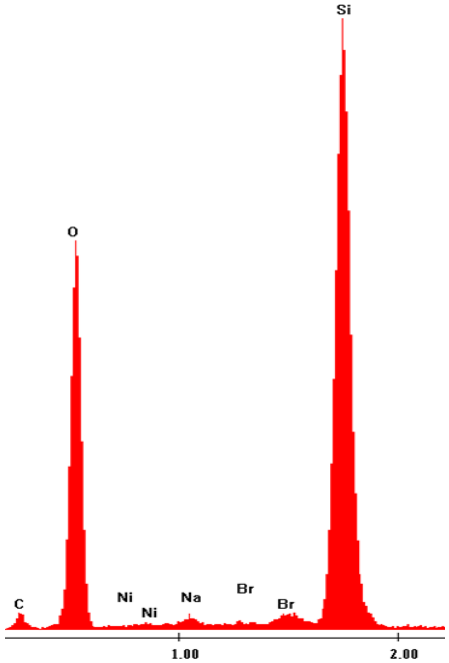

Figure 4.6: SEM images using a backscatter detector and EDX spectra of silica macrospheres prepared using DTC complex **8**.

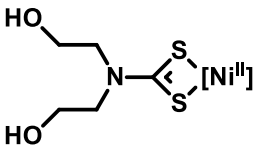

10

Interior

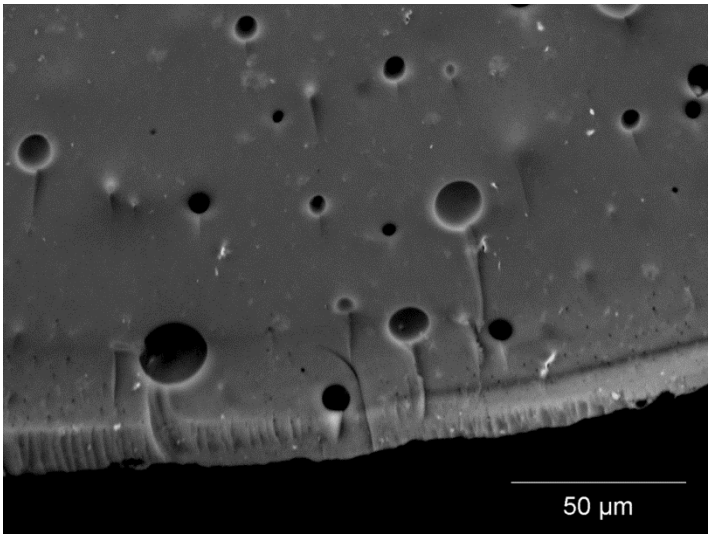

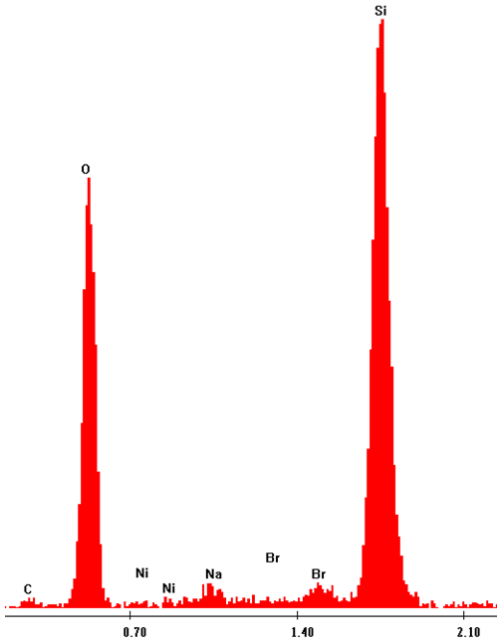

Surface

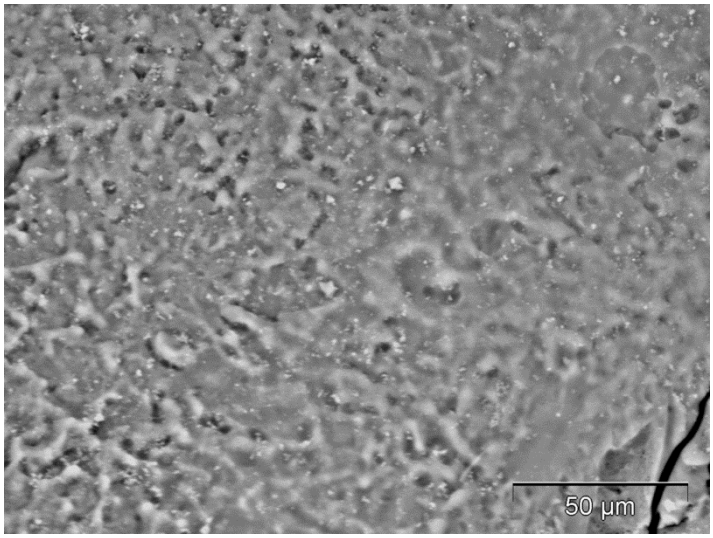

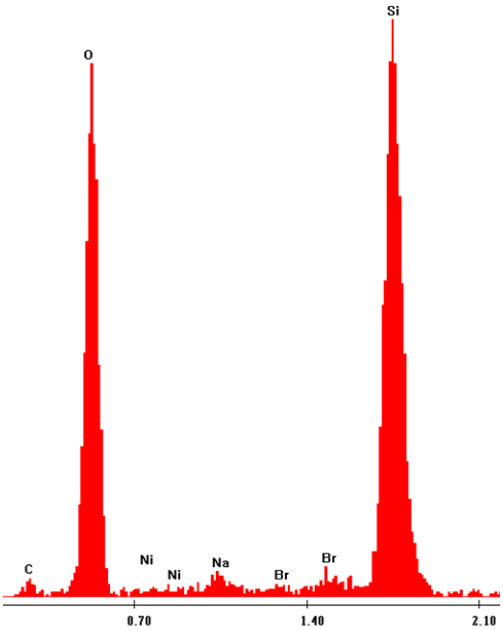

Figure 4.7: SEM images using a backscatter detector and EDX spectra of silica macrospheres prepared using DTC complex **10**.

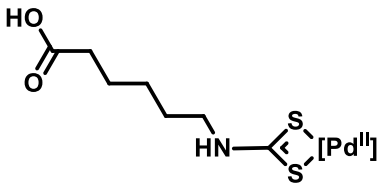

3

Interior

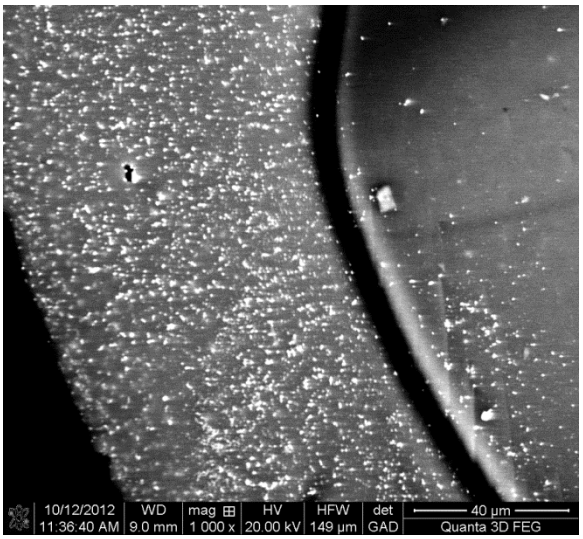

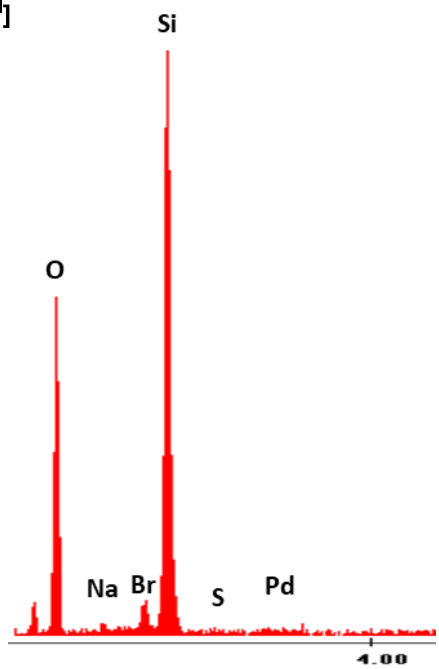

Surface

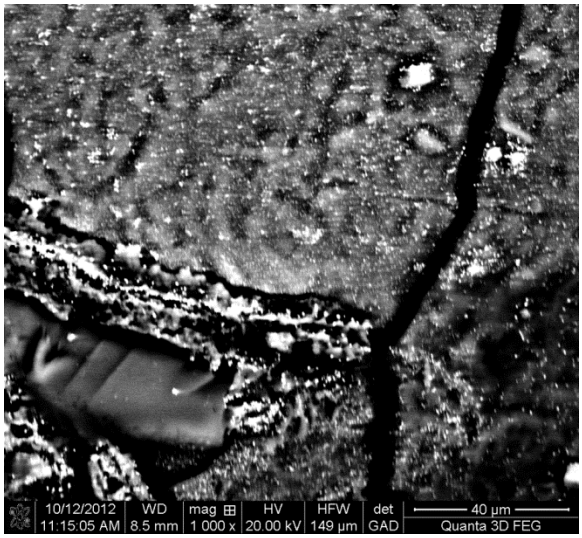

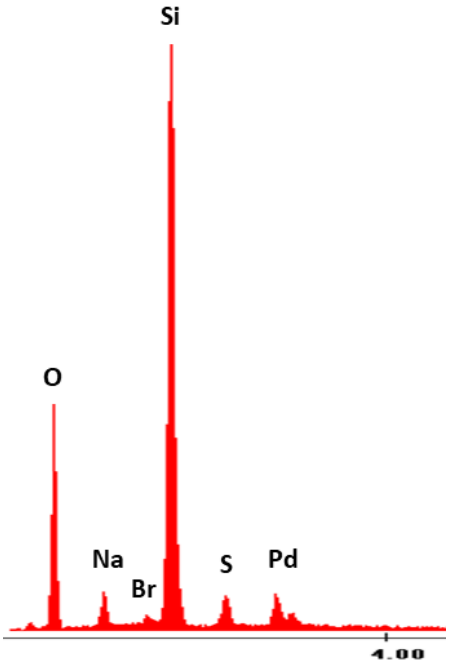

Figure 4.8: SEM images using a backscatter detector and EDX spectra of silica macrospheres prepared using DTC complex **3**.

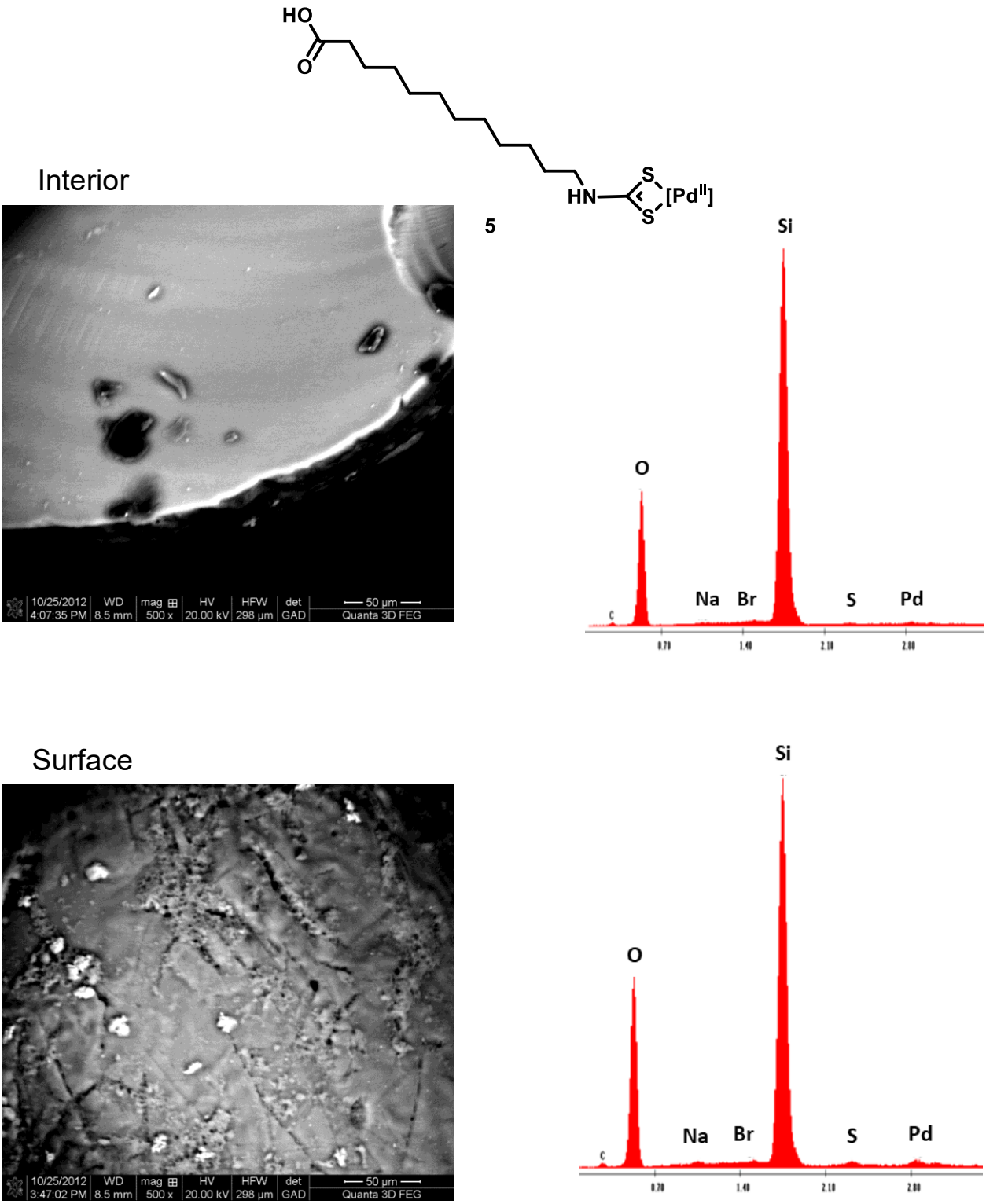

Figure 4.9: SEM images using a backscatter detector and EDX spectra of silica macrospheres prepared using DTC complex **5**.

4.4: Conclusions

Transition metal complexes containing DTC ligands were synthesized and confirmed to contain DTC functionality using IR spectroscopy, as the expected bands for N-CS_2 and C-S vibrations were present. However, the exact structures of the complexes were not determined.

Metal complexes containing DTC ligands that had carboxylic acid functionality were able to provide some preference for loading of transition metals towards the surface of silica macrospheres. The metal is not loaded exclusively on the surface of the macrospheres, but within an area towards the outer surface of the macrospheres. A significant portion of metal still remains within the interior of the macrospheres.

DTC ligands containing non-functionalized alkyl chains or alkyl chains containing alcohol functionalities did not seem to provide any selectivity for the metal incorporation into the macrospheres.

Chapter 5: Inorganic-Organic Hybrid Macrospheres as Catalyst Supports

5.1: Introduction

Silica materials can also be prepared containing organic functionality that can be used as ligating groups to bind desired metals, tethering them to surfaces. These tethering groups can also help to reduce catalyst leaching from supports, increasing the lifetime of the supported catalyst and reducing contamination of product mixtures with heavy metals.[27],[32]

The preparation of inorganic-organic hybrid macrospheres, containing functionality for the coordination of metals may allow for not only reduced catalyst leaching over the *is*PdSMSs, but also allow for selective catalyst loading in only areas accessible by reaction mixtures. Metal loading by scavenging would allow catalyst uptake only in areas where the solution can penetrate, giving more efficient catalyst loading than obtained for the *is*PdSMSs.

5.2: Experimental

5.2.1: Materials and Methods

TBOS, 3-aminopropyltriethoxysilane (APTES), N-[3-(trimethoxysilyl)propyl]-ethylenediamine (enPTMS), *tert*-butyl acrylate, methyl acrylate, iodobenzene, 4-iodotoluene, triethylamine, DMF, and DCM were purchased from Sigma Aldrich. Palladium(II) acetate trimer (Pd 45.9-48.4%) and 3-mercaptopropyl)triethoxysilane (MPTES) were obtained from Alfa Aesar. Cetyltrimethylammonium bromide (CTAB) was purchased from British Drug Houses.

Samples were prepared for SEM imaging by mounting on an aluminum stub using carbon tape. SEM images and EDX spectra were recorded on a FEI XL30 ESEM equipped with an EDAX energy dispersive spectrometer. TEM samples were prepared by grinding macrospheres, suspending in ethanol, then placing onto a copper grid. TEM imaging was performed on a

Philips EM201 electron microscope. NMR spectroscopy was performed using a Bruker ARX 400 MHz spectrometer. Elemental analysis was performed at Galbraith Laboratories, Inc. in Knoxville TN.

5.2.2: Preparation of Inorganic-Organic Hybrid Macrospheres

The same procedure described in Chapter 2.2.3 to prepare the silica macrospheres was used, with the addition of an organotrialkoxysilane. The desired organotrialkoxysilane (MPTES, APTES, or enPTMS) was added along with the TBOS in the desired quantity.

After formation, the macrospheres were filtered and washed with distilled water and then ethanol, before drying in air for 24 hours.

Hardening was accomplished by placing the resulting inorganic-organic hybrid macrospheres in a tube furnace and heating at 100°C under flowing argon gas for 16 hours.

5.2.3: Metal Loading of Inorganic-Organic Hybrid Macrospheres

The dried inorganic-organic hybrid macrospheres were placed in a solution of either 0.010M or 0.10M palladium(II) acetate in DMF (10 mL/g macrospheres) and let soak for the desired length of time, with occasional mixing by light agitation. The palladium(II) acetate solution was then decanted, and the macrospheres washed with ethanol until the wash was visibly colourless. The macrospheres were then dried in air for 24 hours.

5.2.4: Preparation of Palladium Nanoparticle-Loaded Macrospheres (Pd^0@SMSs) by Calcination of Metal-Loaded Inorganic-Organic Hybrid Macrospheres

The dried palladium-loaded inorganic-organic hybrid macrospheres were placed in a muffle furnace and heated at 500ºC in air overnight. Hydrogen reduction was performed in the same manner as for the *is*PdSMSs described in Chapter 2.2.3.

5.2.5: Batch Heck Cross-Coupling Reactions Using Palladium-Loaded Macrospheres

Aryl iodide (0.40 mmol), methyl or tert-butyl acrylate (0.60 mmol), triethylamine (0.084 mL, 0.60 mmol) and 2.0 mL DMF were added to a 5 mL microwave vial. Pd-loaded macrospheres (*is*PdSMSs, Pd^{II}@MIOMSs, or Pd^0@SMSs) (0.020 g) and a stir bar were added to the vial, and the vial then sealed. The vial was heated at 130ºC in the batch microwave for the desired amount of time.

Workup was performed using the same procedure described in Chapter 2.2.5 for batch Heck cross-coupling reactions using *is*PdSMSs.

5.2.6: Continuous-Flow Heck Cross-Coupling Reactions Using the MACOS System

Macrosphere-loaded reactor capillaries were prepared using the same procedure described in Chapter 3.2.2, using silicon carbide reactor capillaries.

Heck cross-coupling reactions were performed in the second-generation MACOS system, using the procedure in Chapter 3.2.4 for Heck cross-coupling reactions using the *is*PdSMSs in MACOS. For reactions involving 20 µL/minute flow rates, sampling valve switches were performed after 4 and 5 mL of reaction solution were infused.

5.3: Results and Discussion

5.3.1: Inorganic-Organic Hybrid Macrospheres

Inorganic-organic hybrid macrospheres (IOMSs) with different functionalities were prepared through a modified version of the silica macrosphere synthesis developed by Huo et al.[52] (Scheme 5.1). The addition of an organotrialkoxysilane to the emulsion as a secondary silica source and co-condensation with TBOS leads to IOMSs with functionality throughout their entire structure. Functionality could also be added by grafting organotrialkoxysilanes onto silica macrospheres (Scheme 5.2), but this method tends to lead to lower densities of functionalization than can be achieved using co-condensation methods.[95]

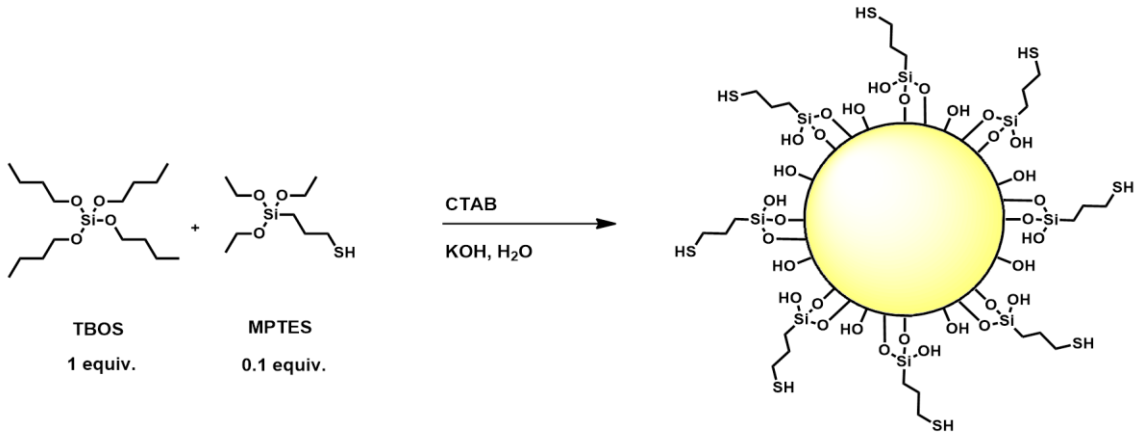

Scheme 5.1: Formation of IOMSs by co-condensation of TBOS and an organotrialkoxysilane.

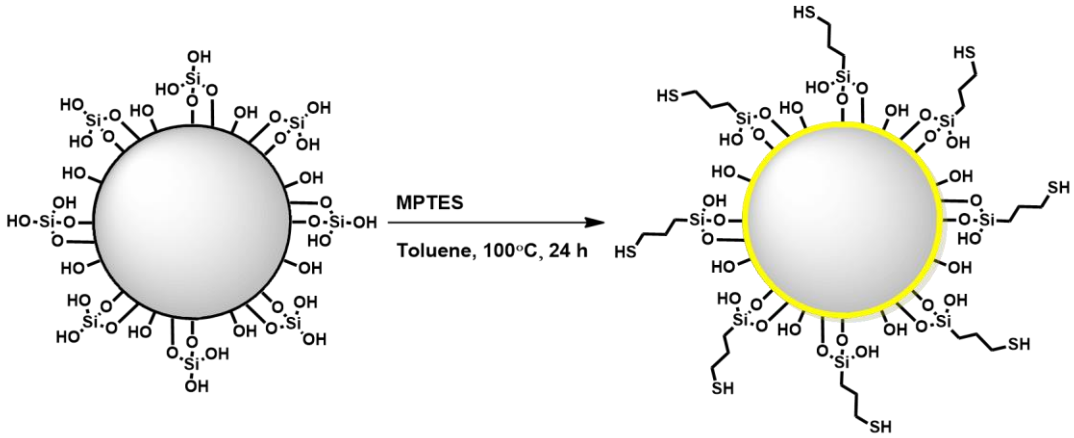

Scheme 5.2: Formation of IOMSs by grafting MPTES onto a pre-formed silica macrosphere.

Organotrialkoxysilanes with thiol and amine functionality, 3-mercaptopropyl triethoxysilane (MPTES), aminopropyltriethoxysilane (APTES), and N-[3-(trimethoxysilyl)propyl]-ethylenediamine (enPTMS), were used to prepare IOMSs using the co-condensation process shown in Scheme 5.1. IOMSs could only be formed when a small proportion of organotrialkoxysilane was used in conjunction with the TBOS (Table 5.1). At higher organotrialkoxysilane amounts, only amorphous pieces or oils formed. The maximum amount of the organotrialkoxysilane that could be used while retaining the ability to form macrospheres varied for each, but was significantly higher for the MPTES than for APTES and enPTMS, which were of similar values. Incorporations of MPTES and APTES of 20-40%, have been reported for other hybrid materials,[96],[97] but the constraints required for the formation of macrospheres using this method does not seem to allow for high loadings. Higher proportions of

Table 5.1: Inorganic-organic hybrid materials formed when adding organotrialkoxysilanes to the precursor emulsion for the formation of silica macrospheres.

Organotrialkoxysilane	Organotrialkoxysilane/TBOS (mole ratio)	Resulting Material
MPTES	0.11	amorphous blobs
	0.10	clear macrospheres
	0.086	white macrospheres
	0.044	white macrospheres
APTES	0.031	macrospheres + amorphous powder
	0.024	macrospheres + amorphous powder
	0.015	clear macrospheres
enPTMS	0.066	oil
	0.026	macrospheres + amorphous powder
	0.017	white macrospheres

the organotrialkoxysilane interfere with the formation of cross-linkages in the resulting structures,[97] which would make the macrospheres more unstable and unable to harden. Only amorphous powders were obtained at high organotrialkoxysilane proportions.

Amine-containing silanes may be water miscible,[95] so their increased presence may affect the phase separation required for the formation of the macrospheres. This could also cause a significantly lower incorporation of APTES and enPTMS into the macrospheres than would be expected from the amounts of each organotrialkoxysilane used.

EDX spectra were obtained for the IOMSs formed using MPTES (MIOMSs), and their sulfur to silicon atomic ratios compared to the stoichiometric ratios of MPTES and TBOS (Table 5.2). The ratio was also compared for the surface and interior of the IOMSPs to see if there is any selectivity towards where the MPTES is incorporated in the macrosphere structure.

Table 5.2: Sulfur incorporation of IOMSs prepared using different MPTES proportions.

Entry	MPTES/TBOS (mole ratio)	S/Si (atom ratio)[a]	
		Interior	Surface
1	0.044	0.10±0.01	0.16±0.001
2	0.086	0.10±0.01	0.17±0.01
3	0.10	0.14±0.004	0.20±0.01
4	Grafted		0.055±0.006

[a] Measured using EDX after drying in air following preparation

There was a slight increase in the sulfur to silicon ratio in the MIOMSs as the amount of MPTES was increased during synthesis. However, the ratio was always greater than the expected ratio based on the stoichiometry of MPTES and TBOS. As was noted for the *is*PdSMSs, there is likely incomplete reaction or incorporation of TBOS in the formation of the macrospheres. While the butoxy substituents of TBOS undergo hydrolysis slowly, the ethoxy substituents of MPTES

undergo hydrolysis more readily. Some of these oligomers may not be able to cross-link sufficiently with TBOS-rich phases, preventing their incorporation into the macrospheres.

Higher loadings of MPTES may cause more oligomeric structures to form due to homocondensation of MPTES early in the reaction. There does however seem to be a slight preference for incorporation of the MPTES-rich phase towards the surface of the SIOMSs. The mechanism of formation of the silica macrospheres determined by Serrano et al.[53] (Figure 2.3), suggests that steady growth of macrospheres is unlikely, with the MPTES being incorporated later in the formation. The cause of the increased incorporation of MPTES at the surface of the macrospheres may be the higher miscibility of the ethanol formed during the hydrolysis of MPTES with the water in the emulsion than the n-butanol formed during hydrolysis of the TBOS. MPTES-rich oligomers not incorporated into the bulk macrosphere structure may later adsorb onto the surface of the macrospheres after formation.

SIOMSs prepared by the grafting of MPTES onto the surface of pre-prepared macrospheres showed significantly lower levels of sulfur content than those prepared by the co-condensation of MPTES and TBOS. This is generally expected,[95] confirming that co-condensation is the best choice for the formation of IOMSs.

5.3.2: Metal Loading of IOMSs

The IOMSs were loaded with metals by soaking them in a solution of metal salt to scavenge metal ions from solution (Scheme 5.3). The ability of the IOMSs to adsorb palladium was examined and compared to pure silica macrospheres. Each set of macrospheres was soaked in 0.010M and 0.10M palladium(II) acetate in DMF solutions to determine an effective

concentration of metal in solution for achieving high metal loading on the macrospheres. A large visual difference was observed in the palladium-loaded MIOMSs (Pd^{II}@MIOMSs) between soaking in 0.010M and 0.10M palladium(II) acetate in DMF. MIOMSs soaked in the 0.10M solution were a much darker orange colour (Figure 5.1), suggesting higher metal loading, than the IOMSs soaked in the 0.010M solution. This is not surprising, but shows that higher metal concentrations are preferable for achieving high metal loading.

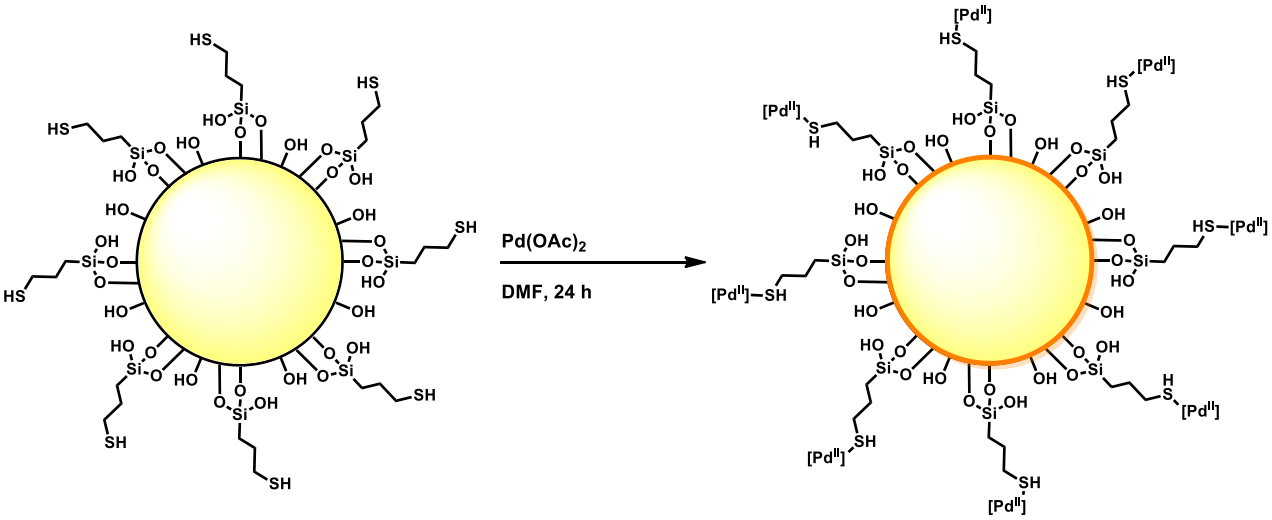

Scheme 5.3: Palladium loading of MIOMSs by soaking in a solution of palladium(II) acetate for 24 hours.

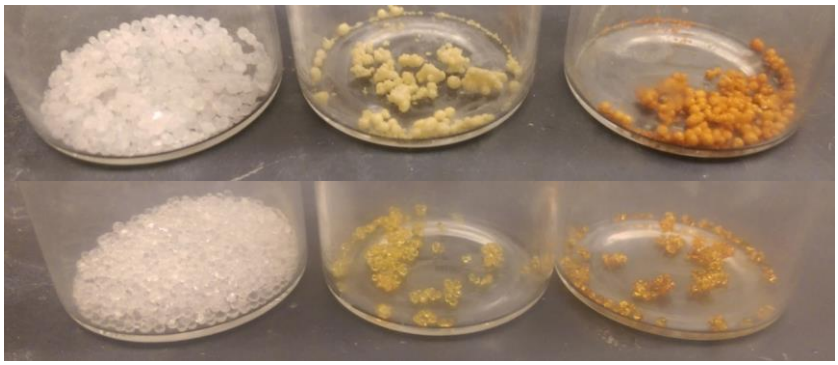

Figure 5.1: MIOMSs prepared with 0.086 (top) and 0.10 (bottom) MPTES/TBOS, Pd^{II}@MIOMSs soaked in 0.10M (middle) and 1.0M (right) palladium(II) acetate in DMF solutions.

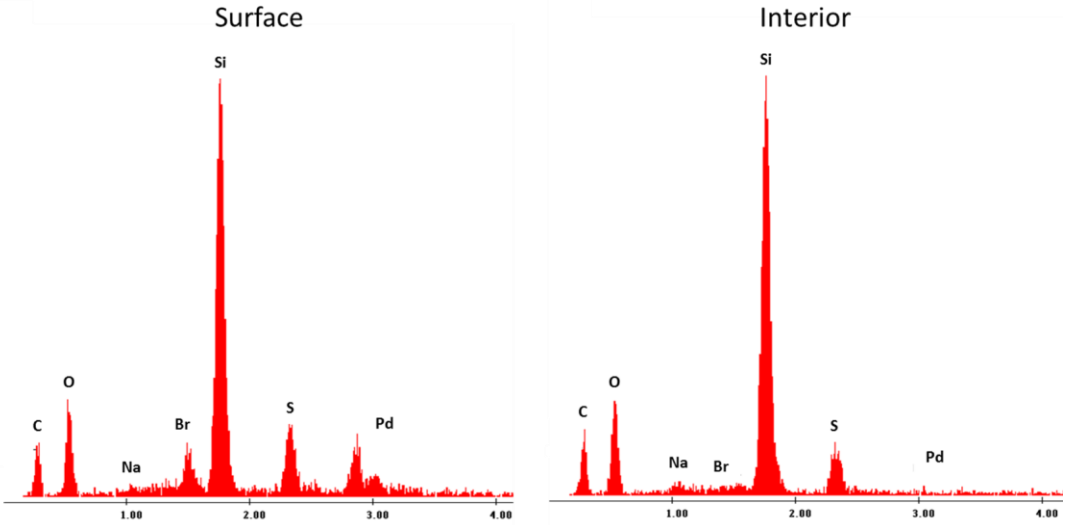

Figure 5.2: EDX spectra of interior and surface of Pd^{II}@MIOMSs prepared using 0.10 MPTES/TBOS after soaking in 0.10M palladium(II) acetate in DMF for 24 h

Table 5.3: Palladium content relative to silicon in Pd@MIOMSs after soaking in 0.10M palladium(II) acetate in DMF for 24 hours.

Entry	MPTES/TBOS (mole ratio)	S/Si (atom ratio)[a]		Pd/Si (atom ratio)[a]	
		Interior	Surface	Interior	Surface
1	0			0.002±0.001	0.004±0.002
3	0.086	0.13±0.01	0.17±0.01	0.022±0.013	0.073±0.002
3	0.10	0.14±0.004	0.16±0.005	0.002±0.002	0.048±0.025
4	Grafted		0.055±0.006		0.006±0.005
5	*is*PdSMS			0.026±0.002	0.026±0.002

[a] Measured using the atom ratios determined by EDX

EDX confirmed that the palladium was present on the surface of the Pd^{II}@MIOMSs, with no significant presence of palladium measured in the interiors of macrospheres that had been broken open (Figure 5.2). Several samples did contain relatively high interior palladium loadings, but the surface loading was still significantly higher than the interior loading in those cases. Those samples may have larger cracks or contain some porosity, allowing the palladium(II) acetate solution to permeate the macrospheres (Table 5.3). Therefore, most palladium present on these catalyst supports should therefore be accessible to reactions, unlike for the *is*PdSMSs.

The relative amount of palladium relative to silicon on the surface of the palladium-loaded, mercaptopropyl-functionalized IOMSs (Pd@MIOMSs) was significantly higher than for the *is*PdSMSs in all cases, suggesting that the effective palladium loading is significantly higher. Silica macrospheres, with no added mercapto functionality (Table 5.3, Entry 1), adsorbed palladium(II) acetate in negligible amounts, so palladium uptake by the MIOMSs is due to the mercapto functionality, not simply adsorption by the silica. The silica macrospheres with MPTES grafted on the surface also had negligible palladium loading, suggesting that a certain graft density may be necessary for effective binding of the palladium salt. It was noted that the surface sulfur to silicon ration on the MIOMSs decreased from 0.20 (Table 5.3, Entry 3) to 0.16 (Table 5.3, Entry 3) after palladium loading. It is possible that the DMF solution was able to wash away some of the surface of the macrospheres, reducing the amount of functionality present.

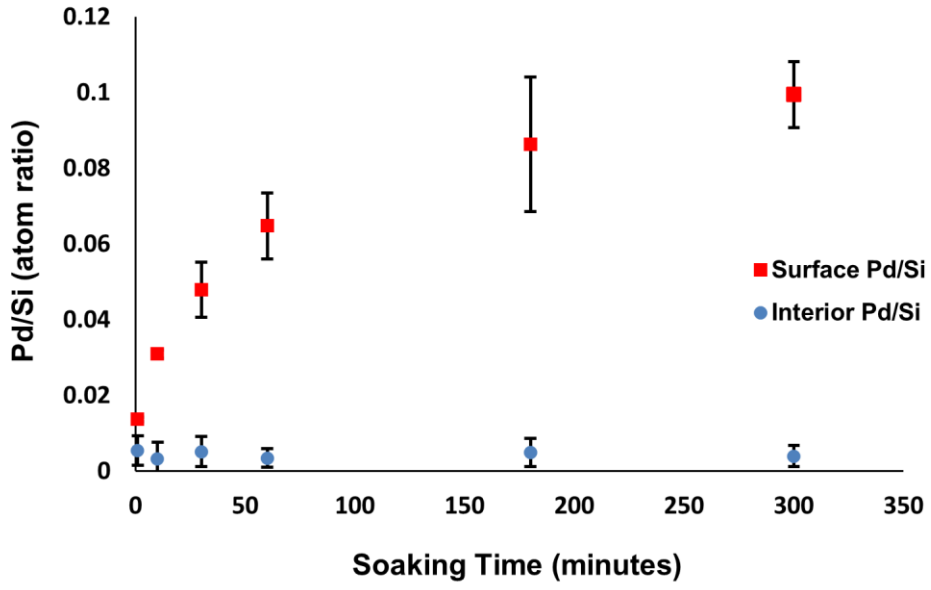

Figure 5.3: Palladium to silicon atomic ratio on the surface and interior of Pd@MIOMSs at various soaking times in 0.10M palladium(II) acetate in DMF. Determined by EDX.

Table 5.4: Average Palladium to silicon mole ratios in IOMSs formed using MPTES after soaking in 0.10M palladium(II) acetate in DMF for 5 hours.

Entry	IOMS	Pd/Si[a]	
		Interior	Surface
1	MIOMS (0.086 MPTES/TBOS)	0.003±0.002	0.118±0.002
2	MIOMS (0.10 MPTES/TBOS)	0.004±0.003	0.099±0.009
3	AIOMS (0.015 APTES/TBOS)	0.007±0.002	0.027±0.003
4	enIOMS (0.017 enPTMS/TBOS)	0.018±0.002	0.018±0.002

[a] Determined by EDX.

The loading of the SIOMSs with palladium was studied over a period of 5 hours to determine optimal soaking times for palladium loading (Figure 5.3). The paladium loading on the surface increased quickly, but began to slow down after the first hour. However, the interior loading remained constant and negligible. Palladium seems to be selectively loaded on the exterior of the MIOMSs, as the palladium(II) acetate solution does not penetrate the macrospheres within 5 hours.

The IOMSs prepared from the co-condensations of APTES (AIOMSs) or enPTMS (enIOMSs) with TBOS were also loaded with palladium by scavenging from a palladium(II) acetate in DMF solution. The AIOMSs did not have as high of a palladium loading as either of the MIOMSs, but also contained a significantly lower proportion of organotrialkoxysilane added during synthesis, so may have less coordinating functionality available. Although the palladium loading of the MIOMSs formed using 0.086 MPTES/TBOS was slightly higher than those formed using 0.10 MPTES/TBOS, this may be due to the rough, amorphous surface of the former.

Interestingly, the Pd^{II}@enIOMSs contained the same relative proportion of palladium both in the interior and on their surface. The palladium(II) acetate in DMF solution must be able to

penetrate those macrospheres, meaning they contain a level of porosity not present within the other IOMSs. The increased water miscibility of enPTMS over MPTES may allow for increased water presence within the macrospheres, giving a larger pore volume that solutions may more easily penetrate. This may be beneficial, as there could be potentially an enormous increase in catalytic surface area, but may also trap solution within them, limiting mass transfer in the flow system.

Unfortunately, the mechanical stability of the surface of Pd^{II}@MIOMSs was very low due to intense cracking, which was observed from SEM imaging (Figure 5.4a). The surface would flake off of the macrospheres after mild agitation, leaving clear macrospheres without palladium loading and an orange powder (Figure 5.4b).

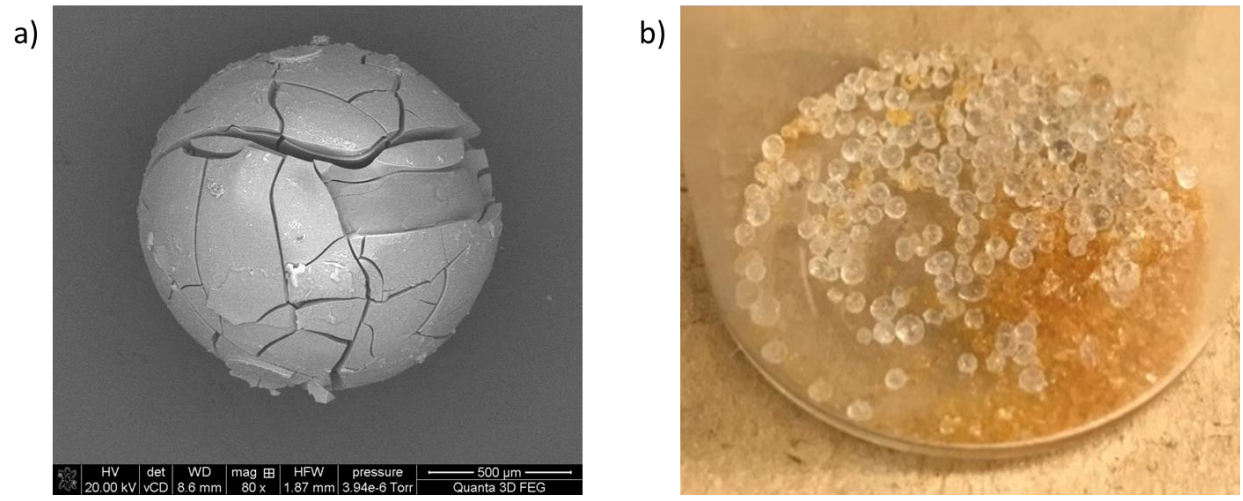

Figure 5.4: a) SEM image of a Pd^{II}@MIOMS. b) Pd^{II}@MIOMSs after shaking the vial they were stored in. Colourless macrospheres remain, while the orange palladium-loaded surface was dislodged.

In order to strengthen the surface of the MIOMSs, an additional heat treatment step was employed to promote further cross-linking and hardening of the macrospheres. Calcination of the MIOMSs was not originally performed because it could cause decomposition and loss of the

organic functionality at high temperatures. To ensure the organic portion of the MIOMS was retained, a temperatue of 100°C was selected for the additional hardening step (Scheme 5.4).

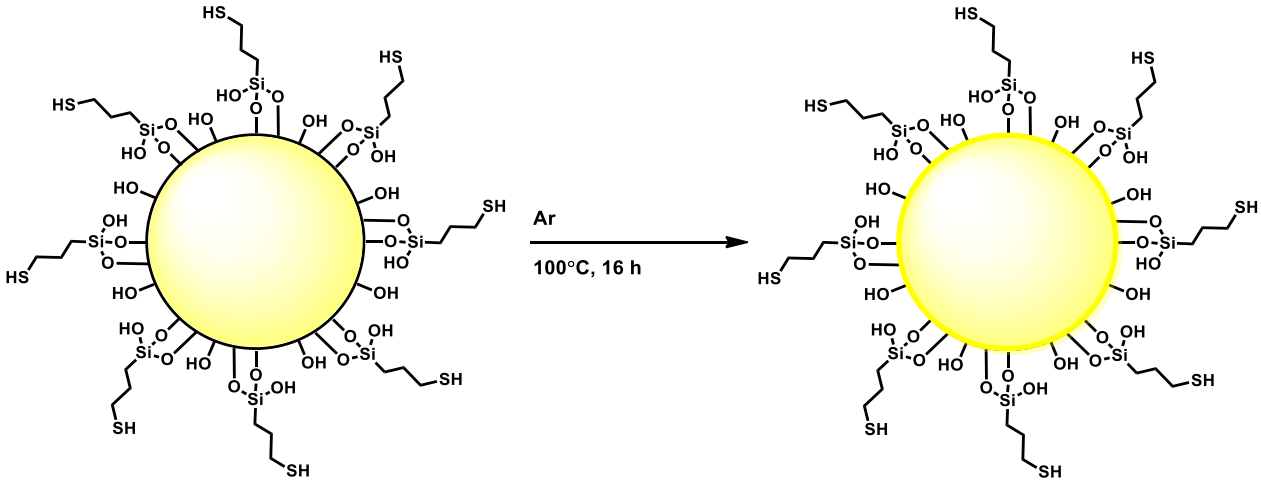

Scheme 5.4: Hardening of MIOMS by heat treatment under flowing argon gas at 100°C.

The heat treatment was successful in hardening the MIOMSs to withstand the soaking in DMF for the palladium loading. The resulting macrospheres contained significantly fewer cracks, as observed by SEM (Figure 5.5a), and the surface did not flake off during agitation.

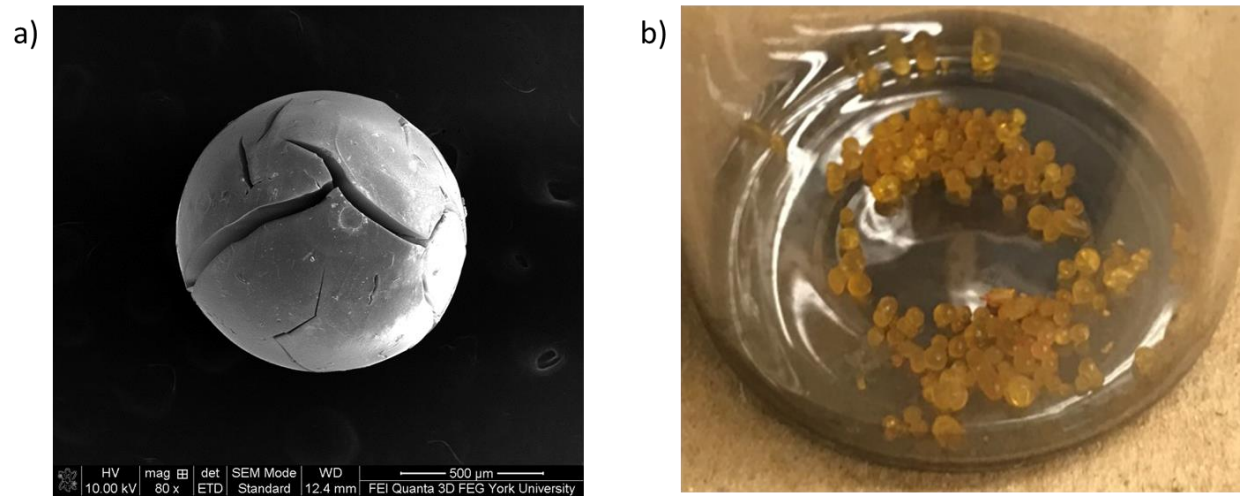

Figure 5.5: a) SEM image of a Pd^{II}@MIOMS that had undergone an additional heat treatment at 100°C for 16 hours (left). b) Pd^{II}@MIOMSs after shaking the vial they were stored in (right).

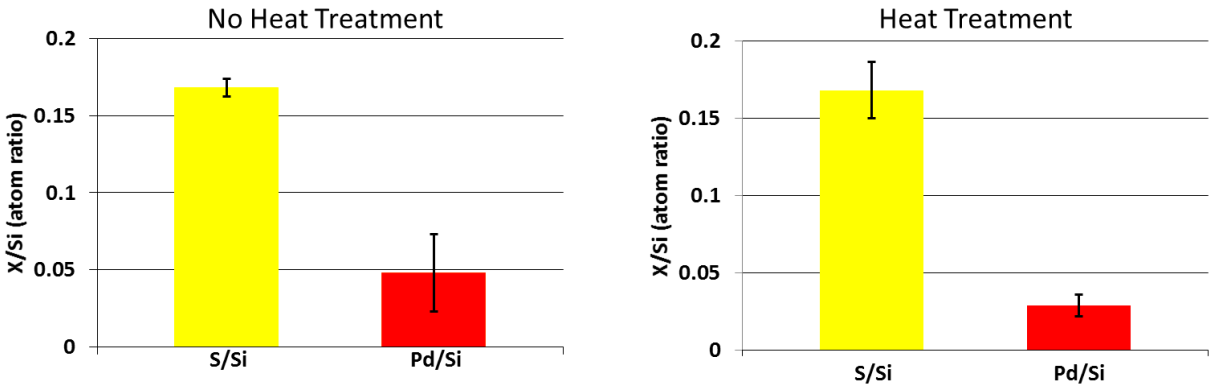

Figure 5.6: Sulfur to silicon and palladium to silicon atom ratios of Pd^{II}@MIOMSs prepared from MIOMSs that had and had not undergone heat treatment. Determined by EDX.

The average sulfur to silicon atom ratio, measured by EDX, of the Pd^{II}@MIOMSs did not seem to change for those MIOMSs that had undergone the hardening step (Figure 5.6). Therefore, the heat treatment did not seem to cause any significant loss of organic functionality from the MIOMSs. The average palladium to silicon ratio, measured by EDX, however was somewhat lower for the Pd^{II}@MIOMSs that had undergone the heat treatment. This may be due to the increased crosslinking reducing the amount of palladium solution that is able to penetrate

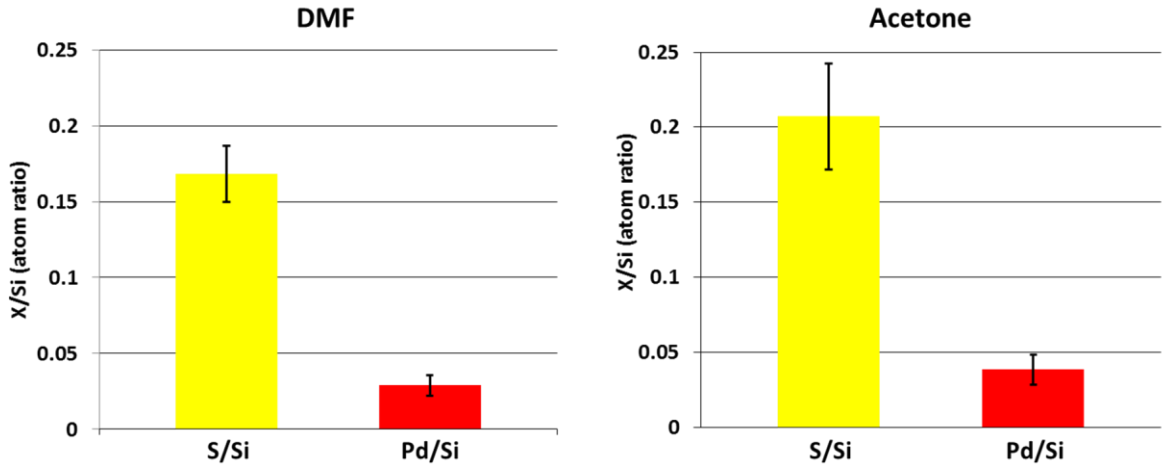

Figure 5.7: Sulfur to silicon and palladium to silicon atom ratios of Pd^{II}@MIOMSs prepared from MIOMSs using 1.0M palladium(II) acetate in DMF or acetone solutions. Determined by EDX.

the surface of the macrospheres during loading. The interaction volume of the x-rays in EDX may extend several microns into the macrosphere surface, giving lower loading measurements if the palladium is unable to penetrate the macrospheres.

When the solvent for the palladium solution used to load the MIOMSs was changed from DMF to acetone, there was not a significant difference in the palladium loading of the Pd^{II}@MIOMSs. However, the average sulfur to silicon atom ratio was higher when the acetone solution was used than with DMF (Figure 5.7). The ratio is in line with the original ratio measured in the MIOMSs after preparation (Table 5.2, Entry 3), confirming that DMF must facilitate the removal of surface functionality on the MIOMSs. The MPTES incorporated at the surface of the MIOMSs may be loosely bound, or the DMF is able to cause loss of the macrosphere surface. Unfortunately, the propensity of palladium black to coat the macrospheres seemed to be higher when acetone was used, causing irreproducibility of the coatings.

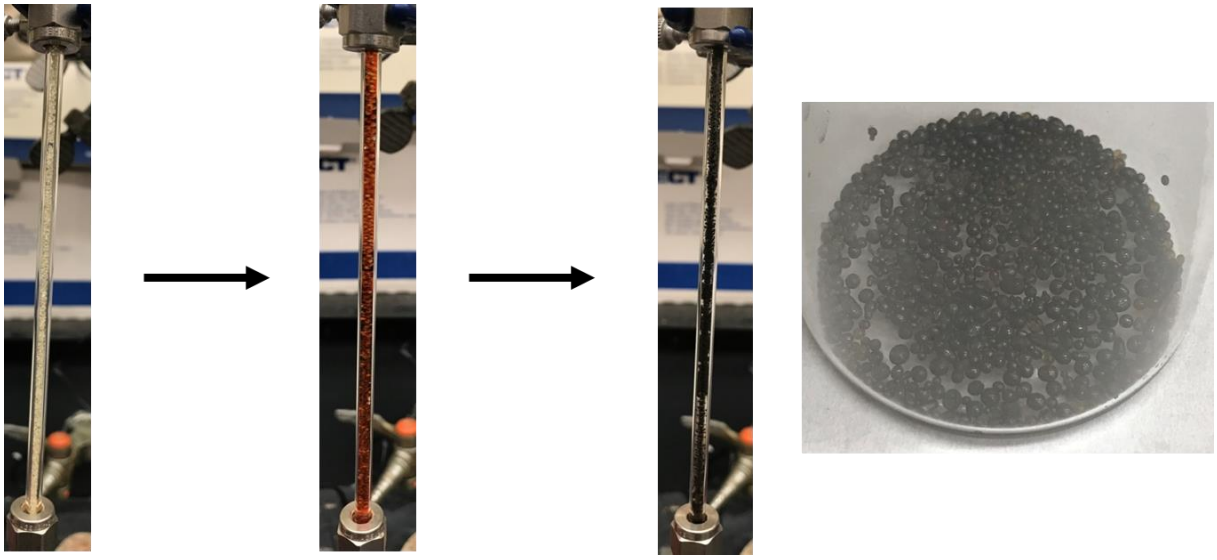

Figure 5.8: Loading of MIOMSs with palladium by flowing a 0.10M solution of palladium(II) acetate in DMF over the macrospheres in a flow capillary. Resulting macrospheres on far right.

Coatings using flow rather than batch soaking of the macrospheres in palladiu(II) acetate in DMF also caused palladium black to coat the macrospheres, giving bulk metallic coatings that may not be suitable for microwave irradiation (Figure 5.8).

5.3.3: Palladium Nanoparticle-Loaded Macrospheres by Calcination of Pd^{II}@MIOMSs

Functionality on the surface of the IOMSPs may be undesirable for certain reactions that may be performed in MACOS. In these cases, supported palladium nanoparticles may be a more desirable catalyst. Calcination of the Pd^{II}@MIOMSs was performed to remove organic functionality and promote the formation of silica macrospheres with palladium nanoparticles selectively on their surface (Pd^{0}@SMSs) (Scheme 5.5).

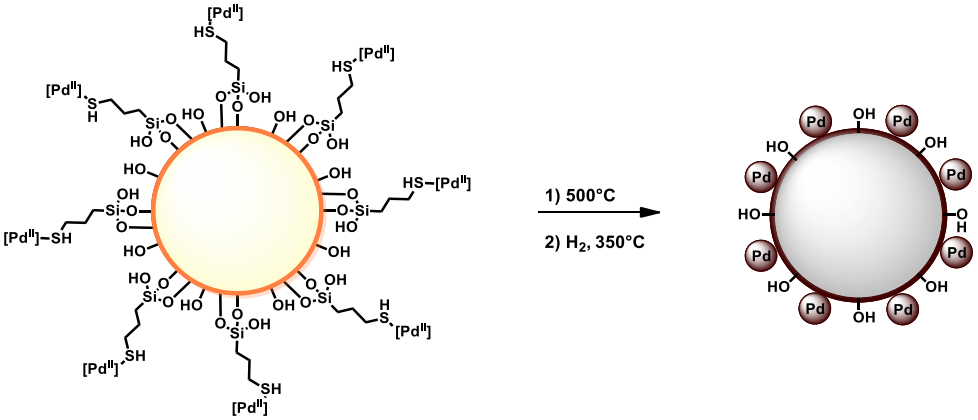

Scheme 5.5: Preparation of Pd^{0}@SMSs by calcination of Pd^{II}@MIOMSs.

The resulting macrospheres should resemble the *is*PdSMSs, but with the palladium nanoparticles only present on their surface, rather than throughout the entire structure. This would also hopefully give increased palladium loading on the surface of the macrospheres, as the Pd^{II}@MIOMSs had a higher atom ratio of palladium to silicon on their surface than the *is*PdSMSs.

Table 5.5: Palladium content of the Pd^{II}@MIOMSs before and after calcination and reduction to form Pd^{0}@SMSs.

Macrosphere Type	Pd/Si (atom ratio)		weight%			
	Surface[a]	Total[b]	Pd[b]	Si[b]	S[a]	C[c]
Pd^{II}@MIOMSs	0.048±0.025	0.0018	0.14	21	5.1	37 (33[b])
Pd^{0}@SMSs	0.052±0.027	0.0017	0.26	40	1.7	3.3
*is*PdSMSs	0.026±0.002	0.033	4.3	40	-	-

[a] Average calculated using EDX. [b] Measured using ICP-AES. [c] Measured using combustion analysis.

The composition of each type of palladium-loaded macrosphere, measured by EDX and combustion analysis or ICP-AES, is shown in Table 5.5. The Pd^{II}@MIOMSs contained 33 weight% carbon, measured by combustion analysis, due to CTAB and MPTES incorporation. Upon calcination, a significant proportion of mass was therefore lost form the macrospheres, which could compromise their stability. The loss of functionality could also allow for more instability of palladium binding, and high levels of leaching during reaction.

Fortunately, the macrospheres retained their structure after calcination and still contained palladium on their surface. The total palladium to silicon atom ratio, determined by ICP-AES

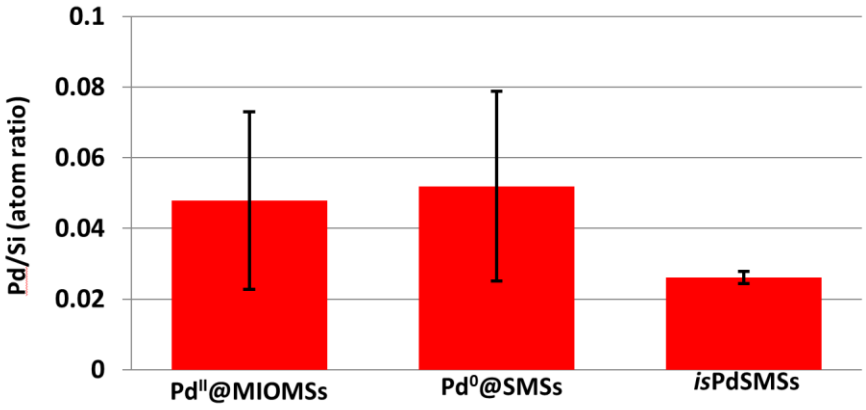

Figure 5.9: Palladium to silicon ratio on the surface of Pd^{II}@MIOMSs that had not undergone heat treatment for hardening before palladium loading, Pd^{0}@SMSs, and *is*PdSMSs. Determined by EDX.

and EDX (Figure 5.9), was similar before and after calcination to form Pd^0@SMSs. This suggests that there was not significant loss of palladium upon calcination. The overall increase in the palladium weight% to 0.26 from 0.14 weight% for the Pd^0@SMSs relative to the Pd^{II}@MIOMSs can be attributed to the loss of organic functionality. Even with the loss of the coordinating functionality, the palladium remained adsorbed to the macrosphere surface. Palladium also appears to still be loaded exclusively on the surface of the macrospheres, as it was not observed in EDX spectra of the interior of the Pd^0@SMSs.

EDX measurements for the carbon content of the Pd^{II}@MIOMSs were in agreement with the value determined by ICP-AES, and spectra for the Pd^0@SMSs confirm the loss of carbon after calcination (Figure 5.10). EDX spectra for the Pd^0@SMSs still show the presence of sulfur within the macrospheres after calcination, but the amount appears to be reduced from before calcination (Figure 5.2).

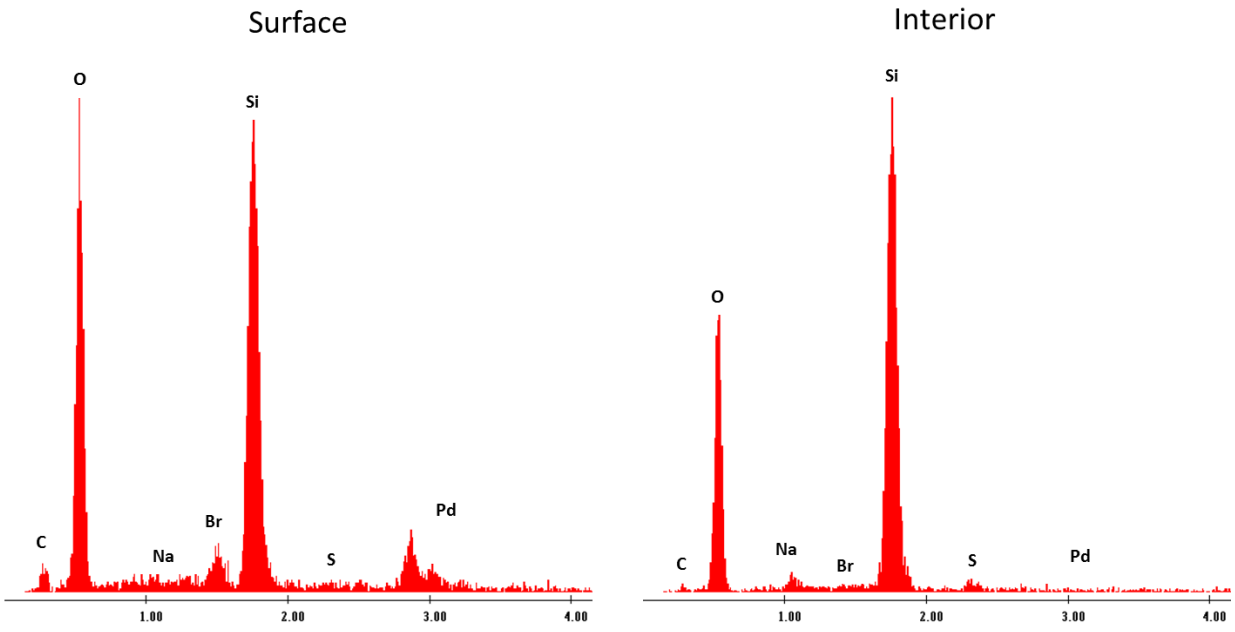

Figure 5.10: EDX spectra of the surface and interior of Pd^0@SMSs.

The size of the palladium nanoparticles in the Pd^0@SMSs was determined from analysis of TEM images (Figure 5.11). When the whole Pd^0@SMSs were simply ground, no particles could be located because the majority of the macrosphere structure did not contain palladium. Instead, the surface was scraped off of several macrospheres and then only the surface scrapings ground and used. The palladium particles were generally larger in the Pd^0@SMSs than those in the *is*PdSMSs, probably due to the increased palladium concentration on the surface of those

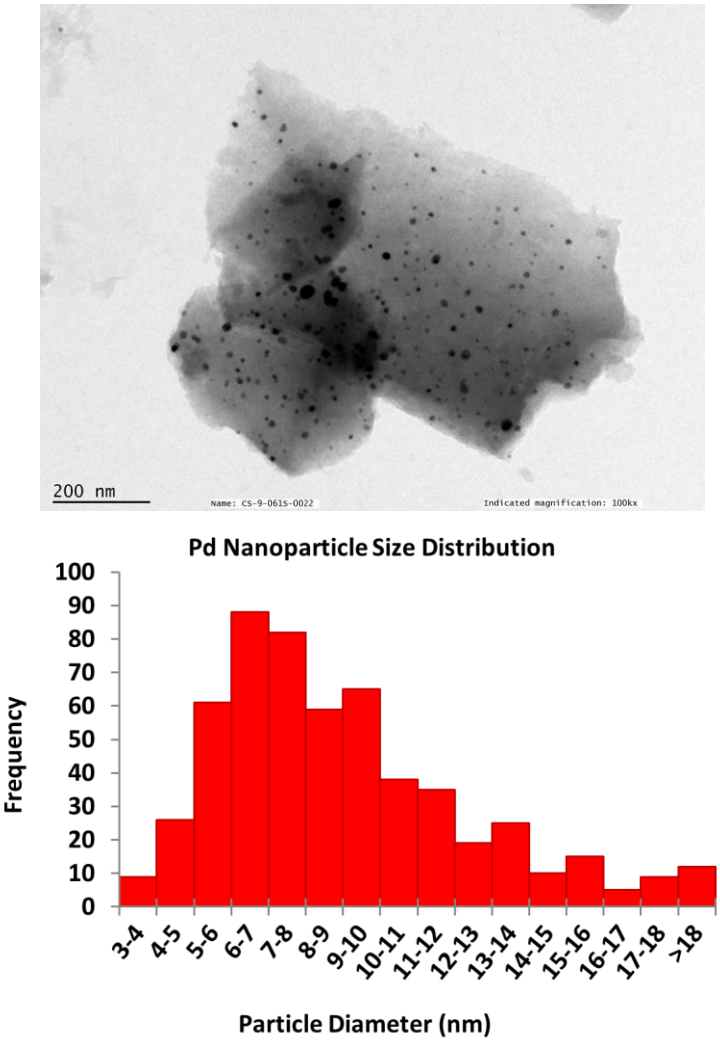

Figure 5.11: TEM image of surface piece of Pd^0@SMS and histogram of measured palladium particle diameters using TEM image analysis.

macrospheres. Most palladium nanoparticles measured were in the range of 6-8 nm in diameter, compared to 2-2.5 nm for the *is*PdSMSs (Figure 2.8).

The Pd^0@SMSs also could not be determined to contain ordered mesoporosity from the TEM images, as many of the pieces had variable thickness. Since the surfactant CTAB was also used in the formation of the MIOMSs, some porosity may have been present. However, pore structure may also be lost due to reorganization during calcination.

5.3.4: Heck Cross-Coupling Reactions in Batch Microwave Conditions

Heck cross-coupling reactions were carried out to test the catalytic abilities of the Pd^{II}@MIOMSs and Pd^0@SMSs in comparison with the *is*PdSMSs (Table 5.6). The coupling of 4-iodotoluene with methyl acrylate was chosen as a test reaction because it gave good yield when used in MACOS with the *is*PdSMSs. The tests were carried out under batch microwave conditions using the same overall mass of each type of palladium-loaded macrosphere. The total

Table 5.6: Heck cross-coupling reactions under batch microwave conditions using Pd^{II}@MIOMSs, Pd^0@SMSs, and *is*PdSMSs.

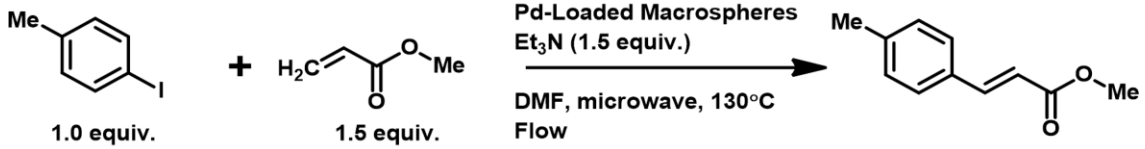

Palladium-Loaded Macrospheres	Macrosphere Quantity (g)	Total Amount of Pd (mg)[a]	Pd/ 4-Iodotoluene (mol%)	Yield (%)
Pd^{II}@MIOMSs	0.020	0.028	0.066	14
Pd^0@SMSs	0.020	0.052	0.12	70
*is*PdSMSs	0.020	0.86	2.0	97

[a] Calculated using mass% of palladium determined by ICP-AES.

amount of palladium species, however, will be different due to the different compositions of each macrosphere. An equal mass of the *is*PdSMSs contains significantly more total palladium than either the Pd^{II}@MIOMSs or Pd^{0}@SMSs, but a large portion of the palladium will be inside of the support, making it inaccessible to reaction. The macrospheres do break apart, however, due to stirring in the batch reactions, so a larger proportion than just what is on the surface of the macrospheres will be available for reaction. On the other hand, the Pd^{II}@MIOMSs and Pd^{0}@SMSs will contain all of their palladium on the macrosphere surface, accessible to reaction, regardless of the extent to which the macrospheres are broken during the reaction.

The *is*PdSMSs gave the highest yield of product (97%), likely due to having more overall catalyst present, and as a high surface area dispersion of nanoparticles. Even with shorter reaction time, the *is*PdSMSs are able to effectively catalyze this reaction with near quantitative yield (Table 2.6, Entry 7).

The Pd^{0}@SMSs also gave good yield (70%), even though they contained a significantly smaller amount of total catalyst than the *is*PdSMSs. However, both supports contained palladium nanoparticles, which had proven to be able to effectively catalyze the Heck cross coupling of aryl iodides previously.

On the other hand, the Pd^{II}@MIOMSs gave a very low product yield (14%) for the same reaction. The Pd^{II}@MIOMSs contained not only overall the lowest amount of palladium, but also thiol groups that could serve to poison the catalyst in high proportions. In this case, the breaking of the macrospheres during reaction could further poison the catalyst, as a greater amount of thiol functionality is exposed. However, the bound palladium proved to be somewhat catalytically active, giving promise for its use in MACOS.

5.3.5: Heck Cross-Coupling Reactions in MACOS

The Pd^{II}@MIOMSs and Pd^{0}@SMSs were used as supported heterogeneous catalysts in the second-generation MACOS system (Figure 3.3) under the same reaction conditions used for the *is*PdSMSs (Table 5.7). Unfortunately, neither the Pd^{II}@MIOMSs nor Pd^{0}@SMSs were found to be as active as the *is*PdSMSs, giving lower overall conversions under the same reaction conditions.

The Pd^{II}@MIOMSs gave fairly consistent conversion over multiple uses of the catalyst. However, there was a slight decrease in conversions after the first reaction, which may be due to removal of some loosely bound palladium during the first reaction. A decrease in the flow rate from 30 to 20 μL/minute did not increase the conversions significantly. This suggests that there was not significant leaching of palladium from the support during reaction. There is expected to

Table 5.7: Heck cross-coupling reaction of 4-iodotoluene and *tert*-butyl acrylate performed in MACOS using Pd^{II}@MIOMSs, Pd^{0}@SMSs, and *is*PdSMS.

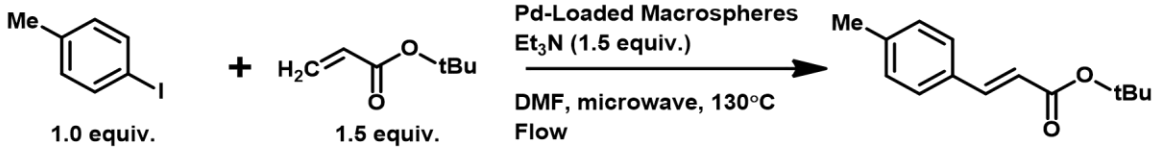

Macrosphere Type	Pd/SiO_2 (g)	Throughput (mmol/min.)	Residence Time (min.)[a]	Conversion (%)[b]				
				1st Use	2nd Use	3rd Use	4th Use	5th Use
Pd^{II}@MIOMS	0.363	0.006	8.6	81	78	77	75	75
	0.360	0.004	10.5	84	81	81	81	84
Pd^{0}@SMS	0.266	0.006	11	85	86	83	-	-
	0.299	0.004	14	89	75	66	-	-
*is*PdSMS	0.281	0.006	10	complete				

[a] Residence time calculated based on the measured total measured volume of the reactor capillary, subtracting the measured volume of the fittings, and flow rate used (20 or 30 μL/minute). [b] Determined using ^{1}H-NMR spectroscopy relative to residual starting material peaks.

be a larger amount of catalyst available on the surface of the Pd^{II}@MIOMSs than on the *is*PdSMSs, but the coordinated catalyst species seems to be less active than the dispersed nanoparticles present on the other macrospheres.

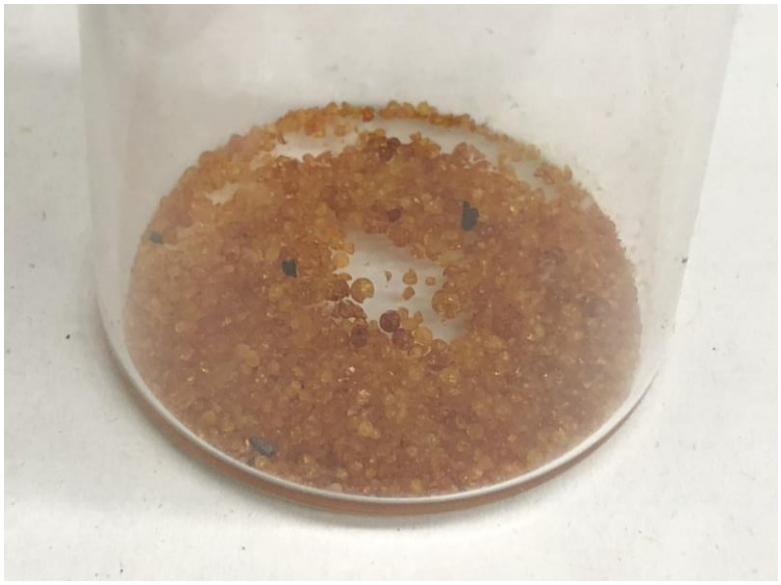

Figure 5.12: Pd^{II}@MIOMSs after being used in MACOS for 5 Heck cross-coupling reactions.

After being used in MACOS for a total of 5 reactions (Figure 5.12), the Pd^{II}@MIOMSs do not appear different than before use (Figure 5.5b), further suggesting that there is no decomposition of the support over the course of the 5 uses.

The Pd^{0}@SMSs also gave lower conversion than the *is*PdSMSs, with the conversion decreasing when the flow rate was reduced. The conversion also decreased over multiple uses of the catalyst. Unlike in the batch reactions, the amount of available palladium nanoparticles should have been greater for the Pd^{0}@SMSs than the *is*PdSMSs because the macrospheres remain intact during the MACOS reaction.

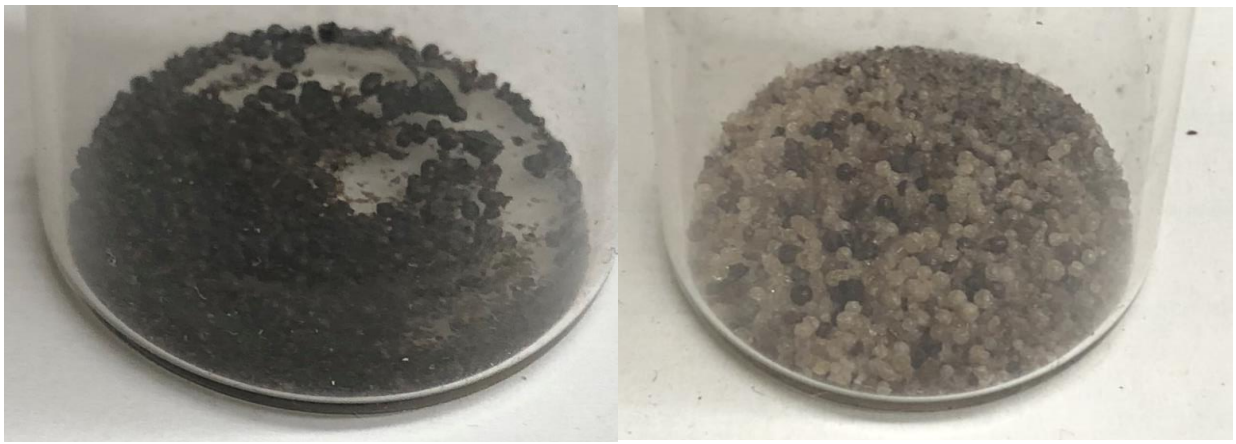

Figure 5.13: Pd^0@SMSs before (left) and after (right) being used in MACOS for 3 Heck cross-coupling reactions.

When the Pd^0@SMSs were removed from the reactor capillary after use, significant loss of palladium from the support could be observed (Figure 5.13). Many of the macrospheres were much lighter in colour than before reaction. This loss of palladium during reaction explains the decrease in conversion observed over multiple uses and the lower conversion than obtained with the *is*PdSMSs under the same conditions.

Pd^{II}@enIOMSs caused significant blockages of the MACOS system when used for Heck cross-coupling reactions in MACOS due to decomposition of the enIOMSs support under reaction conditions. As the palladium loading of the Pd^{II}@enIOMSs was the same in the interior as on the surface, it is likely that the reaction solution is also able to permeate these macrospheres, but unfortunately also weakens the support.

5.4: Conclusions

IOMSs could be prepared with amine and thiol functionality for ligating transition metals, then loaded with palladium by scavenging from solution. The formation of thiol-functionalized

IOMSs with palladium loading (Pd^{II}@MIOMSs) is outlined in Scheme 5.5 below. In this way, the metal is loaded solely on the exposed surface of the macrospheres, where it will be accessible for reaction. The palladium-loaded IOMSs could then undergo calcination to promote the formation of palladium nanoparticles on the surface of silica macrospheres and removal of the organic functionality (Scheme 5.4).

The surface loading of palladium on these macrospheres seems to be significantly higher than the *is*PdSMSs, while the macrospheres contain significantly less palladium in total. The palladium loading is more catalyst efficient, as only the areas likely to be encountered by reagents when used in flow reactions contain palladium.

The Pd^{II}@MIOMSs were able to catalyze Heck cross-coupling reactions in batch and flow processes, but were not as active as the *is*PdSMSs, giving lower conversion to product. Consistent conversions were achieved over 5 uses of the catalyst, showing that the catalyst is stable and reusable.

Pd^{0}@SMSs were also able to catalyze Heck cross-coupling reactions in batch and flow, but were prone to loss of catalyst when used in MACOS, decreasing reactivity over multiple uses of the catalysts.

Chapter 6: Conclusions and Future Work

6.1: Silica Macrosphere-Based Catalyst Supports

Controlled-size silica macrospheres were able to act as a microwave-transparent support for use in MACOS. A dispersion of palladium nanoparticles incorporated into the macrospheres did not cause the supports to heat significantly under microwave irradiation, but were catalytically active for Suzuki-Miyaura and Heck cross-coupling reactions. The *in situ* palladium-loaded macrospheres were re-usable over multiple reactions, with small amounts of palladium leaching over repeated uses. Unfortunately, the majority of the palladium was encapsulated within the interior of the *in situ*-loaded macrospheres, where it is inaccessible to the reaction mixture.

Although macrospheres containing nickel and copper were also prepared, they were not characterized or utilized significantly. The utility of the macrosphere-supported catalysts in MACOS may be extended beyond palladium-catalyzed cross-coupling reactions through the use of dispersions of nanoparticles of other catalytically-active metals.

Inorganic-organic hybrid macrospheres with thiol functionality were able to load palladium selectively on their surface by scavenging from a solution of the metal salt. These supports were able to achieve higher surface palladium loadings than those loaded *in situ*, while using significantly less overall palladium. The thiol-bound palladium, however was not as effective of a catalyst as the dispersion of palladium nanoparticles. The supported catalyst was also reusable several times for Heck cross-coupling reactions in MACOS without a significant decrease in product conversion over multiple uses.

Although there was limited success with the use of amine-functionalized macrospheres due to low palladium uptake and structural instability, other functionalities could be incorporated onto the macrosphere surfaces to form tethered catalysts. Phosphine[27]b,[72],[73] and carbene-

based[25]b,[74] tethers have been used in other heterogeneous catalysts, and could possibly be incorporated onto the macrospheres.

The thiol-bound palladium were used to form palladium nanoparticles through calcination and reduction, yielding silica macrospheres with dispersions of palladium nanoparticles incorporated only on their surfaces. These palladium nanoparticles were effective for catalyzing Suzuki-Miyaura and Heck cross-coupling, but were observed to leach palladium when used in flow reactions, giving decreasing yields over multiple uses.

As the silica macrospheres themselves were not capable of scavenging much palladium from solution, the palladium nanoparticles formed from the tethered palladium were unstable on the surface of the macrospheres. A dispersion of nanoparticles with tethering functionality incorporated onto the surface of macrospheres may allow for the combination of the higher activity of the palladium nanoparticles with the low leaching observed in tethered catalysts.[32]

6.2: Silica Macrosphere-Based Catalyst Supports in MACOS

Unfortunately, Suzuki-Miyaura cross-coupling reactions were unable to be performed in MACOS using the silica macrosphere-supported palladium catalysts due to the formation of precipitates. Further testing would be beneficial to expand the scope of reactions that can be performed using the supported catalysts in MACOS. Other palladium-catalyzed reactions may also be tested.

Due to technical limitations of the microwave devices used, reactions could not be run for extended periods of time, as they required continuous monitoring. This prevented long timeframe reactions from being attempted, and lead to the repeated use of the supported catalysts in

multiple reactions instead. Ideally, one would want to perform a continuous, uninterrupted reaction over multiple days to determine the lifetime of the catalyst under continuous use.

6.3: Amphiphilic Coordination Complexes as a Means of Selective Catalyst Loading

The exact structure of the DTC complexes formed was not determined, but they showed promise for concentrating metals towards the macrosphere surface during formation. The gradient in palladium loading in the macrosphere observed in Figure 4.8 suggests a preference for the palladium complex to be close to the oil-water interface during macrosphere formation.

Further study may allow for the full characterization of complex 3, and development of a complex with higher selectivity to be incorporated on the surface of the macrospheres. Silica macrospheres with metal nanoparticles encapsulated close to their surface may prove to be as catalytically-active as the *in situ* palladium-loaded silica macrospheres, while reducing the amount of inaccessible metal in the interior of the macrospheres.

Chapter 7: References

[1] (a) Raqqaz, T.; Kappe, C. O. *Chem. Asian J.*, **2010**, 5, 1274-1289. (b) Porta, R.; Benaglia, M.; Puglisi, A. *Org. Process Res. Dev.*, **2016**, 20, 2-25. (c) Plutschack, M. B.; Pieber, B.; Gilmore, K.; Seeberger, P. H. *Chem. Rev.*, **2017**, 117, 11796-11893.

[2] (a) Yoshida, J.-i.; Nagaki, A.; Yamada, T. *Chem. Eur. J.*, **2008**, 14, 7450-7459; (b) Yoshida, J.-i. Flash Chemistry—Fast Organic Synthesis in Microsystems, Wiley-VCH, Weinheim, 2008.

[3] Roberge, D. M.; Durcy, L.; Bieler, N.; Cretton, P.; Zimmermann, B. *Chem. Eng. Technol.*, **2005**, 28, 318-323.

[4] Schwalbe, T.; Autze, V.; Hohmann, M.; Stirner, W. Org. Proc. Res. Dev., 2004, 8, 440-454.

[5] Trachsel, F.; Hutter, C.; von Rohr, P. R. *Chem. Eng. J.*, **2008**, 135, S309-S316.

[6] Fukuyama, T.; Shinmen, M.; Nishitani, S.; Sato, M.; Ryu, I. *Org. Lett.*, **2002**, 4, 1691-1694.

[7] (a) Tiggelaar, R. M.; Benito-López, F.; Hermes, D. C.; Rathgen, H.; Egberink, R. J. M.; Mugele, F. G.; Reinhoudt, D. N.; van den Berg, A.; Verboom, W.; Gardeniers, H. J. G. E. *Chem. Eng. J.*, **2007**, 131, 163-170. (b) Garcia-Egido, E.; Wong, S. Y. F.; Warrington, B. H. *Lab Chip*, **2002**, 2, 31-33.

[8] He, P.; Haswell, S. J.; Fletcher, P. D. I. *Lab Chip*, **2004**, 4, 38-41.

[9] Jachuck, R. J. J.; Selvaraj, D. K.; Varma, R. S. *Green Chem.*, **2006**, 8, 29-33.

[10] For the development of the MACOS reactor concept and applications in synthetic chemistry, see: (a) Comer, E.; Organ, M. G. *J. Am. Chem. Soc.*, **2005**, 127, 8160−8167. (b) Organ, M. G.; Comer, E. *Chem. Eur. J.*, **2005**, 11, 7223−7227. (c) Bremner, S.; Organ, M. G. *J. Comb. Chem.*, **2007**, 9, 14−16.

[11] For the use of MACOS technology in multi-step natural product synthesis, see: Achanta, S.; Liautard, V.; Paugh, R.; Organ, M. G. *Chem. Eur. J.*, **2010**, 16, 12797−12800.

[12] For applications of MACOS technology in medicinal chemistry, see: (a) Ullah, F.; Samarakoon, T.; Rolfe, A.; Rurtz, Hanson, P. R.; Organ, M. G. *Chem. Eur. J.*, **2010**, 16, 10959-10962. (b) Zang, Q.; Javed, S.; Ullah, F.; Zhou, A.; Knudtson, C. A.; Bi, D.; Basha, F. Z.; Organ, M. G.; Hanson, P. R. *Synthesis*, **2011**, 2743−2750. (c) Hanson, P. R.; Organ, M. G.; Rolfe, A.; Samarakoon, T. B.; Ullah, F. *J. Flow Chem.*, **2011**, 1, 32−39. (d) Rolfe, A.; Ullah, F.; Samarakoon, T. B.; Kurtz, R. D.; Porubsky, P.; Neuenswander, B.; Lushington, G. H.; Santini, C.; Organ, M. G.; Hanson, P. R. *ACS Combin. Sci.*, **2011**, 13, 653−658. (e) Zang, Q.; Javed, S.; Porubsky, P.; Ullah, F.; Neuenswander, B.; Lushington, G. H.; Basha, F. Z.; Organ, M. G.; Hanson, P. R. *ACS Combin. Sci.*, **2012**, 14, 211−217. (f) Ullah, F.; Zang, Q.; Javed, S.; Porubsky, P.; Neuenswander, B.; Lushington, G. H.; Bash, F. Z.; Hanson, P. R.; Organ, M. G. *Synthesis*, **2012**, 44, 2547−2554. (g) Zang, Q.; Javed, S.; Hill, D.; Ullah, F.; Bi, D.; Porubsky, P.; Neuenswander, B.; Lushington, G. H.; Santini, C.; Organ, M. G.; Hanson, P. R. *ACS Combin. Sci.*, **2012**, 14, 456−459. (h) Ullah, F.; Zang, Q.; Javed, S.; Zhou, A.; Knudtson, C. A.; Bi, D.; Hanson, P. R.; Organ, M. G. *J. Flow. Chem.*, **2012**, 2, 118−123. (i) Faisal, S.; Ullah, F.; Maity, P. K.; Rolfe, A.; Samarakoon, T. B.; Porubsky, P.; Neuenswander, B.; Lushington, G. H.; Basha, F. Z.; Organ, M. G.; Hanson, P. R. *ACS Combin. Sci.*, **2012**, 14, 268−272.

[13] For larger-scale applications of MACOS technology in process chemistry applications, see: (a) Benaskar, F.; Patil, N.; Rebrov, E.; Meuldijk, J.;

Benabdelmoumen, A.; Hessel, V.; Hulshof, L.; Schouten, J. *ChemSusChem*, **2013**, 6, 353−366. (b) Benaskar, F.; Patil, N.; Rebrov, E.; Meuldijk, J.; Hessel, V.; Schouten, J.; Hulshof, L. *Ind. Eng. Chem. Res.*, **2012**, 51, 14344−14354. (c) Benaskar, F.; Patil, N.; Rebrov, E.; Meuldijk, J.; Hessel, V.; Schouten, J. *Chem. Eng. J.*, **2012**, 207−208, 426−439.

[14] For the use of Pd thin films in MACOS applications, see: (a) Shore, G.; Morin, S.; Organ, M. G. *Angew. Chem., Int. Ed.*, **2006**, 45, 2761−2766. (b) Shore, G.; Morin, S.; Mallik, D.; Organ, M. G. *Chem. Eur. J.*, **2008**, 14, 1351−1356. (c) Shore, G.; Organ, M. G. *Chem. Commun.*, **2008**, 838−840.

[15] For the use of Au thin films in MACOS applications, see: (a) Organ, M. G.; Shore, G.; Tsimerman, M. *Beilstein J. Org. Chem.*, **2009**, 5, No. 35; (b) Shore, G.; Organ, M. G. *Gold Bull.*, **2010**, 43, 105−113. (c) Shore, G.; Organ, M. G. *Chem. Eur. J.*, **2008**, 14, 9641−9646.

[16] For the use of Cu thin films in MACOS applications, see: Shore, G.; Yoo, W. J.; Li, C. J.; Organ, M. G. *Chem. Eur. J.*, **2010**, 16, 126−133.

[17] Sauks, J. M.; Mallik, D.; Lawryshyn, Y.; Bender, T.; Organ, M. G. *Org. Process Res. Dev.*, **2014**, 18, 1310-1314.

[18] Somerville, K.; Tilley, M.; Li, G.; Mallik, D.; Organ, M. G. *Org. Process Res. Dev.*, **2014**, 18, 1315-1320.

[19] Schruder, C. W., Organ, M. G., Pietro, W. J. *Current Nanoscience*, **2016**, 12, 448-454.

[20] Tilley, M.; Li, G.; Savel, P.; Mallik, D.; Organ. M. G. *Org. Process Rev. Dev.*, **2016**, 20, 517-524.

[21] Köll, K.; Metzger, *J. Angew. Chem. Int. Ed. Engl.*, **1978**, 17, 754-755.

[22] Tsubogo, T.; Oyamada, H.; Kobayashi, S. *Nature*, **2015**, 520, 329-332.

[23] Kirschning, A.; Solodenko, W.; Mennecke, K. *Chem. Eur. J.*, **2006**, 12, 5972–5990.

[24] Frost, C. G.; Mutton, L. *Green Chem.* **2010**, 12, 1687−1703.

[25] For Negishi coupling reactions in flow, see: (a) Egle, B.; Muñoz, J.; Alonso, N.; De Borggraeve, W.; de la Hoz, A.; Díaz-Ortiz, A.; Alcázar, J. *J. Flow Chem.*, **2015**, 4, 22−25.; (b) Price, G. A.; Bogdan, A. R.; Aguirre, A. L.; Iwai, T.; Djuric, S. W.; Organ, M. G. *Catal. Sci. Technol.*, **2016**, 6, 4733−4742.

[26] Shimizu, K.-I.; Koizumi, S.; Hatamachi, T.; Yoshida, H.; Komai, S.; Kodama, T.; Kitayama, Y. *J. Catal.*, **2004**, 228, 141-151.

[27] (a) Crudden, C. M.; Sateesh, M.; Lewis, R. *J. Am. Chem. Soc.*, **2005**, 127, 10045-10050.; (b) Lemay, M.; Pandarus, V.; Simard, M.; Marion, O.; Tremblay, L.; Béland, F. *Top. Catal.*, **2010**, 53, 1059-1062.

[28] (a) Mehnert, C. P.; Ying, J. Y. *Chem. Commun.*, **1997**, 2215-2216.; (b) Mehnert, C. P.; Weaver, D. W.; Ying, J. Y. *J. Am. Chem. Soc.*, **1998**, 12289-12296.

[29] Augustine, R.; Tanielyan, S.; Anderson, S.; Yang, H. *Chem. Commun.*, **1999**, 1257-1258.

[30] (a) Djakovitch, L.; Köhler, K. *J. Mol. Cat. A: Chem.*, **1999**, 142, 275-284.; (b) Djakovitch, L.; Heise, H.; Köhler, K. *J. Organomet. Chem.*, **1999**, 584, 16-26.; (c) Djakovitch, L.; Köhler, K. *J. Am. Chem. Soc.*, **2001**, 123, 5990-5999.

[31] (a) Bremeyer, N.; Ley, S. V.; Ramarao, C.; Shirley, I. M.; Smith, S. C. *Synlett*, **2002**, 1843–1844.; (b) Ley, S. V.; Ramarao, C.; Gordon, R. S.; Holmes, A. B.; Morrison,

A. J.; McConvey, I. F.; Shirley, I. M.; Smith, S. C.; Smith, M. D. *Chem. Commun.*, **2002**, 1134–1135.; (c) Ramarao, C.; Ley, S. V.; Smith, S. C.; Shirley, I. M.; DeAlmeida, N. *Chem. Commun.*, **2002**, 1132–1133.; (d) Yu, J.-Q.; Wu, H.-C.; Ramarao, C.; Spencer, J. B.; Ley, S. V. *Chem. Commun.*, **2003**, 678–679.; (e) Lee, C. K. Y.; Holmes, A. B.; Ley, S. V.; McConvey, I. F.; Al-Duri, B.; Leeke, G. A.; Santos, R. C. D.; Seville, J. P. K. *Chem. Commun.*, **2005**, 2175–2177.

[32] Greco, R.; Goessler, W.; Cantillo, D.; Kappe, C. O. *ACS Catal.*, **2015**, 5, 1303-1312.

[33] For Suzuki-Miyaura coupling reactions in flow, see: (a) Hattori, T.; Tsubone, A.; Sawama, Y.; Monguchi, Y.; Sajiki, H. *Catalysts*, **2015**, 5, 18−25.; (b) He, P.; Haswell, S. J.; Fletcher, P. D. I.; Kelly, S. M.; Mansfield, A. *Beilstein J. Org. Chem.*, **2011**, 7, 1150-1157.; (c) Pavia, C.; Ballerini, E.; Bivona, L. A.; Giacalone, F.; Aprile, C.; Vaccaro, L.; Gruttadauria, M. *Adv. Synth. Catal.*, **2013**, 355, 2007-2018.; (d) Pascanu, V.; Hansen, P. R.; Bermejo Gómez, A.; Ayats, C.; Platero-Prats, A. E.; Johansson, M. J.; Pericàs, M. À.; Martín-Matute, B. *ChemSusChem*, **2015**, 8, 123−130.; (e) Martinez, A.; Krinsky, J. L.; Penafiel, I.; Castillon, S.; Loponov, K.; Lapkin, A.; Godard, C.; Claver, C. *Catal. Sci. Technol.*, **2015**, 5, 310-319.; (f) Mateos, C.; Rincón, J. A.; Martín-Hidalgo, B.; Villanueva, J. *Tetrahedron Lett.*, **2014**, 55, 3701-3705.; (g) Reynolds, W. R.; Plucinski, P.; Frost, C. G. *Catal. Sci. Technol.*, **2014**, 4, 948−954.; (h) Trinh, T. N.; Hizartidis, L.; Lin, A. J. A.; Harman, D. G.; McCluskey, A.; Gordon, C. P. *Org. Biomol. Chem.*, **2014**, 12, 9562-9571.; (i) Estrada, G. O. D.; Flores, M. C.; Silva, J. F. M.; de Souza, R. O. M. A.; e Miranda, L. S. M. *Tetrahedron Lett.*, **2012**, 53, 4166−4168.

[34] For Heck coupling reactions in flow, see: (a) Stouten, S. C.; Wang, Q.; Noël, T.; Hessel, V. *Tetrahedron Lett.,* **2013**, 54, 2194−2198.; (b) Jumde, R. P.; Marelli, M.; Scotti, N.; Mandoli, A.; Psaro, R.; Evangelisti, C. *J. Mol. Catal. A: Chem.*, **2016**, 414, 55−61.

[35] For Sonogashira coupling reactions in flow, see: (a) Borcsek, B.; Bene, G.; Szirbik, G,; Dormán, G; Jones, R.; Ürge, L.; Darvas, F. *Arkivoc*, **2012**, 5, 186-195.; (b) Tan, L.-M.; Sem, Z.-Y.; Chong, W.-Y.; Liu, X.; Hendra; Kwan, W. L.; Lee, C.-L. K. *Org. Lett.*, **2013**, 15, 65−67.; (c) Battilocchio, C.; Bhawal, B. N.; Chorghade, R.; Deadman, B. J.; Hawkins, J. M.; Ley, S. V. *Isr. J. Chem.*, **2014**, 54, 371−380.

[36] (a) Heck, R. M.; Gulati, S.; Farrauto, R. J. *Chem. Eng. J.*, **2001**, 82, 149-156.; (b) Kiwi-Minsker, L. *Chimia*, **2002**, 56, 143-147.

[37] Glasnov, T. N.; Findenig, S.; Kappe, C. O. *Chem. Eur. J.*, **2009**, 15, 1001-1010.

[38] Cantillo, D.; Kappe, C. O. *ChemCatChem*, **2014**, 6, 3286-3305.

[39] (a) Kresge, C. T.; Leonowicz, M. E.; Roth, W. J.; Vartuli, J. C.; Beck, J. S. *Nature*, **1992**, 359, 710-712.; (b) Beck, J. S.; Vartuli, J. C.; Roth, W. J.; Lenowicz, M. E.; Kresge, C. T.; Schmitt, K. D.; Chu, C. T.-W.; Olson, D. H.; Sheppard, E. W.; McCullen, S. B.; Higgins, J. B.; Schlenker, J. L. *J. Am. Chem. Soc.*, **1992**, 114, 10834-10843.

[40] Nakanishi, K. *J. Porous Mater.*, **1997**, 4, 67-112.

[41] For the development of sol-gel processes for the formation of metal oxides, see: (a) Ebelmen, M. *Ann. Chimie. Phys.*, **1846**, 16, 129-166.; (b) Graham, T. *J. Chem. Soc.*, **1864**, 17, 318-327.

[42] Cushing, B. L.; Kolesnichenko, V. L.; O'Connor, C. J. Chem. Rev. 2004, 104, 3893-3946.

[43] Stober, W.; Fink, A.; Bohn, E. *J. Colloid Interface Sci.*, **1968**, 26, 62-69.

[44] (a) Yang, H.; Shi, Q.; Liu, X.; Xie, S.; Jiang, D.; Zhang, F.; Yu, C.; Tu, B.; Zhao, D. *Chem. Commun.*, **2002**, 2842 –2843; (b) Liang, C.; Dai, S.; Guiochon, G. *Chem. Commun.*, **2002**, 2680 –2681.

[45] Kamiya, K.; Sakka, S.; Tatemichi, Y. *J. Mater. Sci.*, **1980**, 15, 1765-1771.

[46] Schacht, S.; Hou, Q.; Volgt-Martin, I. G.; Stucky, G. D.; Schueth, F. *Science*, **1996**, 273, 768-771.

[47] Kleitz, F.; Marlow, F.; Stucky, G. D. *Chem. Mater.*, **2001**, 15, 3587-3595.

[48] Zhao, D.; Sun, J.; Li. Q.; Stucky, G. D. *Chem. Mater.*, **2000**, 12, 275-279.

[49] Bruinsma, P. J.; Kim, A. Y.; Liu, J.; Baskaran, S. *Chem. Mater.*, **1997**, 9, 2507-2512.

[50] Kievsky, Y.; Sokolov, I. *T-Nano*, **2005**, 4, 490-494.

[51] Yang, M.; Sokolov, I. Y.; Coombs, N.; Kresge, C. T.; Ozin, G. A. *Adv. Mater.*, **1999**, 11, 1427-1431.

[52] Huo, Q.; Feng, J.; Schüth, F.; Stucky, G. D. *Chem. Mater.*, **1997**, 9, 14-17.

[53] Serrano, D. P.; van Grieken, R.; Melgares, A. M.; Moreno, J. *J. Porous Mater.*, **2010**, 17, 387-397.

[54] Unger, K.; Berg, K.; Gallei, E. *Kolloid-Z.u.Z.Polymere*, **1969**, 234, 1108-1114.

[55] Unger, K. K.; Becker, N.; Roumeliotis, P. *J. Chromatogr.*, **1976**, 125, 115-127.

[56] Fowler, C. E.; Burkett, S. L.; Mann, S. *Chem. Commun.*, **1997**, 1769-1770.

[57] (a) Anderson, M. L.; Morris, C. A.; Stroud, R. M.; Merzbacher, C. I.; Rolison, D. R. *Langmuir*, **1999**, 15, 674-681.; (b) Morris, C. A.; Anderson, M. L.; Stroud, R. M.;

Merzbacher, C. I.; Rolison, D. R. *Science*, **1999**, 284, 622-624. (c) Tai, Y.; Watanabe, M.; Kaneko, K.; Tanemura, S.; Miki, T.; Murakami, J.; Tajiri, K. *Adv. Mater. (Weinheim, Ger.)*, **2001**, 13, 1611-1614.; (d) Wallace, J. M.; Rice, J. K.; Pietron, J. J.; Stroud, R. M.; Long, J. W.; Rolison, D. R. *Nano Lett.* **2003**, 2003, 1463-1467.

[58] Richard-Plouet, M.; Guille, J.-L.; Frere, Y.; Danicher, L. *J. Sol-Gel Sci. Technol.*, **2002**, 25, 207-213.

[59] Fonseca, F. C.; Goya, G. F.; Jardim, R. F.; Carreno, N. L. V.; Longo, E.; Leite, E. R.; Muccillo, R. *Appl. Phys. A*, **2003**, 76, 621-623.

[60] Bharathi, S.; Fishelson, N.; Lev, O. *Langmuir*, **1999**, 15, 1929-1937.

[61] Ueno, A.; Suzuki, H.; Kotera, Y. *J. Chem. Soc., Faraday Trans. 1*, **1983**, 79, 127-136.

[62] Lopez, T.; Bosch, P.; Moran, M.; Gomez, R. *J. Phys. Chem.*, **1993**, 97, 1671-1677.

[63] (a) Breitscheidel, B.; Zieder, J.; Schubert, U. *Chem. Mater.*, **1991**, 3, 559-566.; (b) Schubert, U.; Breitscheidel, B.; Buhler, H.; Egger, C.; Urbaniak, W. *Mater. Res. Soc. Symp. Proc.*, **1992**, 271, 621-632.; (c) Morke, W.; Lamber, R.; Schubert, U.; Brietscheidel, B. *Chem. Mater.*, **1994**, 6, 1659-1666.

[64] Kozuka, H.; Sakka, S. *Chem. Mater.*, **1993**, 5, 222-228.

[65] Kiviaho, J.; Hanaoka, T.; Kubota, Y.; Sugi, Y. *J. Mol. Catal.*, **1995**, 101, 25-31.

[66] Cai, M.-Z.; Song, C.-S.; Huang, X. *J. Chem. Soc., Perkins Trans.*, **1997**, 1, 2273-2274.

[67] Lagasi, M.; Mogi, P. *J. Mol. Catal.*, **2002**, 61, 182-183.

[68] Yi, P.; Zhuangyu, Z, Hongwen, H. *J. Mol. Catal.*, **1990**, 62, 297-306.

[69] Clark, J. H.; Macquarrie, D. J.; Mubofu, E. B. *Green Chem.*, **2000**, 2, 53-58.

[70] Macquarrie, D. J.; Gotov, B.; Toma, S. *Plat. Met. Rev.*, **2001**, 45, 102-110.

[71] Mubofu, E. B.; Clark, J. H.; Macquarrie, D. J. *Green Chem.*, **2001**, 3, 23-25.

[72] Tyrrell, E.; Al-Saardi, A.; Millet, J. *Synlett*, **2005**, 3, 487-488.

[73] Bemi, L. Clark, H. C.; Davies, J. A.; Fyfe, C. A.; Wasylishen, R. E. *J. Am. Chem. Soc.*, **1982**, 104, 438-445.

[74] (a) Çetinkaya, B.; Gürbüz, N.; Secükin, T.; Özdemir, I. *J. Mol. Catal. A: Chem.*, **2002**, 184, 31-38. (b) Schürer, S. C.; Gessler, S.; Buschmann, N.; Blechert, S. *Angew. Chem., Int. Ed.* **2000**, 39, 3898-3901. (c) Schwarz, J.; Böhm, V. P. W.; Gardiner, M. G.; Grosche, M.; Herrmann, W. A.; Hieringer, W.; Raudaschl-Sieber, G. *Chem.-Eur. J.*, **2000**, 6, 1773-1780. (d) Mayr, M.; Buchmeiser, M. R.; Wurst, K. *AdV. Synth. Catal.* **2002**, 344, 712-719.

[75] J.-S. Schanche, *Mol. Diversity*, **2003**, 7, 293-300.

[76] (a) Gedye, R; Smith, F.; Westaway, K.; Ali, H.; Baldisera, L.; Laberge, L; Rousell, J. *Tetrahedron Letters*, **1986**, 27, 279-282.; (b) Giguere, R. J.; Bray, T. L.; Duncan, S. M. *Tetrahedron Letters*, **1986**, 27, 4945-4948.

[77] Hayes, B. L. Microwave Synthesis: Chemistry at the Speed of Light. CEM Publishing, Matthews NC, 2002.

[78] (a) Westaway, K. C.; Gedye, R. *J. Microwave Power*, **1995**, 30, 219-230.; (b) Langa, F.; de la Cruz, P.; de la Hoz, A.; Díaz-Ortiz, A.; Díez-Barra, E. *Contemp. Org. Synth.*, **1997**, 4, 373-386.

[79] Perreux, L.; Loupy, A. *Tetrahedron*, **2001**, 57, 9199-9223.

[80] (a) Kuhnert, N. *Angew. Chem.*, **2002**, 114, 1943-1946.; *Angew. Chem. Int. Ed.*, **2002**, 41, 1863-1866.; (b) Strauss, C. R. *Angew. Chem.*, **2002**, 114, 3741-3743.; *Angew. Chem. Int. Ed.*, **2002**, 41, 3589-3590.

[81] (a) D. Stuerga, M. Delmotte in Microwaves in Organic Synthesis (Ed.: A. Loupy), Wiley-VCH, Weinheim, 2002, pp. 1-34; b) M. D. P. Mingos in Microwave-Assisted Organic Synthesis (Eds.: P. LidstrUm, J. P. Tierney), Blackwell, Oxford, 2004, Chap. 1.

[82] Baghurst, D. R.; Mingos, D. M. P. *Chem. Soc. Rev.*, **1991**, 20, 1-47.

[83] Gabriel, C.; Gabriel, S.; Grant, E. H.; Halstead, B. S.; Mingos, D. M. P. *Chem. Soc. Rev.*, **1998**, 27, 213-223.

[84] Kappe, C. O. *Angew. Chem. Int. Ed.*, **2004**, 43, 6250-6284.

[85] Herrero, M. A.; Kremsner, J. M.; Kappe, C. O. *J. Org. Chem.*, **2008**, 73, 36-47.

[86] Kappe, C. O.; Pieber, B.; Dallinger, D. *Angew. Chem.*, **2012**, 52, 1088-1094.

[87] Cheng, J.; Roy, R.; Agrawal, D. *J. Mater. Sci. Lett.*, **2001**, 20, 1561-1563

[88] Mishra, R. R,; Sharma, A. K. *Compos Part A: Appl. Sci. Manuf.*, **2016**, 81, 78-97.

[89] Organ, M. G. unpublished results

[90] Nakanishi, K.; Komura, H.; Takahashi, R.; Soga, N. *Bull. Chem. Soc. Jpn.*, **1994**, 67, 1327-1335.

[91] (a) Marquardt, P.; Börngen, L.; Nimitz, G.; Sonnberger, R. *Phys. Lett. A*, **1986**, 114, 39-42. (b) Nimitz, G.; Marquardt, P.; Gleiter, H. *J. Crystal Growth*, **1988**, 86, 66-71.

[92] Griffiths, P. C.; Fallis, I. A.; Churnpratoom, T.; Watanesk, R. *Adv. Colloid Interface Sci.*, **2006**, 122, 107-117.

[93] Jervis, H. B.; Raimondi, M. E.; Raja, R.; Maschmeyer, T.; Seddon, J. M.; Bruce, D. W. *Chem. Commun.*, **1999**, 2031-2032. (b) Danks, M. J.; Jervis, H. B.; Nowotny, M.; Zhou, W.; Maschmeyer, T. A.; Bruce, D. W. *Catalysis Letters*, **2002**, 82, 95-98.

[94] Ivanov, A. V.; Korneeva, E. V.; Gerasimenko, A. V.; Forsling, W. *Russ. J. Coord. Chem.*, **2005**, 31, 695-707.

[95] Khatib, I. S.; Parish, R. V. *J. Organomet. Chem.*, **1989**, 369, 9-16.

[96] Fowler, C. E.; Burkett, S. L.; Mann, S. *Chem Comm.*, **1997**, 1769-1770.

[97] Hall, S. R.; Fowler, C. E.; Lebeau, B.; Mann, S. *Chem. Comm.*, **1999**, 201-202.